FINAL TECHNICAL REPORT

Providing building vulnerability data and analytical fragility functions for PAGER

Submitted to the
U.S. Geological Survey
Under the National Earthquake Hazards Reduction Program
USGS Award G10AP00011
(Award period 1/1/10—12/31/11)

Principal Investigator: Jay Berger
Earthquake Engineering Research Institute
499 14th St., Suite 220, Oakland, CA 94612

Authors:
Dina D'Ayala
Andreas Kappos
Helen Crowley
Panagiotis Antoniadis
Miriam Colombi
Emre Kishali
Georgios Panagopoulos
Vitor Silva

[Dina D'Ayala, editor]

Earthquake Engineering Research Institute

May 2012

Funding for this report was provided by the U.S. Geological Survey under grant G10AP00011.

This report is published by the Earthquake Engineering Research Institute (EERI), a nonprofit corporation. The objective of EERI is to reduce earthquake risk by advancing the science and practice of earthquake engineering by improving understanding of the impact of earthquakes on the physical, social, economic, political, and cultural environment, and by advocating comprehensive and realistic measures for reducing the harmful effects of earthquakes.

Any opinions, findings, conclusions, or recommendations expressed herein are the authors' and do not necessarily reflect the views of EERI, the U.S. Geological Survey, or the participants' organizations.

This publication is available in PDF format from http://pager.world-housing.net/

AUTHORS AND AFFILIATIONS:

Dina D'Ayala
Senior Lecturer
University of Bath
Dept of Architecture and Civil Engineering
Bath BA2 7AY United Kingdom
absdfda@bath.ac.uk

Andreas Kappos
Civil Engineering Department
Aristotle Univ of Thessaloniki
54124 Thessaloniki Greece
Phone +30 2310995743; Fax +30 2310995614
ajkap@civil.auth.gr

Helen Crowley
Eucentre
Via Ferrata 1
Pavia, 27100 Italy
Phone +39 (0382) 5169874; Fax + 39 (0382) 529131
helen.crowley@eucentre.it

Panagiotis Antoniadis
Civil Engineering Department
Aristotle Univ of Thessaloniki
54124 Thessaloniki Greece
panton@3dr.edu

Miriam Colombi
Eucentre
Via Ferrata 1
Pavia, 27100 Italy
miriam.colombi@eucentre.it

Emre Kishali
Kocaeli University Architecture and Design Faculty
Anitpark 41300 İzmit/KOCAELİ, Turkey
Phone: +902623034252; Fax: +90262304253
emre.kishali@kocaeli.edu.tr

Georgios Panagopoulos
Civil Engineering Department
Aristotle Univ of Thessaloniki
54124 Thessaloniki Greece
panagop@civil.auth.gr

Vitor Silva
Eucentre
Via Ferrata 1
Pavia, 27100 Italy
vitor.silva@eucentre.it

ACKNOWLEGMENTS

The authors would like to thank those researchers who provided data as well as thoughtful comments on various drafts of this report, including Hemant Kaushik of the Indian Institute of Technology, Guwahati and Polat Gülkan and Murat Altug Erberik of the Middle East Technical University in Turkey. Thanks also go to Craig Comartin of CDComartin Inc and Kishor Jaiswal of the U.S. Geological Survey for careful reviews of earlier drafts, and to David Wald of the US Geological Survey for encouraging the strong intellectual exchanges throughout the PAGER-WHE collaboration. Many other researchers have participated in earlier phases, and the authors are grateful for some of the earlier discussions that led to this final phase. The authors are grateful to EERI and its World Housing Encyclopedia project for embarking on such an ongoing collaboration with PAGER. And finally the authors, and EERI, are most grateful to the U.S. Geological Survey for their support of this work.

ABSTRACT:

This report summarizes the research findings of the fourth and final phase of the Earthquake Engineering Research Institute (EERI)'s World Housing Encyclopedia (WHE)-Prompt Assessment of Global Earthquakes for Response (PAGER) initiative. Since the launch of the WHE-PAGER collaboration in early spring of 2008, this joint effort has led to identifying and compiling a range of input parameters on structural inventory and vulnerability of non-U.S. construction types. The information compiled through this effort over the years has benefited the development of PAGER's engineering-based loss estimation models.

Earlier phases of this collaboration identified wide variation in the capacity curves provided by different researchers for similar structure types. It was thus decided that the core of the work in Phase IV should concentrate on understanding these discrepancies. To that end, five groups of modellers (that had already contributed to Phase III) agreed to exchange the structural model and vulnerability data on construction typologies that were derived by each of them separately in the previous phase and to perform vulnerability analyses (using their own procedures) on data provided by the other groups.

This report thus presents capacity curves and fragility curves for concrete and masonry buildings that do not comply with the HAZUS typologies, either because they are not designed to code standards or because the construction details substantially differ from U.S. code provisions. The main difference with respect to the HAZUS typologies is the ductility ratio at the level of the element and at the global level. Four main concrete typologies are studied: bare frames designed according to seismic code requirements (C1), bare frames designed only for gravitational loads or very low seismic capacity but without ductility detailing provisions (C4), infilled frames designed according to seismic code requirements (C1-I), infilled frames designed only for gravitational loads or very low seismic capacity but without ductility detailing provisions (C3). For each of the infilled frame typologies the case of irregularity of the infill in elevation, i.e. lack of infill at the ground floor, has also been considered. For masonry, adobe (A), stone (S), unreinforced fired brick (UFB) and unreinforced concrete block (UCB) masonry have been considered. For each of the main typologies some different sub-typologies have been considered, either dependent on the masonry fabric, rubble and dressed stone, or on the type of horizontal structures, timber or concrete floors. The typologies are representative of different regions of the world: the concrete frames studied represent buildings from India, Italy, Greece and Turkey; the masonry typologies represent buildings from Turkey.

Contents

1. Introduction

This report summarizes the research findings of the fourth and final phase of the Earthquake Engineering Research Institute (EERI)'s World Housing Encyclopedia (WHE)-Prompt Assessment of Global Earthquakes for Response (PAGER) initiative. Since the launch of the WHE-PAGER collaboration in early spring of 2008, this joint effort has led to identifying and compiling a range of input parameters on structural inventory and vulnerability of non-U.S. construction types. The information compiled through this effort over the years has benefited the development of PAGER's engineering-based loss estimation models.

The WHE-PAGER phase IV is a natural extension of ongoing collaboration between PAGER and WHE team members since its earlier phases. The primary objective of this joint effort has been to benefit from the professional expertise available within the WHE community in order to identify, retrieve and harmonize the structural inventory and seismic vulnerability data of non-US constructions around the world. In the phase I of this initiative, the effort resulted in the compilation of structural, occupancy, and vulnerability parameters for building typologies in 26 countries aggregated at national level. The structural inventory dataset was useful in harmonizing and validating PAGER's existing inventory database, and ultimately serving as structural and population exposure input for the PAGER's engineering based loss estimation models. The aggregated inventory and vulnerability assessment were also useful in developing global regionalization schemes for the PAGER's empirical vulnerability models. The empirical models now serve as a backbone of operational loss-PAGER system to provide a quick assessment of earthquake shaking-induced fatalities and economic impacts following a significant earthquake (magnitude greater than 5.5) worldwide (Jaiswal and Wald, 2010a). Moving forward, the PAGER system also aims at providing robust estimate of building and infrastructure damage and associated casualties (injuries and deaths) based on its engineering-based loss estimation models. The content produced concerning the structural damage, losses and socio-economic impacts can lead to informing emergency responders, government and aid agencies, and the media about the true scope of the potential disaster following a significant earthquake and to determining potential humanitarian needs in the aftermath.

The major milestones achieved in earlier phases can be summarized as follows:

- During Phase I of the project, WHE experts helped identifying and providing, on a country basis, inventory data of predominant building typologies and intensity-based building collapse fragilities of building types for 26 countries.
- In Phase II the Phase I results were analyzed[1] and the Phase I approach was slightly modified in order to obtain data for additional countries. The analysis and modifications made included:
    - the identification of problematic data,
    - an updated and more complete taxonomy of building typologies,
    - a new (updated) protocol/questionnaire for the collection of (fragility) data,
    - a new definition of damage states,

[1] http://pager.world-housing.net/wp-content/uploads/2009/08/JaiswalWald2009Analysis-of-Phase-I.pdf

    - a new framework for the definition of collapse rates influencing casualty rates,and
    - modification of the data collection process to facilitate a second round of expert opinion solicitation for a new set of countries.
- During Phase III, critically important non-HAZUS building typologies were identified. The objective of this phase was to seek assistance from a group of experts in order to collate capacity and fragility parameters of selected non-US building types. These parameters were to be incorporated within the analytical framework of performance-based assessment, constituting the basis for structure-specific damage and loss estimation within the PAGER system. Capacity and fragility parameters were developed in accordance with the HAZUS-MH model and format. Phase III data, analysis and documentation can be accessed at the WHE-PAGER website (http://pager.world-housing.net/). Data was provided on a variety of reinforced concrete and unreinforced masonry non-US typologies by five groups of researchers. An attempt was also made to validate the capacity curves obtained analytically with evidence from experimental work on similar structural typologies, concentrating specifically on shaking table tests or push-over tests of entire structures that could provide reference for the analytical models. (see http://pager.world-housing.net/background-papers-2/presentations-from-sept-09-workshop)

Scarcity of experimental data on material strength, stiffness and dynamic response properties of certain existing building types, and the scatter associated with vulnerability and fragility parameters of similar construction typologies between different countries was evident from the analysis of Phase III data (D'Ayala et al. 2010). This analysis led to the initiation of Phase IV, under the leadership of Dr. Dina D'Ayala, chair of the steering committee in Phases II and III[2].

The analytical model implemented in the current USGS PAGER system is based on the HAZUS capacity-spectrum methodology, which estimates the response of a structure from demand spectra and spectral-capacity curves (NIBS-FEMA, 2008, Porter 2009). A demand spectrum represents the site-adjusted input ground motion typically derived from elastic acceleration response spectra, whereas the spectral capacity of a structure is expressed in terms of an idealized force-displacement curve defined by yield and ultimate control points. The capacity-spectrum method provides the estimate of the median response of an idealized nonlinear single degree of freedom (SDOF) oscillator as the point of intersection between the spectral-capacity and demand curves in the Spectral displacement-Spectral acceleration space (S_d-S_a). This point is referred to as the performance point of the SDOF representing the structure and it is obtained by adjusting the response to account for site soil amplification and hysteretic energy dissipation through an iterative procedure. The performance point coordinates are compared with the corresponding quantities of spectral displacement or spectral acceleration, defined based on limit states or performance limits, in order to identify specific damage state thresholds. The spectral displacement S_d associated with the performance point forms an input to fragility functions that

[2] Participants in Phases II and III included: M. Blondet, C. Comartin, D. D'Ayala, A. Goretti, P. Gulkan, W. Holmes, S. Jain, K. Jaiswal, A. Kappos, M. Lutman, R. Meli, A. Muñoz, S. Pampanin, K. Porter, D. Rai, M. Tomazevic, D. Wald and A. Yakut. Additional researchers who participated in Phase III included N. Ahmad, Q. Ali, G.Benzoni, R.Deoliya, H. Kaushik, A. Lang, D. Lang, N. Luco, G. Panagopoulos, J. Prasad, H. Ryu, and Y. Singh.

gives the probability of different damage states. The damage and casualties associated with slight, moderate and extensive damage states are discounted for PAGER purposes since these damage state thresholds (and casualties resulted from these damage states) do not contribute significantly to total fatalities. Porter (2009) simplifies the iterative process for PAGER purposes and directly tabulates the mean-collapse fragilities and indoor fatality rates as a function of 5% damped spectral accelerations at 0.3 and 1.0 sec periods. The fatality rates given structural collapse (FR) are the same as in the case of the PAGER's semi-empirical approach (Jaiswal and Wald, 2010b).

Initial work in this phase mainly focused on reviewing the earthquake damage and loss estimation methodologies adopted within the HAZUS-MH and the EC8 –N2 documents. This work documented the substantial differences in the calculation of the performance points within the two methods. Such differences are mainly attributed to the derivation of the non-linear spectra, starting from the same initial elastic demand spectrum, but also to the choice of reference period (secant as opposed to initial) used to compute the coordinate of the performance points, and finally, to the hysteretic energy dissipation model adopted within the two methodologies. Such differences, compounded with conceptual and numerical differences in the derivation of the fragility curves from the performance points, lead to substantially different estimate on collapse and ultimately casualty estimates from the two procedures.

For this reason, and given the scatter observed in Phase III of the project for the capacity curves provided by different researchers for similar structure types, it was decided that the core of the work in Phase IV should concentrate on understanding the discrepancies discussed above. To this end, five groups of modellers (that had already contributed to Phase III) agreed to exchange the structural model and vulnerability data on the construction typologies (that were derived by each of them separately in the previous phase) and to perform the vulnerability analyses (using their own procedures) on data provided by the other groups. The teams participating to Phase IV are:

- Dina D'Ayala, University of Bath, U.K. (UBATH) Model: FaMIVE, developed to model different types of masonry structures.
- Helen Crowley, ROSE School (ROSE). Model: DBELA, simplified approach developed to model reinforced concrete frames with and without infill. ROSE provided also data on Italian index buildings to AUTh team.
- Andreas Kappos, University of Thessaloniki, Greece (AUTh). Used ETABS-SAP and Seismostruct to model reinforced concrete frames with and without infill. AUTh provided data on Greek index buildings to ROSE team.
- Polat Gülkan, Murat Altug Erberik, Middle East Technical University, Turkey, (METU) provided data on masonry to UBATH team and on reinforced concrete frames with infill to ROSE team.
- Hemant B. Kaushik, Indian Institute of Technology Guwahati (IITG). Provided data on concrete frames to AUTh team and ROSE team.

Phase IV was organised into 3 tasks:

1.1 Task 1. Choice of structural typologies to be analyzed

From a list of 25 critical non-HAZUS building types identified at the end of Phase III, a subset was selected for which the modellers had available data and suitable numerical procedures to conduct push-over analyses and derive performance points and fragility curves. Two broad structural types were identified to conduct the vulnerability analysis according to details in Tasks 2 and 3:

- reinforced concrete frames, with or without infill;
- unreinforced masonry made of fired bricks, stonework, sundried brick or concrete blocks, with different types of horizontal structures.

The structural typologies are classified according to the PAGER Construction type catalogue (http://pager.world-housing.net/wp-content/uploads/2009/09/LISTING-OF-PAGER-CONSTRUCTION-TYPES-AND.pdf) by choosing the closest type in relation to the description associated with the data provided. Table 1.1 and Table 1.2 summarize the building typologies analyzed, their regions of pertinence, the team that provided the data and the team/s that performed the analyses, respectively, for various unreinforced masonry and concrete typologies.

Table 1.1 List of unreinforced masonry structural typologies analyzed in Phase IV

PAGER building typology	Building typology description	Region of pertinence	Team providing data	MODELLING PROCEDURE	Team conducting analysis
A1	Adobe masonry, single story, timber floors, 2 openings on façade	Turkey	METU	FaMIVE	UBATH
A1	Adobe masonry, single story, timber floors, 3 openings on façade	Turkey	METU	FaMIVE	UBATH
RS2	Rubble stone masonry, single story, timber floors, 2 openings on façade	Turkey	METU	FaMIVE	UBATH
RS2	Rubble stone masonry, single story, timber floors, 3 openings on façade	Turkey	METU	FaMIVE	UBATH
RS2	Rubble stone masonry, two story, timber floors, 2+2 openings on façade	Turkey	METU	FaMIVE	UBATH
RS2	Rubble stone masonry, two story, timber floors, 2+2 openings on façade with timber bands	Turkey	METU	FaMIVE	UBATH
RS2	Rubble stone masonry, two story, timber floors, 2+3 openings on façade	Turkey	METU	FaMIVE	UBATH
RS2	Rubble stone masonry, two story, timber floors, 2+3 openings on façade with timber bands	Turkey	METU	FaMIVE	UBATH
MS	Massive stone masonry, two story, timber floors, 2+2 opening on façade	Turkey	METU	FaMIVE	UBATH
UFB1	Unreinforced brick masonry, single story, mud mortar, timber floors, 2 openings on façade	Turkey	METU	FaMIVE	UBATH
UFB1	Unreinforced brick masonry, single story, mud mortar, timber floors, 3 openings on façade	Turkey	METU	FaMIVE	UBATH
UFB1	Unreinforced brick masonry, two story, mud mortar, timber floors, 2+3 openings on façade	Turkey	METU	FaMIVE	UBATH
UFB4	Unreinforced brick masonry, single story, cement mortar, timber floors, 2 openings on façade	Turkey	METU	FaMIVE	UBATH
UFB4	Unreinforced brick masonry, two story, cement mortar, timber floors, 2+2 openings on façade	Turkey	METU	FaMIVE	UBATH
UFB4	Unreinforced brick masonry, two story, cement mortar, timber floors, 3+2 openings on façade	Turkey	METU	FaMIVE	UBATH
UFB5	Unreinforced brick masonry, two story, cement mortar, concrete floors, 2+2 openings on façade	Turkey	METU	FaMIVE	UBATH
UCB	Unreinforced concrete block masonry, two story, lime/cement mortar, reinforced concrete floors, 2+3 openings	Turkey	METU	FaMIVE	UBATH
UCB	Unreinforced concrete block masonry, three story, lime/cement mortar, reinforced concrete floors, 3+2+2 openings	Turkey	METU	FaMIVE	UBATH

Table 1.2. List of reinforced concrete structural typologies analyzed in Phase IV

PAGER building typology	Building typology description	Region of pertinence	Team providing data	MODELLING PROCEDURE	Team conducting analysis
C4L (RC1LL)	RC frame, Low seismic code design (1959), Low-rise (2 stories), No infill walls	Mediterranean	AUTh	DBELA	ROSE
C3L (RC3.1LL)	RC frame, Low seismic code design (1959), Low-rise (2 stories), Fully infilled	Mediterranean	AUTh	DBELA	ROSE
C4M (RC1ML)	RC frame, Low seismic code design (1959), Medium-rise (4 stories), No infill walls	Mediterranean	AUTh	DBELA	ROSE
C3M (RC3.1ML)	RC frame, Low seismic code design (1959), Medium-rise (4 stories), Fully infilled	Mediterranean	AUTh	DBELA	ROSE
C4H (RC1HL)	RC frame, Low seismic code design (1959), High-rise (9 stories), No infill walls	Mediterranean	AUTh	DBELA	ROSE
C3H (RC3.1HL)	RC frame, Low seismic code design (1959), High-rise (9 stories), Fully infilled	Mediterranean	AUTh	DBELA	ROSE
C1L (RC1LH)	RC frame, High seismic code design (1995), Low-rise (2 stories), No infill walls	Mediterranean	AUTh	DBELA	ROSE
C1L-I (RC3.1LH)	RC frame, High seismic code design (1995), Low-rise (2 stories), Fully infilled	Mediterranean	AUTh	DBELA	ROSE
C1M (RC1MH)	RC frame, High seismic code design (1995), Medium-rise (4 stories), No infill walls	Mediterranean	AUTh	DBELA	ROSE
C1M-I (RC3.1MH)	RC frame, High seismic code design (1995), Medium-rise (4 stories), Fully infilled	Mediterranean	AUTh	DBELA	ROSE
C1H (RC1HH)	RC frame, High seismic code design (1995), High-rise (9 stories), No infill walls	Mediterranean	AUTh	DBELA	ROSE
C1H-I (RC3.1HH)	RC frame, High seismic code design (1995), High-rise (9 stories), Fully infilled	Mediterranean	AUTh	DBELA	ROSE
C4M (RC_PC)	RC frame, No Seismically designed, 4 stories, No Infill walls	Mediterranean	ROSE	ETABS	AUTh
C4M (RC_5%)	RC frame, Seismically designed (horizontalload:5%), 4 stories, No Infill walls	Mediterranean	ROSE	ETABS	AUTh
C4M (RC_12.5%)	RC frame, Seismically designed (horizontalload:12.5%), 4 stories, No Infill walls	Mediterranean	ROSE	ETABS	AUTh
C3M (RC_PC)	RC frame, No Seismically designed, 4 stories, Infill walls	Mediterranean	ROSE	ETABS	AUTh
C3M (RC_5%)	RC frame, Seismically designed (horizontalload:5%), 4 stories, Infill walls	Mediterranean	ROSE	ETABS	AUTh
C3M (RC_12.5%)	RC frame, Seismically designed (horizontalload:12.5%), 4 stories, Infill walls	Mediterranean	ROSE	ETABS	AUTh
C4M (1)	RC frame without masonry infill,modern	Northern India	IITK	ETABS	AUTh
C3M (2)	RC frame with masonry infill	Northern India	IITK	ETABS	AUTh
C3M-SS (3)	RC frame open first story	Northern India	IITK	ETABS	AUTh
C3M (9)	RC 4 story Residential Building with Masonry Infills in all stories	North-eastern India	IITG	SEISMOSTRUCT	AUTh
C3M-SS (10)	RC 4 Story Residential Building with Open First Story	North-eastern India	IITG	SEISMOSTRUCT	AUTh
C4M	mid-rise, reinforced concrete, MRF	Turkey	METU	DBELA	ROSE

For concrete structures it is worth noting that the PAGER taxonomy does not differentiate between presence/absence of infill for ductile frames, including all of them in class C1. (see PAGER Inventory Database v1.4) PAGER STR category C1 is basically as defined in the HAZUS technical manual. The C1 typology is assumed to be detailed for ductile behavior and expected to undergo large deformations during an earthquake without brittle failure of any frame members and collapse of the structural system. Hence any 'structural concrete frame' system that has been designed specifically for earthquake shaking (to exhibit the ductile behavior due to specific ductile detailing provisions) should be classified as C1 type (in PAGER-STR) as it is assumed that the

presence of infill will not alter the collapse behavior and will not reduce the ultimate ductility. In this respect the class C1 is treated differently than non ductile structures, as in these the presence of infills affects the ultimate and collapse behavior in a much more substantial way, and hence the rationale of subdividing this typology in the two classes C3 and C4.However even for ductile structures, while in the initial stage the contribution of the infill is considered as positive in terms of lateral shear capacity, in the post-failure phase, the shear strength of concrete columns may be affected and shear failures might become an issue, thus resulting in semi-ductile behavior of the system.In the non-linear push-over analysis approach described in section 3, the relevance of shear failure to the ultimate capacity for the index buildings analyzed is monitored during the analysis to check whether it becomes critical at any stage.

Given the above considerations, in table 1.1 buildings classified as C1 have been given an extra digit for their identity, I, if infills are present. Moreover as some of the analyses have also considered the case of buildings with infill at all stories except the first one, leading to a soft story configuration, the digit SS have been added to classify this cases.

1.2 Task 2. Choice of analytical approaches to derive capacity curves and fragility functions

Of the possible approaches available in literature to assess the ultimate capacity of structures subjected to seismic activity, namely, non-linear static equivalent analysis, elastic dynamic analysis with response spectrum, direct integration non linear dynamic analysis, and incremental dynamic analysis, the choice was made to employ non-linear static equivalent analysis, associated with the capacity spectrum method, as this is the current platform for the PAGER analytical model. This entails using a non-linear static analysis approach, also known as push-over analysis, to determine the capacity of the structure in terms of lateral acceleration and displacement, beyond the elastic limits of the materials and components, up to widespread failure and collapse.

The capacity curve and the associated performance point can represent the performance of one specific structure or the average performance of a class of structures for which a median performance point coordinates and standard deviation can be computed.The standard deviation represents the uncertainty in the computation of such capacity. Similarly performance points can be calculated for a number of different demand spectra with a probability of occurrence at the site, or one spectrum can represent a family of events. If the latter approach is chosen also the uncertainty in the demand can be represented in terms of a median value and a standard deviation. By considering the probability density distribution of performance points for a given structural typology located in a given region with a given probabilistic distribution of events for a set return period, fragility curves can be developed, providing the probability of reaching or exceeding different damage states, given a level of nonlinear response in terms of spectral displacement.Furthermore additional varaibility in the performance due to the fact that dynamic response is treated as static, should also be considered. This can be explictly computed or expert judgement can be used in determining its value.

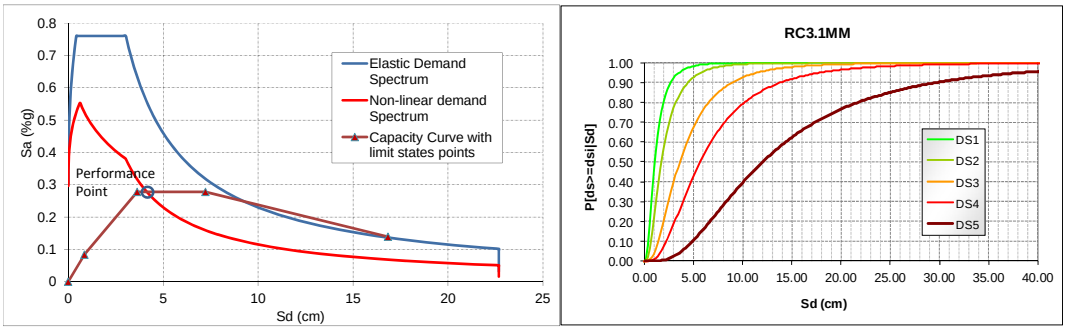

Figure 1.1:a) representative capacity/demand spectrum and performance point ;b) representative fragility curves

Three approaches of different levels of complexity have been chosen by each of the modellers' teams, working on the same basic assumptions, but requiring substantially different levels of detail in terms of data input. A central element of this task is the identification of the parameters needed to run the analysis for each of the approaches, whether this are obtained through the data providing team, which in general used yet a different approach, or whether they are estimated by the modeller, and in this case how.

For the masonry structures modelling, the approach adopted by UBATH's team is a limit state-based mechanical approach, where an optimization routine is used to identify the most likely collapse mechanism to take place, given a geometric configuration and material characteristics for a masonry structure. The approach, coded in the programme FaMIVE, is further described in section 4.2 together with the procedure adopted to compute capacity curves, performance points and fragility curves provided in section 4.5.

For the concrete structures two substantially different approaches are adopted by AUTh's and ROSE' teams. ROSE uses a simplified method, DBELA, which leads to the derivation of median capacity curves and fragility curves for a class of buildings, given a modest number of parameters describing the characteristics of the structures at elemental and material level. The method considers only flexural behavior and two possible collapse mechanisms, beam sway or column sway, i.e. the frame could fail by either hinges forming prevalently in the beams or in the columns. Further details of the procedure, its simplifying assumptions and algorithm to obtain capacity curves and fragility functions are provided in section 2.2 and 2.5.

Finally AUTh's used commercialy available nonlinear analysis software to analyze either representative 2D-frames of regular buildings or full 3D models of irregular concrete structures. For the regular 2D frames AUTh employed ETABS/SAP2000 software, using lamp plasticity and cracked r/c resistant cross sections. In-house developed software is used to control length and capacity of plastic-hinges, concrete confinement and shear capacity of the elements. For the 3D analyses, Seimsostruct was used. Further details relating to the structural modelling, together with the procedure adopted to derive the bilinear capacity curve and the fragility functions are provided in section 3.2 and 3.5.

Each modellers' report contains specific information on the level of detail required for the modelling, the list of significant parameters and minimum requirement to run the analysis, the conditions defining collapse, and the source and treatment of uncertainties.

The fact that the analysis procedures chosen represent the full spectrum of approaches for the derivation of capacity curves, with different levels of simplifying assumptions, input parameters,

and computational burden, helps establish the variability of estimates to be expected, which is a principal aim of this effort.

1.3 Task 3. Comparison and discussion of results

As expected, substantial variation is present in the results produced in this phase and when comparared to the capacity curves and fragility functions provided by the contributors to Phase III of the project. In each of chapters 2 to 4 of this report, for each of the structures analyzed, the results are compared in terms of capacity curves. However in order to make greater sense of the differences obtained, a summative and in-depth discussion is included in chapter 5 of this report. Some critical modeling solutions are reviewed in terms of their effect on the results; for the concrete structures these relate to concrete confinement (type and spacing of shear links), plastic hinge limits, shear failure considerations, and simulation of the effects of the infill. For the masonry structures the effects of window lay-out in determining the size of the piers, of connections of the analyzed façade with the side walls, and of gravitational loads are analyzed with respect to the type of mechanism triggered and the level of lateral acceleration capacity obtained.Secondly, as can be seen from Table 1.2, many of the index buildings chosen belong to the same PAGER typology. Results are compared to understand regional differences vis-à-vis construction practice and code requirements.Finally results obtained are compared in terms of capacity curve characteristic points, ductility, displacement at collapse and value of parameters used to derive the fragility functions. These will be compared with the equivalent parameters used in HAZUS.

1.4 Report structure and content

The present report contains the results of the modeling conducted by Kappos et al. (AUTh) and Crowley et al. (ROSE) on concrete typologies, and D'Ayala et al. (UBATH) on masonry typologies. Details of each approach methodology and results are contained in sections 2, 3, and 4 respectively of this report. Each section outlines the methodology underlying the procedure used by each modeler, the results obtained, a comparison in terms of capacity curves, and the methodology used to derive the fragility curves, as well as the results obtained for the fragility curves. In Section 5 of the report the outcomes of the comparison of the analyses conducted and presented in the previous chapters are summarized and further discussed. As it can be seen from Table 1.2, many of the index buildings chosen belong to the same PAGER typology. Results are hence compared to understand the influence of the analytical approach used on the vulnerability assessment of a given structure as well as regional differences vis-à-vis construction practice and code requirements.

1.5 Executive summary and conclusions

This report presents capacity curves and fragility curves for concrete and masonry buildings that do not comply with the HAZUS typologies, either because they are not designed to code standards or because the construction details substantially differ from U.S. code provisions. The main difference with respect to the HAZUS typologies is the ductility ratio at the level of the element and at the global level. Four main concrete typologies are studied: bare frames designed according to seismic code requirements (C1), bare frames designed only for gravitational loads or very low seismic capacity but without ductility detailing provisions (C4), infilled frames designed according to seismic code requirements (C1-I), infilled frames designed only for gravitational loads or very

low seismic capacity but without ductility detailing provisions (C3). For each of the infilled frame typologies the case of irregularity of the infill in elevation, i.e. lack of infill at the ground floor, has also been considered. For masonry, adobe (A), stone (S), unreinforced fired brick (UFB) and unreinforced concrete block (UCB) masonry have been considered. For each of the main typologies some different sub-typologies have been considered, either dependent on the masonry fabric, rubble and dressed stone, or on the type of horizontal structures, timber or concrete floors. The typologies are representative of different regions of the world: the concrete frames studied represent buildings from India, Italy, Greece and Turkey; the masonry typologies represent buildings from Turkey.

Three different procedures have been used to analyze data provided by other research teams, which had already contributed analytical capacity curves to the PAGER model in Phase III of the WHE-PAGER project. For the concrete buildings two procedures were used: a simplified procedure called DBELA was used to produce capacity curves for buildings in Italy, Greece, Turkey, with and without infill; and a more sophisticated procedure relying on non-linear pushover analysis by f.e. modeling (AUTh procedure) was also used to analyze the same set of building as above, plus buildings from India with regular and irregular plan and elevation. For the masonry buildings only one procedure called FaMIVE was used, based on limit state analysis and collapse mechanism identification.

For each typology a capacity has been defined and compared with the capacity curve obtained by the team that analyzed it in Phase III of the WHE-PAGER project. The comparison is carried out in terms of the yield limit point (Dy, Ay) and ultimate point (Du, Au) that define the bilinear capacity curve, and the natural period. Comparisons are aimed at identifying differences between different computational approaches and regional differences for the same typologies, due to either code requirement or typical construction practices.

Results indicate that:

- For the concrete frames, the comparison between IITG and AUTh procedures lead to differences for Dy in the range of 14 to 58%, for a regular frame, while are 2 or 3 orders of magnitude higher for the irregular frames, indicating that the SAP program is not suitable for the analysis of this type of building. For Du, differences are greater ranging between 45% and 145%, further proving the limitation of SAP in defining the post yielding behavior.
- For the concrete frames, comparison between the DBELA and AUTh procedures, leads to differences for Dy in the range of 32% to 68%, for the Italian index buildings and in the range of 17% to 88% for the Greek index buildings. In almost all cases the AUTh procedure resulted in smaller displacements, i.e. stiffer structures. For Du, differences are in the range of 7% to 126% for the Italian index frames and of 12% to 96% for the Greek index frames. It should be noted that agreement improves consistently for infilled frames of low and medium rise where differences are between 6% and 13%.
- For the masonry typologies, comparison between the METU procedure and FaMIVE leads to differences for Dy in the range of -4.7% and 80%, while for Du differences are in the range of 0.76% to 77%. The best agreement is obtained for unreinforced brickwork with RC slabs (UFB5) and for unreinforced concrete block masonry, as in both cases the prevalent behavior is in plane-failure. For massive stone and unreinforced brickwork with mud mortar and light timber floors, with a prevalent out-of-plane behavior the differences are greater. All considered the agreement is quite good.

- For the concrete frames typologies analyzed in this study, it appears that shear failure was not an issue, notwithstanding the coupling with stiff and strong infill as in the case of the Indian irregular index building.
- For the regular Indian index frames the Infill strength affected both displacement and strength capacity of both yielding and ultimate performance points. However a variation in infill strength of 74% resulted in variations of 30% in ultimate displacement and 42% in ultimate capacity.
- Confinement of the concrete was also investigated, affecting particularly the ultimate displacement of the bare and soft story frames. The reduction in ultimate displacement for both cases with open stirrups is of the order of 90%.
- For the masonry buildings connection with orthogonal walls is the major factor in determining collapse mechanisms and collapse load multipliers, hence this is the most important parameter for the definition of capacity curves in masonry structures. Spanning of the floor is also a relevant parameter, has the gravity load surcharge provided by the floor structure and its restraining action on the walls, affect both mechanisms and collapse load multipliers.
- In masonry buildings the number of stories affects the overall stiffness and the drift limits at ultimate and collapse state hence different capacity curves for different number of stories should be derived.

Comparison of capacity curves obtained from this work with capacity curves contained in the HAZUS database show that in the case of concrete frames which do not have seismic provisions or that are designed with low code provisions, the HAZUS model underestimates the displacement both at yielding and at ultimate and the ultimate strength capacity for both bare and infilled frames, irrespective of the procedure chosen for the analysis. For masonry structures the results are less clear as in some cases the HAZUS curve for unreinforced masonry is in relatively good agreement with the results obtained by this study, and in some cases it overestimates substantially both displacement and capacity. This is principally the case for adobe and stone masonry, which, as already highlighted, behave differently from the assumption of in-plane failure. Hence it is necessary to derive more realistic capacity curves for different regions using the analytical approach to be implemented in PAGER. New capacity curves should be derived for adobe and stone masonry as the HAZUS curves are not at all representative.

2. Application of DBELA Methodology to Reinforced Concrete Frames from Greece, India, Turkey

Helen Crowley, Miriam Colombi and Vitor Silva

2.1 Introduction

Capacity curves of frames can be produced using a number of software packages, which include nonlinear analysis (either through plastic hinge modeling or fiber element analysis). However, this requires a large amount of data on the buildings (e.g. detailing of sections, nonlinear properties of the concrete and steel, mass distribution), the variability of which is often not available for a class of buildings. If a single building is chosen to represent a certain building class to reduce computation time (e.g. mid-rise non-ductile reinforced concrete buildings with masonry infill panels), the resulting capacity curve might not actually represent the median capacity curve of that class of buildings.

The aim of this chapter is to present a simplified method for generating median capacity and fragility functions when only a limited amount of information on the buildings is available; it is not proposed that this method should be used in the case that detailed information is available, or when capacity curves for individual buildings are to be derived. The methodology considers only flexural behavior, and requires further calibration to model shear failure. The capacity curves resulting from the simplified method (which take seconds to calculate) are compared with those from more robust nonlinear analyses for a number of frames to understand how different the predictions of global behavior are. For a given building class, populations of buildings are generated using Monte Carlo simulation to identify the median capacity curves (which are compared with the capacity curves of the single buildings originally considered), and then associated fragility functions (for use with the equivalent linearization approach of FEMA440) are derived. These fragility functions explicitly include the uncertainty in the capacity, to which an estimation of the uncertainty in the response needs to be added.

2.2 Summary of DBELA Approach Methodology

The formulae that have been used to produce simplified capacity curves for both beam-sway (i.e. strong column/weak beam) and column-sway (i.e. weak column/strong beam) mechanisms for three different limit states to damage are summarized in the following section. Different equations have been used for bare frame and infilled frame structures. The following has the objective of presenting the formulae used in the capacity curve calculation, rather than the theory behind the methodology; the reader is referred to Crowley *et al.* [2004] and Bal *et al*. [2010] for more detailed information on the methodology presented herein.

Structures are modeled as SDOF equivalent systems with a given mechanism in DBELA, and the displacement capacity of the equivalent system is calculated as a function of the sectional strains in the plastic hinges of the mechanism. The sectional limit states to damage used herein relate to the levels of strain in the materials, and are different according to the building construction code. The studied structures are divided between those that do not have adequate confinement and are thus treated as non-ductile, and those that are well-confined and thus have ductile behavior. Crowley *et al.* [2004] have suggested the use of limit state strains for both inadequately and adequately confined members; the former have been updated using the work of Bal [2008]. The first limit state (LS1) relates to yield of the structure, the second limit state (LS2) refers to the point

beyond which significant damage is experienced, and the third limit state (LS3) refers to the point beyond which the structure collapses. The post-yield sectional limit state strains considered in this evaluation are described in the following table, where ε_c denotes the strain in the concrete and ε_s denotes the strain in the steel.

Table 2.1 Values of the post-yield sectional limit state strains for reinforced concrete buildings

	Non-ductile		Ductile	
LS2 strains	$\varepsilon_{C(LS2)} = 0.0035$	$\varepsilon_{S(LS2)} = 0.015$	$\varepsilon_{C(LS2)} = 0.0035$	$\varepsilon_{S(LS2)} = 0.015$
LS3 strains	$\varepsilon_{C(LS3)} = 0.0075$	$\varepsilon_{S(LS3)} = 0.035$	$\varepsilon_{C(LS3)} = 0.015$	$\varepsilon_{S(LS3)} = 0.05$

The frames are transformed from MDOF structures to SDOF equivalent systems, with an effective height. The effective height coefficient ef_h (that is multiplied by the height) is different according to the response mechanism (either beam-sway or column-sway as mentioned previously) [Glaister and Pinho, 2003]. For what concerns the beam-sway mechanism, the effective height is independent of the ductility and depends on the number of stories *n* as described in the following equations:

$$ef_h = 0.64 \qquad n \le 4 \qquad \textbf{(2.1)}$$

$$ef_h = 0.64 - 0.0125\,(n-4) \qquad 4 < n < 20 \qquad \textbf{(2.2)}$$

$$ef_h = 0.44 \qquad n \ge 20 \qquad \textbf{(2.3)}$$

With regards to the column-sway mechanism, the effective height depends on the ductility. However, the ductility cannot be calculated unless the yield displacement at the effective height is known and thus an iterative procedure should be carried out to find the effective height. Glaister and Pinho [2003] proposed the following equation for the sake of simplicity:

$$ef_h = 0.67 - 0.17\frac{\varepsilon_{S(Lsi)} - \varepsilon_y}{\varepsilon_{S(Lsi)}} \qquad \textbf{(2.4)}$$

The ductility is also considered according to the sway mechanism. In the following equations, the ductility for beam-sway and column-sway mechanism are shown respectively:

$$\mu_{LSi} = 1 + \frac{\left(\varepsilon_{C\,(LSi)} + \varepsilon_{S(LSi)} - 1.7\varepsilon_y\right)h_b}{\varepsilon y \cdot l_b} \qquad \textbf{(2.5)}$$

$$\mu_{LSi} = 1 + \frac{\left(\varepsilon_{C(LSi)} + \varepsilon_{S(LSi)} - 2.14\varepsilon_y\right)h_c}{0.86 \cdot ef_h \cdot H_T \cdot \varepsilon_y} \qquad \textbf{(2.6)}$$

where:

- $\varepsilon_{C(LSi)}$ and $\varepsilon_{S(LSi)}$ are sectional limit state strains for reinforced concrete buildings (see Table 2.1);
- ε_y is the yield strain of the reinforcement steel;
- h_b is the depth of the beam;
- l_b is the length of the beam;
- h_c is the depth of the column;
- ef_h is the effective height;
- H_T is the total height of the building.

To estimate the probable response mechanism of a structure, a stiffness-based (or deformation-based) sway index is used. The probability of having a column sway mechanism increases with the increasing beam section depth, with the decreasing column section depth, with the increasing

column length (story height) and with the decreasing beam length. The value of the index for i^{th} joint for a certain floor is:

$$R_i = \frac{\frac{h_{b,L}}{L_{b,L}} + \frac{h_{b,R}}{L_{b,R}}}{2\left(\frac{h_{c,B}}{L_{c,B}}\right)} \quad \textbf{(2.7)}$$

where sub-indices 'L', 'R' and 'B' refer to 'Left', 'Right', and 'Below' respectively. The index per floor could then be obtained by averaging the result of (2.7) for each floor:

$$S_{def,j} = \frac{\sum_{i=1}^{n} R_{i,j}}{n} \quad \textbf{(2.8)}$$

where n is the total number of joints at floor j. The maximum value of the index between floors is the value that represents the structure. In the following table the limits of the index for different building types are shown (Abo El Ezz, 2008; Shah, 2009):

Table 2.2 Limits of the deformation-based sway index for different building types

	Beam Sway mechanism	Column Sway mechanism
Bare Frame structure	$R_i \leq 1.5$	$R_i > 1.5$
Fully Infilled Frame structure	$R_i \leq 1$	$R_i > 1$
Infilled soft story layout Frame structure	$R_i \leq 0.5$	$R_i > 0.5$

Shear failure is not considered in the calculation of the limit state displacements in DBELA, though it is recognized that it should be considered.

2.2.1 Bare Frame

The structural yield and post-yield period-height equations are represented by the following formula. They are valid both for beam-sway and column-sway mechanisms. It is worth noting that the coefficients of these empirical formulae are different according to the design level in terms of expected base shear. In fact, a newer building that has been designed to higher levels of base shear and with capacity design principles has deeper members, and is thus stiffer than an older one, and its period is lower.

Low Base Shear	High Base Shear	
$T_y = 0.1H_T$	$T_y = 0.07H$	**(2.9)**
$T_{LSi} = T_y\sqrt{\mu_{LSi}}$	$T_{LSi} = T_y\sqrt{\mu_{LSi}}$	**(2.10)**

Beam-Sway mechanism

The structural yield displacement capacity and the structural post-yield displacement capacity (see Figure 2.1) are shown in the following equations respectively:

$$\Delta S_y = 0.5 \cdot ef_h \cdot H_T \cdot \varepsilon_y \cdot \frac{l_b}{h_b} \quad \textbf{(2.11)}$$

$$\Delta S_{LSi} = \Delta S_y + 0.5 \cdot \left(\varepsilon_{C(LSi)} + \varepsilon_{S(LSi)} - 1.7\varepsilon_y\right) ef_h \cdot H_T \quad \textbf{(2.12)}$$

Column-Sway mechanism

The structural yield displacement capacity and the structural post-yield displacement capacity (see Figure 2.1) are shown in the following equations respectively:

$$\Delta S_y = 0.43 \cdot ef_h \cdot H_T \cdot \varepsilon_y \cdot \frac{h_{s1}}{h_c} \quad \textbf{(2.13)}$$

$$\Delta S_{LSi} = 0.43 \cdot ef_h \cdot H_T \cdot \varepsilon_y \cdot \frac{h_{s1}}{h_c} + 0.5 \cdot \left(\varepsilon_{C(LSi)} + \varepsilon_{S(LSi)} - 2.14\varepsilon_y\right) h_{s2} \quad \textbf{(2.14)}$$

where h_{s1} is the average of the inter story height of the building and h_{s2} is the height of the ground floor story.

The base shear force divided by the seismic weight represents the collapse multiplier λ. It can be calculated directly from the displacement capacity (Δ_y) and the period of vibration at yield (T_y) using the following formula. The base shear force divided by the seismic mass of the building (F/m) is then simply computed multiplying the collapse multiplier by g.

$$\lambda = \frac{4 \cdot \pi^2 \cdot \Delta_y}{T_y^{\,2} \cdot g} \quad \textbf{(2.15)}$$

In figure 2.1 a simplified capacity curve for a bare frame structure is shown.

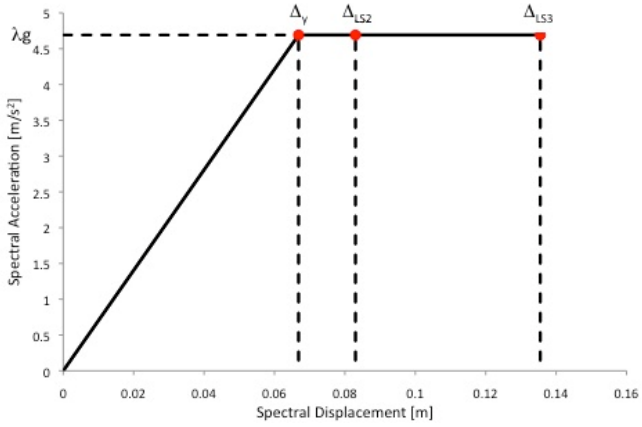

Figure 2.1 Simplified capacity curve for a bare frame structure; the three displacement capacities (one yield and two post-yield) are shown on the curve

2.2.2 Fully infilled Frame

Structures with infill panels are assumed to have a much higher initial stiffness, and thus the formula for the initial period of vibration is modified. The displacement at which yielding is initiated in the structural members has been found from nonlinear analyses of a number of RC frames with infills to be lower than that of frames without infills, and thus the yield displacement is corrected with factors that have been calibrated using the aforementioned analyses. The infill panels are assumed to have failed by the time the significant damage limit state is reached in the structures and thus the structure is assumed to behave as a bare frame for the second and third limit states, and thus the bare frame equations are used. The structural yield and post-yield period-height equations are represented by equation 2.16 and 2.17. They are valid both for beam-sway and column-sway mechanisms. As it is possible to notice, the value of the period is lower and

the initial stiffness of the building is higher than for bare frames (see Figure 2.2). These values have been estimated assuming the infill panel thickness between 0.1 and 0.25 meters. As for the bare frame buildings, the values of these empirical formulae are different according to the design level. It has to be mentioned that the ratio between the formulae for low base shear and high base shear buildings that can be estimated from the bare frame case has also been applied for the fully infilled frame case.

Low Base Shear	High Base Shear	
$T_y = 0.06H_T$	$T_y = 0.048H$	**(2.16)**
$T_{LSi} = T_y\sqrt{\mu_{LSi}}$	$T_{LSi} = T_y\sqrt{\mu_{LSi}}$	**(2.17)**

Beam-Sway mechanism

The structural yield displacement capacity and the structural post-yield displacement capacity are shown in the following equations respectively:

$$\Delta S_y = 0.5 \cdot ef_h \cdot H_T \cdot \varepsilon_y \cdot \frac{l_b}{h_b} \cdot \beta_1 \quad \textbf{(2.18)}$$

$$\Delta S_{LSi} = \Delta S_y + 0.5 \cdot \left(\varepsilon_{C(LSi)} + \varepsilon_{S(LSi)} - 1.7\varepsilon_y\right) ef_h \cdot H_T \cdot \beta_2 \quad \textbf{(2.19)}$$

Column-Sway mechanism

The structural yield displacement capacity and the structural post-yield displacement capacity are shown in the following equations respectively:

$$\Delta S_y = 0.43 \cdot ef_h \cdot H_T \cdot \varepsilon_y \cdot \frac{h_{s1}}{h_c} \cdot \beta_1 \quad \textbf{(2.20)}$$

$$\Delta S_{LSi} = 0.43 \cdot ef_h \cdot H_T \cdot \varepsilon_y \cdot \frac{h_{s1}}{h_c} \cdot \beta_1 + 0.5 \cdot \left(\varepsilon_{C(LSi)} + \varepsilon_{S(LSi)} - 2.14\varepsilon_y\right) h_{s2} \cdot \beta_2 \quad \textbf{(2.21)}$$

where h_{s1} is the average of the inter story height of the building and h_{s2} is the height of the ground floor story.

Both in beam-sway and in column-sway mechanisms, a β parameter is added to the formulae to account for the influence of the infill panels. This parameter slightly decreases the displacement capacity. In the following table the tentative β values suggested by Bal [2008] are shown.

Table 2.3 Tentative β values suggested for the infilled frame structures

Infilled Case	β (*mean*)		
	LS1 (β_1)	LS2 (β_2)	LS3 (β_3)
Bare Frame	1	1	1
Infilled frames	0.52	0.46	0.28

For what concerns the collapse multiplier λ_1, it can be calculated with (2.15). As shown in Figure 2.2, the shape of the simplified capacity curve for infilled frame structures is different from the bare frame capacity curve and a second collapse multiplier λ_2 has to be computed. We can use a proxy for λ_2, which is the value of the bare frame collapse multiplier (as it represents the strength after the infill panels have collapsed).

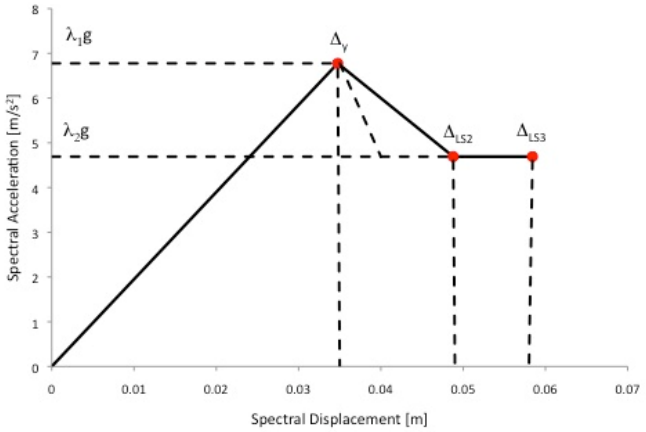

Figure 2.2 Simplified capacity curve for an infilled frame structure.

2.3 Input data and results

As mentioned before, three different sets of data are studied and the corresponding capacity curves are computed. In the following section the input data and results of these analyses are shown.

2.3.1 Data and results for index frames from Greece (provided by AUTH)

In the following table the data required by the DBELA methodology to estimate the capacity curves for the Greek buildings considered in PAGER-WHE Phase III are shown. Note: the reinforcing yield strength is converted to yield strain by assuming a Young's Modulus of 210,000 MPa.

Table 2.4 Data required by DBELA to compute capacity curves

PAGER STRUCTURE TYPOLOGY	Reinforcing steel yield strength [MPa]	Inter-story height [m]		Average beam dimensions in main direction [m]		Average ground floor column depth in main direction [m]
	Long.	upper floors	ground floor	Length	Depth	
C4L (RC1LL)	462	3	4.5	6	0.7	0.28
C3L (RC3.1LL)	462	3	4.5	6	0.7	0.28
C3L-SS* (RC3.2LL)	462	3	4.5	6	0.7	0.28
C4M (RC1ML)	462	3	4.5	6	0.7	0.4
C3M (RC3.1ML)	462	3	4.5	6	0.7	0.4
C3M-SS (RC3.2ML)	462	3	4.5	6	0.7	0.4
C4H (RC1HL)	462	3	4.5	6	0.75	0.6
C3H (RC3.1HL)	462	3	4.5	6	0.75	0.6
C3H- SS (RC3.2HL0	462	3	4.5	6	0.75	0.6
C1L (RC1LH)	440	3	4.5	5.3	0.5	0.35
C1L-I** (RC3.1LH)	440	3	4.5	5.3	0.5	0.35
C1L-SS (RC3.2LH)	440	3	4.5	5.3	0.5	0.35
C1M (RC1MH)	440	3	4.5	5.3	0.55	0.4
C1M-I (RC3.1MH)	440	3	4.5	5.3	0.55	0.4
C1M–SS (RC3.2MH)	440	3	4.5	5.3	0.55	0.4
C1H (RC1HH)	440	3	4.5	5.3	0.57	0.46
C1H-I (RC3.1HH)	440	3	4.5	5.3	0.57	0.46
C1H-SS (RC3.2HH)	440	3	4.5	5.3	0.57	0.46

** SS indicates soft story layout for buildings in classes C1 and C3 with infill; ** I indicates structurally active infills in buildings in classes C1 as per discussion in section 1.1. of this report.*

It is possible to divide these structures into three classes: bare frame, infilled frame and infilled frame with soft story layout. For the purpose of this report, the bare frame and the infilled frame have been studied using the formulae described in Section 2.2. For each structure, the deformation-based sway index is calculated and the mechanism is estimated accordingly. In Table 2.5 and 2.6 the results are shown. It is worth noting that, due to the fact that the thickness of the infill panels is about 0.1 meter, we are likely over predicting the stiffness.

Bare Frame Structures

The bare frame structures studied herein are low, medium, and high rise reinforced concrete structures. The structures are non-ductile with low base shear and ductile with high base shear. The values of the structural yield displacement capacity and the structural post-yield displacement capacity with the values of the collapse multiplier λ and the corresponding base shear force divided by the seismic mass of the building (F/m) are shown in Table 2.5. The value of the sway index and the mechanism types of the buildings are also presented.

Table 2.5 Capacity curve parameters for bare frame structure: Greek data

Structure	Sway index R_i	Mechanism	Δ_{sy} [m]	Δ_{SLS2} [m]	Δ_{SLS3} [m]	λ [-]	F_y/m [m/s^2]
C4L (RC1LL)	1.9	Column Sway	0.080	0.094	0.146	0.574	5.63
C4M (RC1ML)	1.3	Beam Sway	0.086	0.148	0.252	0.189	1.853
C4H (RC1HL)	0.9	Beam Sway	0.152	0.272	0.470	0.075	0.739
C1L (RC1LH)	1.2	Beam Sway	0.039	0.075	0.186	0.573	5.611
C1M (RC1MH)	1.2	Beam Sway	0.064	0.128	0.329	0.289	2.834
C1H (RC1HH)	1.0	Beam Sway	0.118	0.239	0.622	0.119	1.169

Infilled Frame Structures

The infilled frame structures studied herein are low, medium, and high rise reinforced concrete structures. The structures are non-ductile with low base shear and ductile with high base shear. The values of the structural yield displacement capacity and the structural post-yield displacement capacity with the values of the collapse multipliers λ_1 and λ_2 and the corresponding base shear force divided by the seismic mass of the building (F/m) are shown in the Table 2.6. The value of the sway index and the mechanism types of the buildings are also presented.

Table 2.6 Capacity curve parameters for infilled frame structure: Greek data

Structure	Sway index R_i	Mechanism	Δ_{sy} [m]	Δ_{SLS2} [m]	Δ_{SLS3} [m]	λ_1 [-]	λ_2 [-]	F_y/m [m/s^2]	F_2/m [m/s^2]
C3L (RC3.1LL)	1.9	Column Sway	0.042	0.047	0.055	0.829	0.478	8.132	4.692
C3M (RC3.1ML)	1.3	Column Sway	0.053	0.055	0.064	0.242	0.167	3.163	1.642
C3H (RC3.1HL)	0.9	Beam Sway	0.079	0.134	0.168	0.109	0.075	1.068	0.739
C1L-I (RC3.1LH)	1.2	Column Sway	0.032	0.039	0.062	0.987	0.455	9.681	4.468
C1M-I (RC3.1MH)	1.2	Column Sway	0.050	0.053	0.076	0.450	0.199	4.706	1.955
C1H-I (RC3.1HH)	1.0	Column Sway	0.092	0.092	0.108	0.198	0.077	1.938	0.756

2.3.2 *Input data and results for index frames from Italy (provided by EUCENTRE)*

In the following table the data needed by DBELA to estimate the capacity curves are shown.

Table 2.7 Data required by DBELA to compute capacity curves

Id Structure	Yield strain of the reinforcement steel [-]	Inter-story height [m]		Average beam dimensions in main direction [m]		Average ground floor column depth in main direction [m]
	Long.	upper floors	ground floor	Length	Depth	
C4M (RC _PC_x)	0.002	3	3	6	0.32	0.31
C4M (RC_PC_y)	0.002	3	3	5	0.32	0.43
C4M RC_5%_x	0.002	3	3	6	0.34	0.3
C4M RC_5%_y	0.002	3	3	5	0.31	0.37
C4M (RC_12.5%_x)	0.002	3	3	6	0.39	0.33
C4M (RC_12.5%_y)	0.002	3	3	5	0.34	0.45

The bare frame structures studied herein are reinforced concrete medium rise structures (4 stories), non-seismically designed, and seismically designed (but without adequate ductility and capacity design considerations) with horizontal forces corresponding to 5% (low code) and 12.5% (high code) of the weight of the structure. The values of the structural yield displacement capacity and the structural post-yield displacement capacity with the values of the collapse multiplier λ and the corresponding base shear force divided by the seismic mass of the building (F/m) are shown in Table 2.8. The value of the sway index and the mechanism types of the buildings are also presented.

Table 2.8 Capacity curve parameters: Italian data

Structure	Sway index R_i	Mechanism	Δ_{sy} [m]	Δ_{SLS2} [m]	Δ_{SLS3} [m]	λ[-]	F_y/m [m/s^2]
C4M (RC _PC_x)	0.52	Beam Sway	0,144	0,202	0,294	0,403	3,948
C4M (RC_PC_y)	0.45	Beam Sway	0,120	0,178	0,270	0,336	3,290
C4M RC_5%_x	0.57	Beam Sway	0,136	0,194	0,286	0,379	3,716
C4M RC_5%_y	0.50	Beam Sway	0,124	0,182	0,274	0,347	3,396
C4M (RC_12.5%_x)	0.59	Beam Sway	0,118	0,176	0,268	0,675	6,611
C4M (RC_12.5%_y)	0.45	Beam Sway	0,113	0,171	0,263	0,645	6,319

2.3.3 *Input Data and results for index frames from Turkey (provided by METU)*

In Table 2.9 the data needed by DBELA to estimate the capacity curves are shown. Gulkan and Yakut provided the following data that have been used in the analyses:

- Height of the building. Average value: 10.6 m;
- Ground floor height. Average value: 3.1 m.

For consideration of other values needed to calculate the capacity curves, they can be found in Bal et al. (2007). Due to the fact that the exact number of stories is not known, it is not possible to estimate the inter story height of the upper floor. This latter value is essential to compute the displacement capacity in case of a column-sway mechanism. To have a column-sway mechanism,

an inter story height of the upper floor of 3.8 m is necessary, which is unlikely to be the case. For this reason it is assumed that the mechanism will be beam-sway.

Table 2.9 Data required by DBELA to compute capacity curves

Structure	Reinforcing steel yield strength [MPa]	Ground floor height [m]	Average beam dimensions in main direction [m]		Average ground floor column depth in main direction [m]
	Long.		Length	Depth	
C4M	371.13	3.1	3.37	0.6	0.45

The bare frame structures studied herein are reinforced concrete mid-rise structures. The values of the structural yield displacement capacity and the structural post-yield displacement capacity with the values of the collapse multiplier λ and the corresponding base shear force divided by the seismic mass of the building (F/m) are shown in the following table.

Table 2.10 Capacity curve parameters: Turkish data

Structure	Δ_{sy} [m]	Δ_{SLS2} [m]	Δ_{SLS2} [m]	λ [-]	F_y/m [m/s^2]
C4M	0.034	0.086	0.168	0.121	1.183

2.4 Comparison of Capacity Curves

2.4.1 Comparison for index frames from Greece

In the following figures, the capacity curves estimated by AUTH as part of the PAGER-WHE III project (see Section 1.1) and the DBELA method are shown for nonductile, low base shear bare frame buildings and infilled frame buildings. For bare frame structures, it is worth noting that the initial stiffness estimated by AUTH is higher in the case of medium rise and high rise buildings and it is lower in the case of low rise building. It is also worth noting that the capacity curves for the medium rise buildings are very similar. With regards to the infilled frame structures the stiffness estimated by AUTH is always higher than the one estimated herein.

Bare Frame

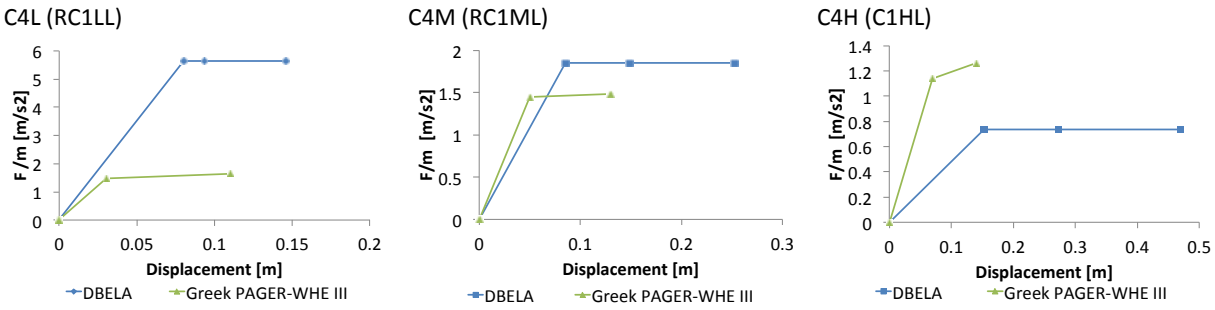

Figure 2.3 Comparison of capacity curves for Greek bare frames

Infilled Frame

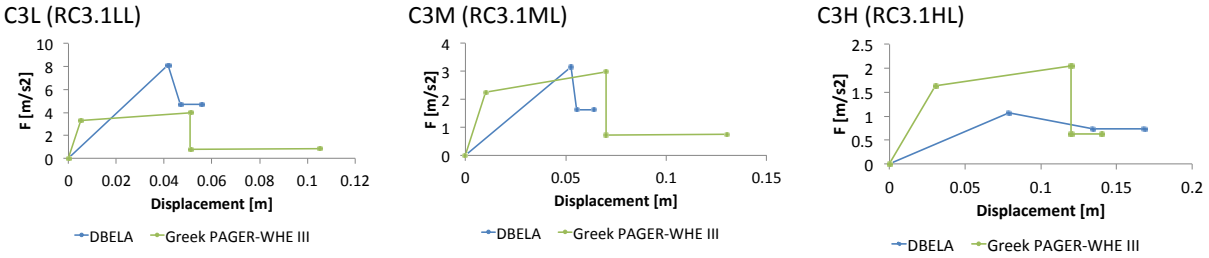

Figure 2.4 Comparison of capacity curves for Greek infilled frames

2.4.2 *Comparison for index frame from Turkey*

In the following figure, the capacity curves estimated by METU (PAGER-WHE Phase III) and those estimated herein are shown for mid-rise bare frame buildings. It is worth noting that the initial stiffness estimated by METU is higher, but nevertheless the lateral strength and ultimate displacement capacities are similar.

Bare Frame

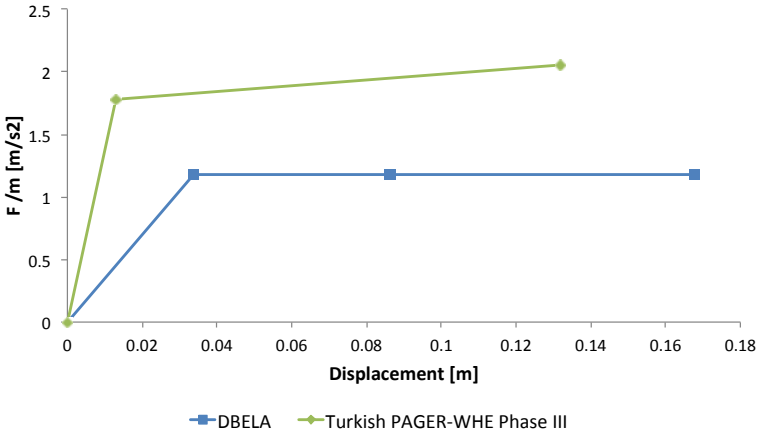

Figure 2.5 Comparison of capacity curves for Turkish frame (C4M)

2.4.1 *General conclusions on the comparisons*

The simplified capacity curves appear to estimate reasonably well the capacity of mid-rise reinforced concrete frames, but fail at adequately represent the behavior of frames with masonry infill. More comparisons and calibration for this building typology is evidently needed. However, it is also worth noting that the capacity curves produced with computer packages might also suffer from modeling errors such as those due to inappropriate material laws or hinge models (depending on whether plastic hinge or fiber element modeling are used) or due to insufficient discretization of elements and fibers (for fiber modeling). Hence the use of the DBELA method within the right context (i.e. for large populations of buildings where detailed information is not available) might still be justified.

2.5 Fragility Functions

2.5.1 Generality

Using a Monte Carlo approach, hundreds of random parameters per building typology were sampled considering the variability in the following parameters:

- Material properties:
  - Yield strain of the steel;
  - Material strains at the limit states.
- Geometric properties:
  - Ground floor height;
  - Upper floor height;
  - Beams length;
  - Beam depth;
  - Column depth;

The values reported previously were assumed to be the mean values, and the coefficient of variation and probabilistic distribution of each parameter was estimated following the study of Bal *et al*. (2007), as reported below and in Tables 2.11, 2.12 and 2.13. Only the bare frames have been considered as the capacity curves for these buildings were better estimated (as presented in the previous section). However, fragility functions for infill buildings could also be generated using the same procedure and random variables.

Table 2.11 Mean, Coefficient of variation (COV in %) and probabilistic distribution assumed for steel modulus and upper floor height

Parameter	Mean	COV (%)	Probability Distribution
Steel Modulus	210000 MPa	5	Normal
Upper floor height	3 m	8	Lognormal
Ground floor/upper floor ratio	1.5	15	Lognormal

Table 2.12 Mean, Coefficient of variation (COV in %) and probabilistic distribution assumed for yield strength and column depth

Class	Steel yield strength (MPa)			Column depth (m)		
	Mean	COV%	Prob Dist	Mean	COV %	Prob Dist
C4L (RC1LL)	462	24	normal	0.28	12	lognormal
C4M (RC1ML)	462	24	normal	0.4	12	lognormal
C4H (RC1HL)	462	24	normal	0.6	12	lognormal
C1L (RC1LH)	440	24	normal	0.35	12	lognormal
C1M (RC1MH)	440	24	normal	0.4	12	lognormal
C1H (RC1HH)	440	24	normal	0.46	12	lognormal

Table 2.13 Mean, Coefficient of variation (COV in %) and probabilistic distribution assumed for beam length and beam depth

Class	Beam length(m)			Beam depth (m)		
	Mean	COV (%)	Prob Dist	Mean/Values	COV(%)	Prob Dist
C4L (RC1LL)	6	38	gamma	0.7	16	normal
C4M (RC1ML)	6	38	gamma	0.7	16	normal

C4H (RC1HL)	6	38	gamma	0.75	16	normal
C1L (RC1LH)	5.3	38	gamma	0.5	16	normal
C1M (RC1MH)	5.3	38	gamma	0.55	16	normal
C1H (RC1HH)	5.3	38	gamma	0.57	16	normal

A few tests were carried out to understand the number of samples after which convergence in the results was obtained; it was concluded that no less than 1000 synthetic buildings should be sampled. Figure 2.6 presents the histogram of spectral displacement for each limit state for a given building class.

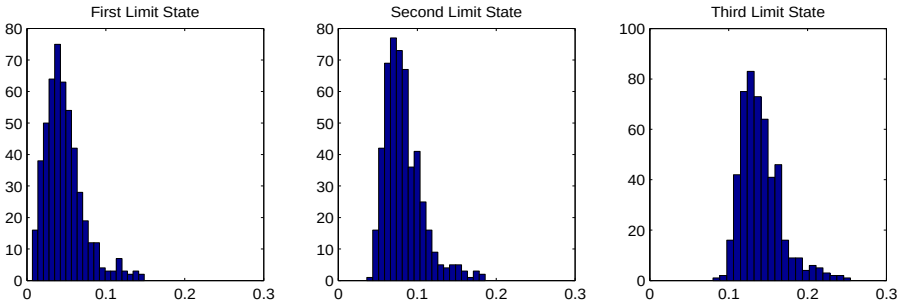

Figure 2.6 Histogram of the spectral displacement (in meters) for each limit state.

By observing the shape of the histograms and employing the maximum likelihood method, it was concluded that a cumulative lognormal distribution proved to give the best fit to the results.

2.5.2 Results

The mean and median capacity curves for each building typology were computed using the formulae presented previously and are presented below. Fragility functions were plotted based on the aforementioned statistics (thus including only the uncertainty in the capacity). Both mean and median capacity curves are provided to show the large difference in these curves. One must use the median capacity curve together with the fragility functions to estimate the damage distribution for a given scenario (by first obtaining the performance point from the median capacity curve). Often a modeler only has one or two buildings of a given typology that can be modelled, but they should not use the mean properties to obtain the representative building typology capacity curve, but instead attempt to model the distribution of the variables and find the median capacity curve.

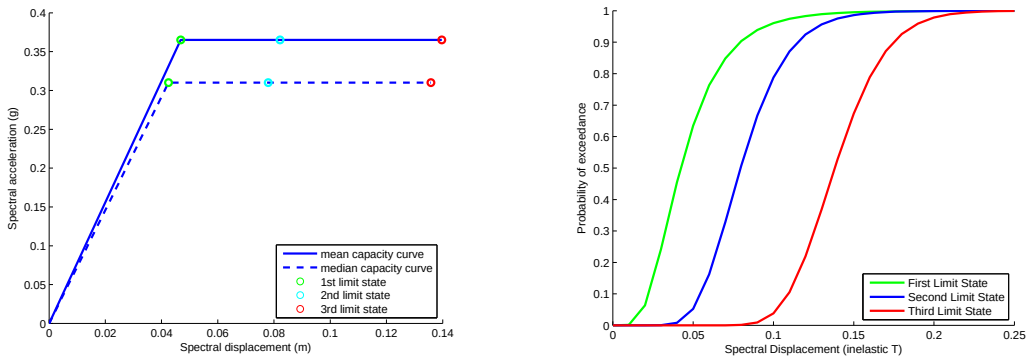

Figure 2.6 Fragility functions for Greek Frames: C4L (RC1LL)

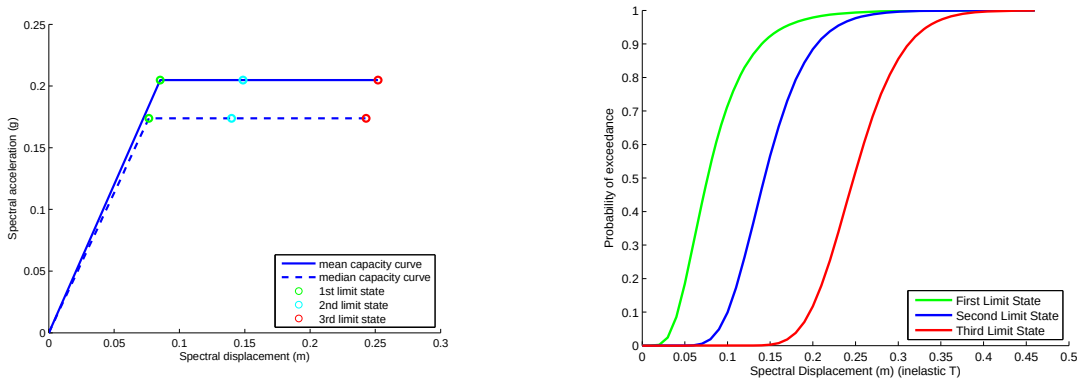

Figure 2.7 Fragility functions for Greek Frames: C4M (RC1ML)

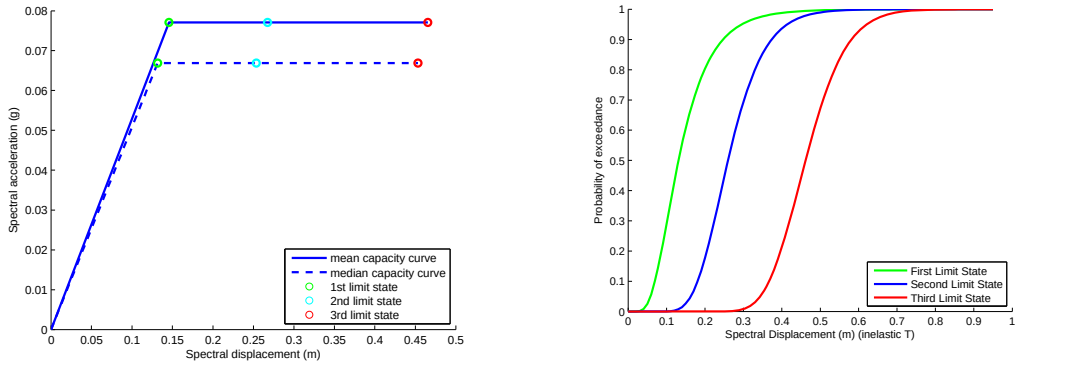

Figure 2.8 Fragility functions for Greek Frames: C4H (RC1HL)

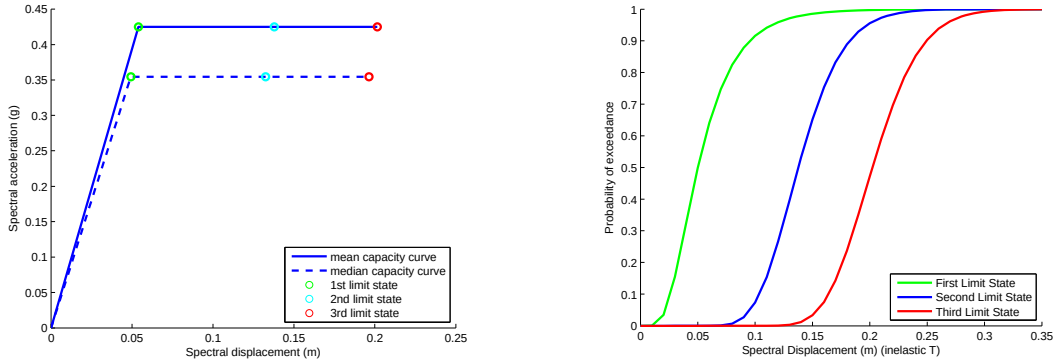

Figure 2.9 Fragility functions for Greek Frames: C1L (RC1LH)

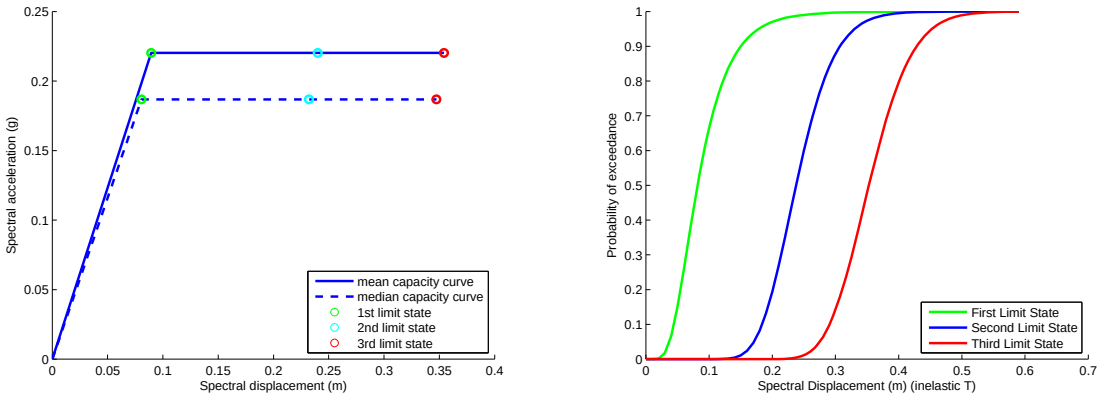

Figure 2.10 Fragility functions for Greek Frames: C1M (RC1MH)

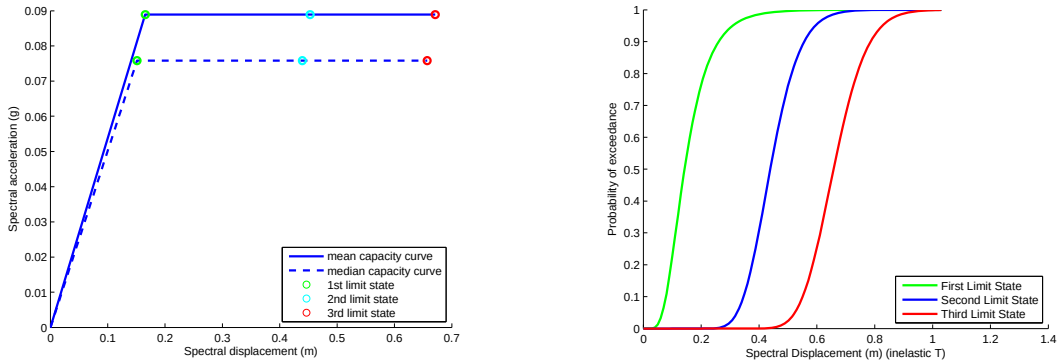

Figure 2.11 Fragility functions for Greek Frames: C1H (RC1HH)

The model uncertainty (due to the simplification of the capacity curves) is not estimated or included in the fragility functions, though this uncertainty appears to be relatively large and should be accounted for. Alternatively, capacity curves of simple, regular 2D frames (randomly generated using the statistics referred to previously) could be produced using a nonlinear analysis package such as OpenSees (which allows for batch analyses). Typical reinforcement ratios (based on code recommendations) and some simple moment distribution analyses based on gravity loads and possibly lateral loads can be used to calculate the required reinforcement. Such an approach is feasible and more robust than the use of simplified capacity curves, but it is rather computationally intensive and requires knowledge of nonlinear analysis. Hence, there may still be a place for simplified methods such as the one presented here in some situations.

The fragility functions presented previously only include the uncertainty in the capacity. To estimate the uncertainty in the response, a comparison of the nonlinear static and nonlinear dynamic response of 7 reinforced concrete non-ductile moment resisting frames has been undertaken. The frames were modeled in OpenSees, the nonlinear static response was calculated using the FEMA 440 Capacity Spectrum Method (ATC, 2005), while the nonlinear dynamic response (in terms of the displacement at the effective height) was calculated considering a large number of natural records. The logarithmic standard deviation has been calculated as approximately 0.45. This is combined with the uncertainty in the capacity (shown in the previous plots) using the SRSS.

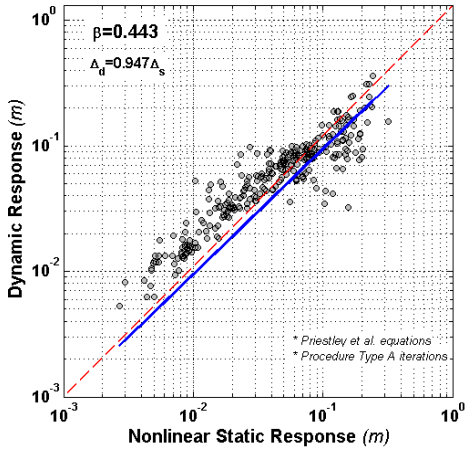

Figure 2.13 Comparison of nonlinear static response estimated with the FEMA 440 method and with nonlinear dynamic analysis for 7 reinforced concrete frames

For each of the bare frames typologies considered the median spectral displacement and the associated logarithmic standard deviation for each limit state are summarized in Table 2.14 and 2.15, when considering only the uncertainty in capacity and when considering also the uncertainty in demand respectively.

The following symbols are used to represent each parameter:

- $SD'(cm)$- median spectral displacement in cm;
- ζ- logarithmic standard deviation of the lognormal distribution.

Table 2.14 Uncertainty in capacity (as shown in Figures 2.7 to 2.12 above)

	LS1		LS2		LS3	
	SD'(cm)	ζ	SD'(cm)	ζ	SD'(cm)	ζ
C4L (RC1LL)	4.221	0.490	7.956	0.287	13.818	0.183
C4M (RC1ML)	7.645	0.473	14.320	0.279	24.786	0.180
C4H (RC1HL)	13.122	0.493	25.999	0.283	46.200	0.180
C1L (RC1LH)	5.004	0.504	13.764	0.220	20.230	0.163
C1M (RC1MH)	8.175	0.475	23.771	0.200	35.296	0.151
C1H (RC1HH)	14.256	0.470	43.889	0.184	65.777	0.139

Table 2.15 Uncertainty in capacity and response:

	LS1		LS2		LS3	
	SD'(cm)	ζ	SD'(cm)	ζ	SD'(cm)	ζ
C4L (RC1LL)	4.221	0.659	7.956	0.525	13.818	0.476
C4M (RC1ML)	7.645	0.646	14.320	0.521	24.786	0.475
C4H (RC1HL)	13.122	0.661	25.999	0.523	46.200	0.475
C1L (RC1LH)	5.004	0.669	13.764	0.492	20.230	0.469
C1M (RC1MH)	8.175	0.647	23.771	0.483	35.296	0.465
C1H (RC1HH)	14.256	0.644	43.889	0.477	65.777	0.461

2.5.3 Comparison with other fragility functions

It is noted that the fragility functions presented above need to be used in conjunction with the median capacity curves (within the framework of the Capacity Spectrum Method), hence comparisons should be made in terms of the losses that are estimated for a given scenario, or in terms of loss exceedance curves. Otherwise, a comparison on just the magnitude of the logarithmic standard deviation in the fragility functions could be made, provided that the same sources of uncertainty are being accounted for.

3. Application of the AUTh Methodology to Reinforced Concrete buildings from India and Italy

A.J. Kappos, G. Panagopoulos, P. Antoniadis

3.1 Introduction

The main goal of Phase IV of the WHE PAGER project is to compare the capacity curves estimated using different models by different researchers worldwide. The sharing of exposure data (building typology, geometry, etc.) will allow researchers to implement their own models to evaluate the capacity of the buildings. As a further goal, fragility curves are derived on the basis of the aforementioned capacity curves and expressing damage states in terms of spectral displacements. The Aristotle University of Thessaloniki (AUTh), Dept of Civil Engineering method, briefly described in Section 3.2 of this report and in more detail in Kappos et al. (2006) and Kappos & Panagopoulos (2010), has been applied to a number of structures representative of typologies that correspond to Indian and Italian reinforced concrete (R/C) buildings, data for which were provided by WHE PAGER colleagues (H. Crowley, H.B. Kaushik). In Section 3.3 of the report the structures are described and grouped according to the researcher that ran his/her model to evaluate the capacity curves. Results derived using the AUTh procedures are presented in Section 3.3 following the description of the structures, while in Section 3.4 some comparisons of the curves derived using different methodologies are shown and briefly discussed. Finally, in Section 3.5, S_d-based fragility curves are derived for all the foregoing typologies.

The specific procedure used herein by the AUTh team is based on the inelastic static (pushover) analysis of the structures and has been previously used for both R/C and URM buildings (Penelis et al. 2003; Kappos et al. 2006). It is one of the two procedures (the other one is inelastic dynamic analysis) that can be used in the analytical part of the 'hybrid' approach (which combines analysis results with empirical data); the procedure can be applied to any R/C building typology, provided that information concerning the geometry of typical structures, material properties and the reinforcement of critical sections is available. The present analysis involves mainly two-dimensional models of the structures in order to maintain the computational cost within reasonable limits, but a case-study involving a more realistic 3D model is also presented in Section 3.3.

3.2 Methodology

3.2.1 Inelastic analysis procedure

To keep the computational cost of vulnerability analysis within reasonable limits and ensure the stability of inelastic analyses at very high seismic motion levels, taking into account the drop in strength of structural elements, the AUTh general approach consisted in analyzing 2D models of structures, with some supplementary 3D analyses described in Section 3.3. R/C members were modeled using lumped plasticity beam-column elements, while infill walls were modeled using the diagonal strut element (see Section 3.2). Cracked sections for R/C members have been taken into account using 40% of the gross flexural rigidity (EI_g) for beams, 60% for external, and 80% for internal, columns (in compression).

Moment – curvature as well as moment – rotation quantities for all plastic hinges have been derived using an in-house developed software (RCCOLA.NET, Figure 3.1), based on the popular RCCOLA application developed initially at UC Berkeley (Mahin et al. 1977), later extended by Kappos (1993). Mean material properties have been utilized, adopting the Kappos (1991) and the Park & Sampson (1972) constitutive laws for confined concrete and reinforcement steel, respectively. The ultimate deformation ε_{cu}, and consequently the ultimate curvature ϕ_u, is conservatively taken as the one that corresponds to the first of the following criteria:

- Drop in concrete stress at the level of $0.85f_c$ along the descending branch of the concrete stress-strain diagram (Figure 3.2)
- First hoop fracture
- Buckling of longitudinal bars

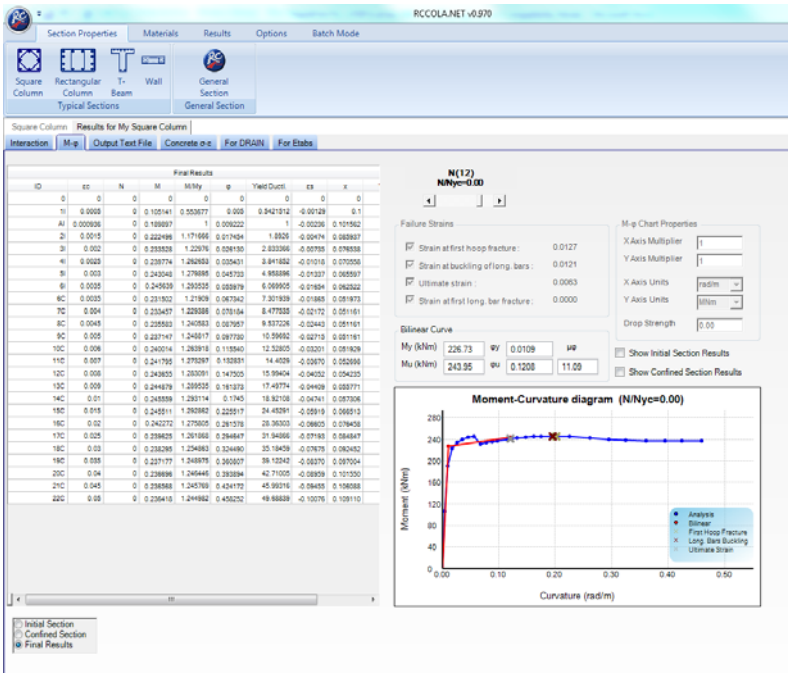

Figure 3.1 Screenshot of the RCCOLA.NET application

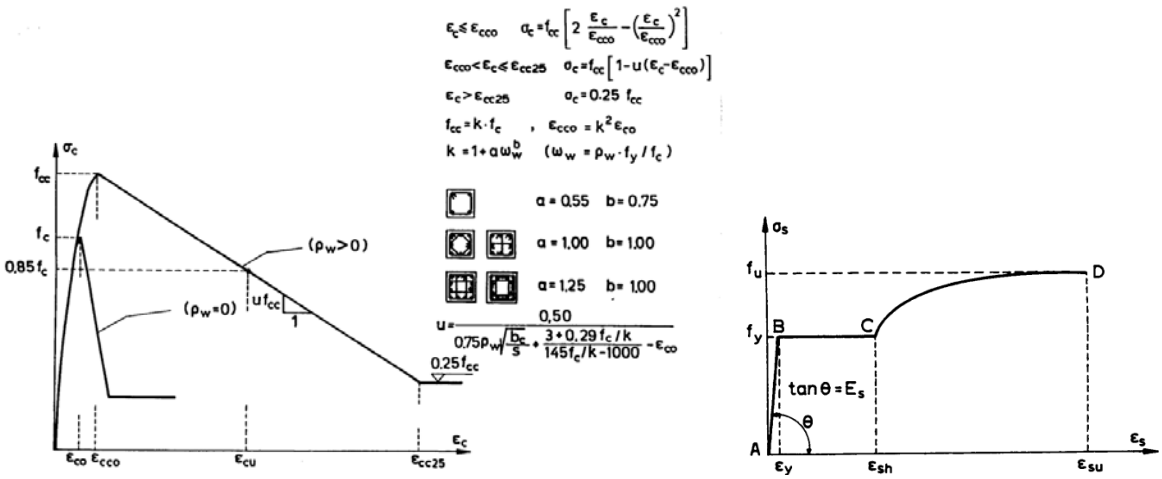

Figure 3.2 Constitutive law for confined concrete (Kappos 1991, left) and steel (Park & Sampson 1972, right)

A bilinear approximation of the derived moment curvature diagram is made adopting the common equal energy absorption (equal areas) rule (see Section 3.2.2). The derived yield (ϕ_y) and ultimate (ϕ_u) curvatures are used to estimate the plastic rotation using equation 3.1.

$$\theta_p = (\varphi_u - \varphi_y)\cdot l_p \quad \theta_p = (\varphi_u - \varphi_y)\cdot l_p \qquad \textbf{(0.22)}$$

The plastic hinge length (l_p) is estimated from the expression (Paulay and Priestley, 1992)

$$l_p = 0.08\cdot l_0 + 0.022\cdot f_{yd}\cdot d_b \qquad \textbf{(0.23)}$$

where

l_0 the length between the maximum moment point and the point where M=0 (≈0.5l for seismic loading)
f_y the steel yield strength
d_b the diameter of longitudinal reinforcement.

Typical moment – rotation diagrams that correspond to the 1st story structural elements of the Italian structures (RC_5%) are presented in Figures 3.3 and 3.4 for beams and columns, respectively, as implemented in Etabs (or SAP2000). A residual rotation of $5\cdot\theta_p$ with a residual strength of $0.2\cdot M_y$ is utilized in order to account for the fact that R/C elements do not actually fail when they reach the ultimate point but they are able to resist substantially lower forces with greater deformations.

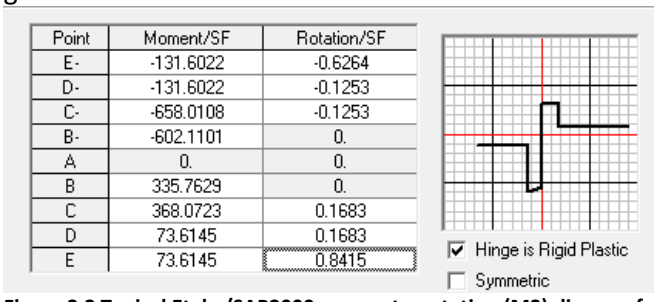

Point	Moment/SF	Rotation/SF
E-	-131.6022	-0.6264
D-	-131.6022	-0.1253
C-	-658.0108	-0.1253
B-	-602.1101	0.
A	0.	0.
B	335.7629	0.
C	368.0723	0.1683
D	73.6145	0.1683
E	73.6145	0.8415

Figure 3.3 Typical Etabs/SAP2000 moment – rotation (M3) diagram for beams

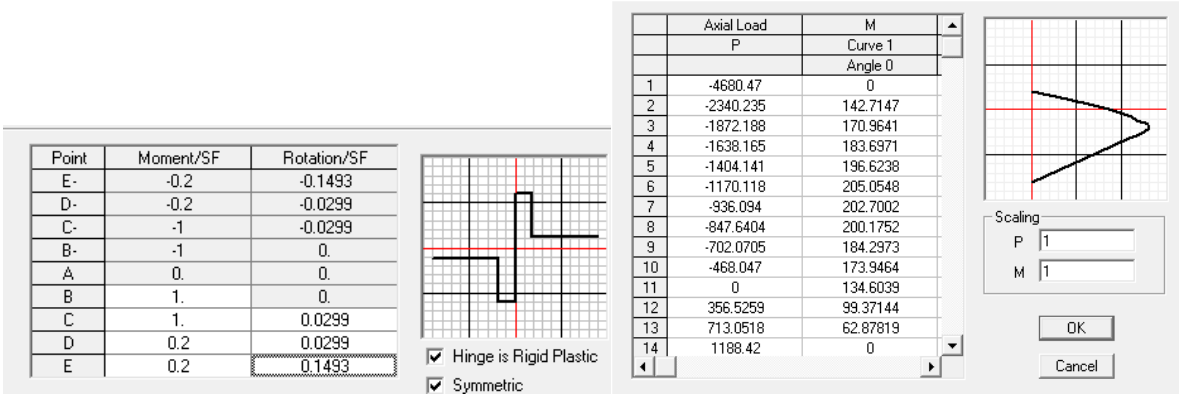

Point	Moment/SF	Rotation/SF
E-	-0.2	-0.1493
D-	-0.2	-0.0299
C-	-1	-0.0299
B-	-1	0.
A	0.	0.
B	1.	0.
C	1.	0.0299
D	0.2	0.0299
E	0.2	0.1493

	Axial Load	M
	P	Curve 1
		Angle 0
1	-4680.47	0
2	-2340.235	142.7147
3	-1872.188	170.9641
4	-1638.165	183.6971
5	-1404.141	196.6238
6	-1170.118	205.0548
7	-936.094	202.7002
8	-847.6404	200.1752
9	-702.0705	184.2973
10	-468.047	173.9464
11	0	134.6039
12	356.5259	99.37144
13	713.0518	62.87819
14	1188.42	0

Figure 3.4 Typical Etabs/SAP2000 moment – rotation and axial load – moment interaction diagrams (PMM)

An additional check is made regarding the ability of each R/C member to develop its flexural strength and deformation, without failing in shear. Hence, in cases where $V_u<V_{My}$, i.e. the shear strength is lower than the shear force corresponding to the development of the member yield moment, the latter is reduced accordingly; moreover, the available rotational capacity (θ_p from equation 3.1) is reduced to $0.5\theta_y$, i.e. 50% the yield rotation of the member. With regard to the effect of ductility demand on shear capacity ($V_u=V(\mu_\theta)$), to avoid the need for iterations, and given that the software used does not have the capability of carrying out shear checks at each step (this was done in the DRAIN2000 software used in previous studies by the AUTh group, see Kappos et al. 2006), the shear capacity V_u is estimated conservatively, i.e. for a value $\mu_\theta=5$, after which a

residual value for the concrete contribution (V_c) is assumed (see Penelis & Kappos 1997, and EPPO 2012). Figure 3.5 presents the moment – plastic rotational ductility $\mu_{\theta,pl}$ diagram ($\mu_{\theta,pl} = \mu_\theta - 1$), along with the moment that corresponds to the shear capacity ($V_u=V(\mu_\theta)$) for the 1st story interior columns of Indian frames (see Figure 3.8), designed for the axial load level that corresponds to the gravity loads of the seismic combination (g+0.3q). It is noted that due to the high transverse reinforcement level of the Indian frames (Ø8/75mm; Figure 3.5) the shear failure was never found to be critical; it is noted that in this assessment no reduction in shear capacity due to poor detailing of the transverse reinforcement was taken into account.

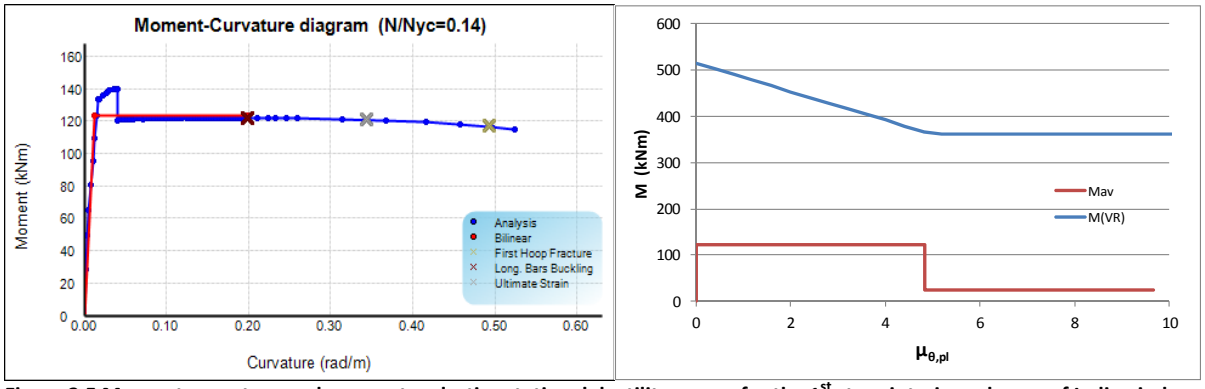

Figure 3.5 Moment-curvature and moment – plastic rotational ductility curves for the 1st story interior columns of Indian index frames

The structures are pushed using a load pattern based on the 1st mode shape until 'failure' of the building. The analysis is terminated when a significant drop of strength occurs (>25% of the maximum base shear), although numerical instabilities may cause the analysis to stop earlier, especially when several elements have a drop in strength or fail at the same step. Minimizing the step size sometimes (but not always!) may solve the problem.

Modeling of masonry infill elements

The model used herein for masonry infills is the one developed by Kappos et al. (1998) and is based on the well-known diagonal strut concept. The relationship between the stiffness of the strut and that of a shear panel can be derived using the condition that the lateral displacement of the two models be equal. Another assumption is that the panel sustains negligible vertical deformations (a reasonable assumption when masonry is constructed subsequent to the completion of the R/C frame).

The axial stiffness coefficient E_sA_s of the strut can be expressed in terms of the shear stiffness G_wA_w of the panel and the inclination (α) of the strut from

$$E_s \cdot A_s = \frac{G_w \cdot A_w}{\cos^2 \alpha \cdot \sin\alpha} \qquad \textbf{(0.24)}$$

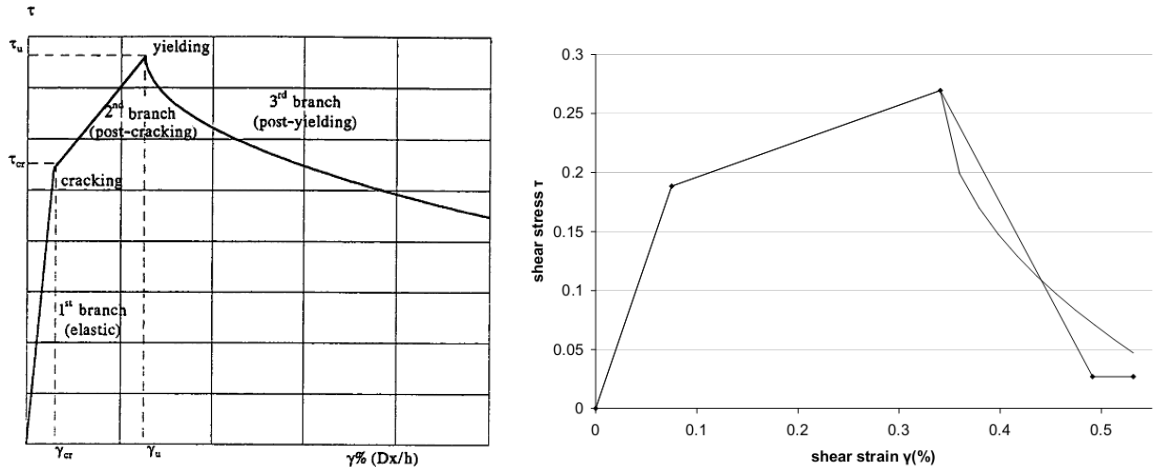

Figure 3.6 Envelope shear stress vs. shear strain curves for infill panel

Based on the assumption of equal areas under the envelope curve, the exponential descending branch of the monotonic τ−γ curve can be substituted by an equivalent bilinear one (Figure 3.5-right). Using the relation between the axial stiffness of the strut and the shear stiffness of the panel it is possible to construct the axial force-displacement diagram of the strut model, which can be directly introduced in the program used (Etabs/SAP2000 in the present study).

3.2.2 Bilinear approximation of pushover curves

Bilinear pushover curves are constructed for each model building type and represent different seismic design and building performance levels. Each curve is defined by two points: (1) the 'yield' capacity and (2) the 'ultimate' capacity. The yield capacity is the point where the building response becomes strongly nonlinear and the strength level is higher than the design strength. Reasons for an actual strength that is higher than the design strength are minimum code requirements, actual material strengths that are higher than the design values (mean values of concrete and steel strength were used in the nonlinear analyses), and, importantly, the presence of masonry infills (this influence is more pronounced in the case of frame systems).. The ultimate capacity is reached after the global structural system has developed a full mechanism and a 20% drop in strength has occurred due to the fact that some members have 'failed' in the sense that they have exceeded their deformation capacity. An in-house developed software (BILIN) has been utilized to automate this procedure (Figure 3.7), adopting equal areas under the 'actual' and the bilinear curve, similar to the FEMA356 guidelines.

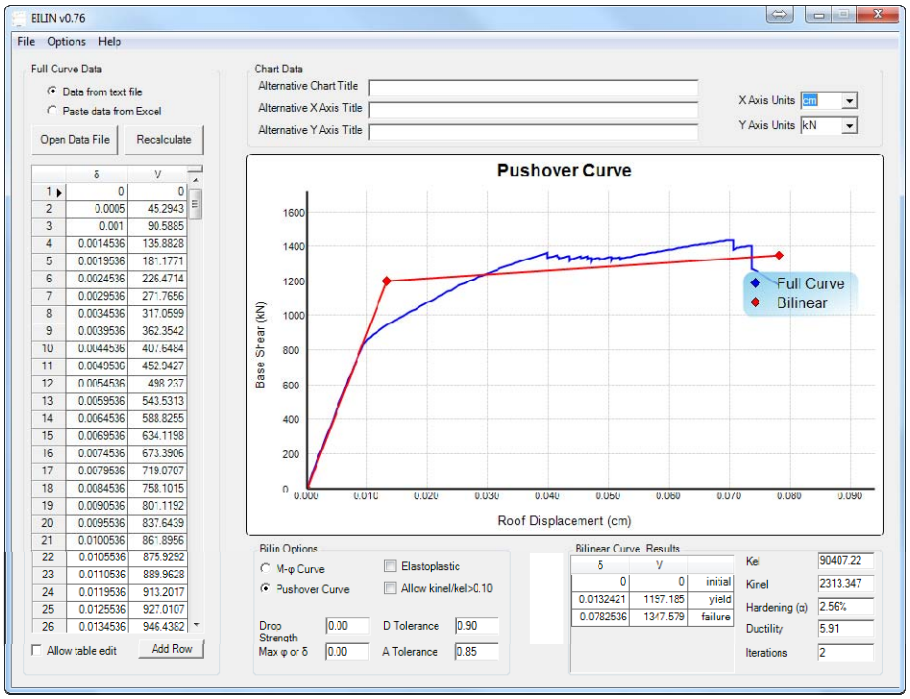

Figure 3.7 Screenshot of the BILIN application

It is emphasised that due to the fact that the pushover curves used for the vulnerability assessment are bilinear versions of the actually calculated curves, a necessity arising from the fact that bilinear behaviour is considered in reducing the elastic spectrum to an inelastic one (or an equivalent elastic one for effective damping compatible with the energy dissipated by the inelastic system), the strength corresponding to the ultimate capacity generally does not coincide with the actual peak strength recorded during the analysis. Moreover, the 'yield' capacity is not the strength of the building when first yielding of a member occurs. The proper way to 'bilinearize' a pushover curve is still a rather controversial issue in the sense that different methods can be appropriate depending on the objective of the specific analysis. It is worth recalling here that in the ATC-40 (1996) manual, where the capacity spectrum method is presented in detail, it is recommended to bilinearize the capacity curve with respect to the previously estimated target point, i.e. the bilinearized curve changes during each iteration, which is not a very convenient procedure.

3.2.3 Derivation of capacity curves from the corresponding pushover curves

The transformation of pushover curves (base shear vs. top displacement) into capacity curves (spectral acceleration vs. spectral displacement) was carried out using the familiar expressions found, among others, in the FEMA-NIBS (2003) and RISK-UE reports:

α_1 fraction of building weight effective in pushover mode

α_2 fraction of building height at the elevation where pushover-mode displacement is equal to spectral displacement.

$$\alpha_1 = \frac{\left[\sum_{i=1}^{N}(m_i\phi_i)\right]^2}{\sum_{i=1}^{N} m_i \cdot \sum_{i=1}^{N}(m_i\phi_i^2)}, \qquad \alpha_2 = \frac{\sum_{i=1}^{N}(m_i\phi_i^2)}{\sum_{i=1}^{N}(m_i\phi_i)\cdot\phi_{cp}}, \qquad PF_{R1} = \frac{1}{\alpha_2} \tag{0.25}$$

where

ϕ_i amplitude of pushover (1^{st}) mode at i^{th} degree of freedom
ϕ_{cp} amplitude of pushover (1^{st}) mode at control point (roof)
m_i the mass at each diaphragm (story) level

Spectral quantities are derived from the equations:

$$S_a = \frac{V/W}{\alpha_1}, \qquad S_d = \frac{\delta}{PF_{R1}} \tag{0.26}$$

where
V base shear
W the total weight of the structure
δ control point (roof) displacement

3.2.4 Alternative 3D approach used for the analysis of the irregular 4-story Indian building

Analysis of the 4-story residential building (considered both as completely infilled with masonry walls, and as having an open first story) was performed via a full 3D finite element model set up in the Seismostruct finite element analysis package. Due to the inherent irregularity (Figure3.9), a 2D modeling approach was deemed meaningless, while insurmountable problems with the SAP/ETABS software forced us to explore alternative but reliable software options (i.e. Seismostruct). Beams and columns were modeled using distributed inelasticity elements; the fiber approach is implemented to represent the cross-sectional behavior where each "fiber" is associated with a uniaxial stress-strain relationship. The sectional stress-strain state of a beam-column element is obtained through the integration of the nonlinear uniaxial stress-strain responses of the individual fibers. Compared to the "concentrated or lumped inelasticity" counterparts, these models feature additional advantages as they do not require a prior moment-curvature analysis, or introducing any element hysteretic response (this is implicitly defined by the material constitutive laws), whereas modeling of axial load-biaxial bending moment interaction is straightforward. On the other hand, such models generally overestimate the initial stiffness of R/C members since they ignore existing cracking (which typically exists due to environmental actions like shrinkage and/or past loading history) and they also cannot model inelastic shear and bond-slip effects without introducing additional features, such as end springs. For the implementation of the distributed inelasticity model, the force-based formulation approach was selected where element equilibrium is strictly satisfied and no restraints are placed to the development of inelastic deformations throughout the member. A member by member modeling approach was used since the force-based formulation permits this level of discretization (as opposed to a more discrete one that should have been applied in case the displacement-based formulation was selected). Masonry infills were modeled using the four-node masonry panel element initially developed by Crisafulli et al. (2000).

A rational architectural configuration was assumed in terms of the location of infill walls, openings etc. as no such data were available. The typical layout of the building plan suggests a possible influence of adjacent buildings; hence the "flat" side of the layout was considered as full of infills (Figure 3.9) in contrast to the other sides where normal opening configuration was assumed, raising some artificial non-symmetry (note that existing symmetry along the y axis was not affected by the infill placement hypothesis). It has to be emphasized, though, that the fully infilled version was modeled with and without the infill panels.

Full diaphragm action was considered at each level apart from the “plinth” one. The “plinth” story, where no R/C slab exists, is a common practice for Indian R/C frame buildings where the foundation lies deeper than half the first story height; columns and foundation elements under the plinth level are fully embedded in the ground while beams are provided only at ground level. Columns were assumed fixed to the ground at the foundation level while modeling of soil-structure interaction due to column-to ground-contact underneath the plinth was simplified; sets of diagonal elastic truss elements were employed, corresponding to a horizontal stiffness calculated upon assumed elastic ground properties (a horizontal spring was not available in the software used).

As mentioned before, due to fiber inelasticity approach, a prior moment-curvature analysis is eliminated at least during the modeling and analysis stages, but during the assessment stage, a cross-sectional analysis was eventually deemed necessary in order to assign realistic failure criteria for the R/C members. For the nonlinear uniaxial stress-strain response of the individual concrete fibers, the Mander et al (1988) constitutive model was used (both for confined or unconfined parts) while for the individual steel counterparts a bilinear one was used.

In terms of the Crisafulli et al (2000) infill panel element parameters, the axial force-displacement diagram of the strut was derived using the approach introduced in Section 3.2.1. Compressive strength was provided by H.B.Kaushik; a relatively high compressive strength was assumed (7.5 MPa). Other properties were taken according to Kaushik et al. (2009). For values not readily inferred from the provided data, the default values of the Crisafulli et al. panel model were adopted.

3.3 Input data and results

The details of the structural typologies analyzed using the aforementioned procedures are outlined here, highlighting the data provided and directly available and the assumptions made where specific parameters needed for the modeling were not available. Results for all analyses carried out are presented following the discussion of the input data for each group of structures. As a rule, the output is provided in terms of normalized pushover curves where the base shear is divided by the total weight of the structure (V/W) and the roof displacement by the total height (δ/H), and in some cases as capacity curves (S_a vs. S_d). Furthermore, the plastic mechanisms at the final stage of the analysis (before failure) are shown in order to describe the inelastic behavior of the structure and the distribution of expected damage.

3.3.1 Input data and results for frames from India provided by IITG

Basic data for the Indian R/C building typologies are summarized in Table 3.1 and Figures 3.8 and 3.9; details of member reinforcement were provided by H.B. Kaushik, while the methodology used by the Indian group for analyzing these buildings is presented in Kaushik et al. (2009) along with the corresponding results. It has to be noted that the aforementioned publications by Kaushik et al. refer to the infilled frame structure of Figure 3.8, while the irregular, 3D building of Figure 3.9 is described only in internal reports by Kaushik.

Table 3.1 Indian R/C building typologies (Kaushik)

PAGER STRUCTURE.	Building type	Reinforcing steel	Concrete Cube Strength	Inter-story height		Average thickness of brick infill walls	Average beam dimensions in main direction		Average ground floor column depth in main direction
				upper floors	ground floor		Length	Depth	
C4M (1)	Reinforced Concrete 4-story Frame without Masonry Infill Walls	HYSD 440 MPa	25 MPa	3.2m	4.4m	-	3m	45cm	30cm
C3M (2)	Reinforced Concrete 4-story Frame with Masonry Infill Walls in all Stories			3.2m	4.4m	22cm	3m	45cm	30cm
C3M-SS (3)	Reinforced Concrete 4-story Frame with Open First Story			3.2m	4.4m	22cm (upper Stories) Absent in Ground or First Story	3m	45cm	30cm
C3M (9)	Reinforced Concrete 4 story Residential Building with Masonry Infills in all Stories		20 MPa	3.15m	3.15m	23cm (external) 11.5cm (internal)	3.1m	51cm	23cm
C3M-SS (10)	Reinforced Concrete 4 Story Residential Building with Open First Story			3.15m	3.15m	23cm (external bays upper stories) 11.5cm (internal bays upper stories) absent in ground or first story	3.1m	51cm	23cm

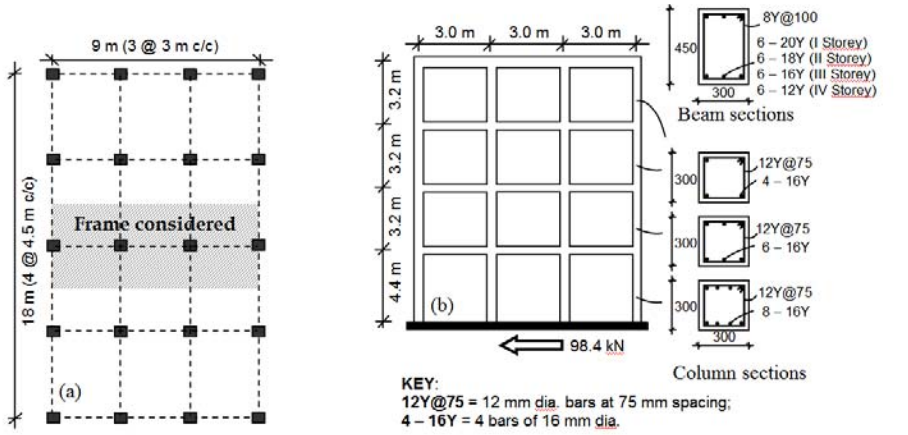

Reduced Live Load (due to earthquake load combination): 0.5 kN/m2 at all floors, 0.25 kN/m2 at roof.

Figure 3.8 Typical layout of the R/C 4-story frames for the index building from India

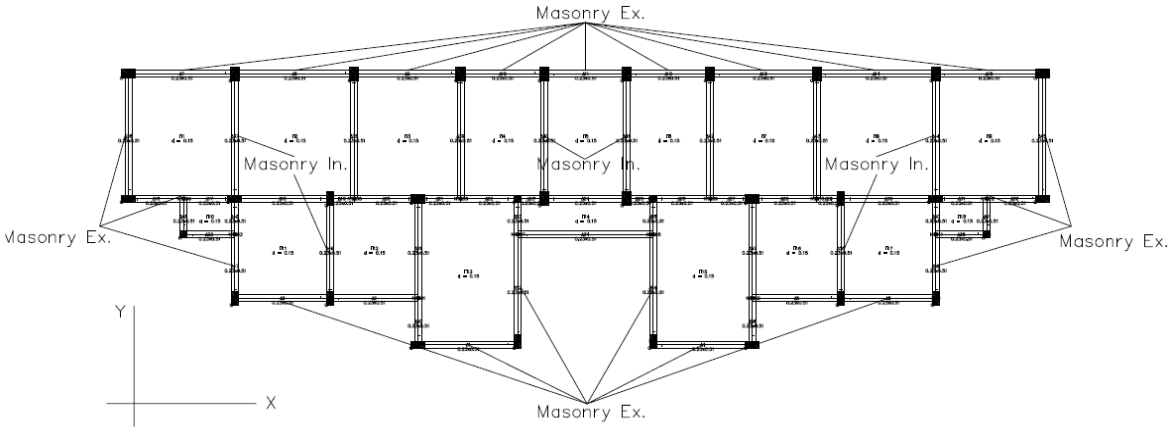

Figure 3.9 Typical plan layout of a 4-story residential index building from India

Compressive strength of masonry infill walls was provided as f_{wc}=7.5MPa with an average brick length of 22cm for the frame structures. For the irregular 3D building the average thickness of brick infill walls is 23cm for external and 11.5cm for internal frames. This value of f_{wc} is significantly higher than the typical masonry properties used in Greece and other European countries (typical values for Greece are 1.5-3.0MPa). Therefore, it was decided to investigate the effect of this parameter on the response of the 2D infilled Indian frames, carrying out some extra analyses with a lower value of f_{wc}=1.91MPa adopted from a recent study by the same Indian group (Kaushik & Manchanda 2010)[3].

The internal frame of the Indian building shown in Figure 3.8 has been modeled using the Etabs v.9.7.2 software (Figure 3.10). The irregular building presented in Figure 3.9 has been modeled as a 3-dimensional structure using the Seismostruct software (Figure 3.11).

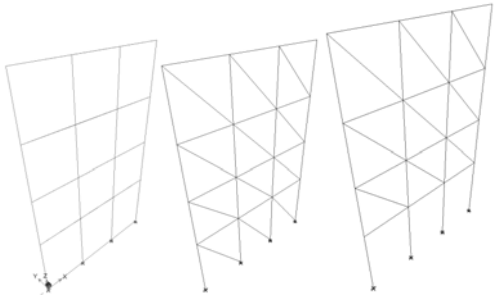

Figure 3.10 Typical models for bare (left), infilled (center) and soft story (right) Indian index frames for buildings with regular layout

[3] It should be noted that the two types of masonry used for infill as examples in India, belong to different regions; the first is from Kanpur, in northern India, the second is from Guwahati in Northeastern India.

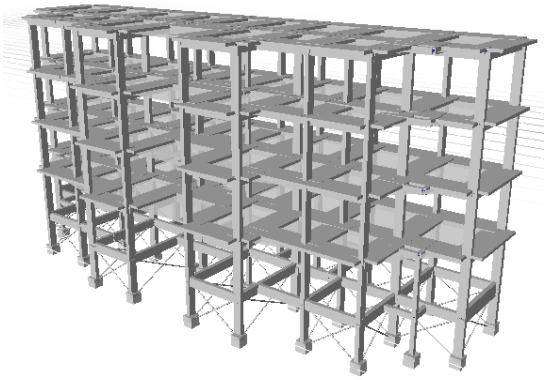

Figure 3.11 3D model of irregular plan layout, reinforced concrete 4 story residential index building with masonry infills in all stories

Results for building types C4M (1), C3M (2), C3M-SS (3)

Normalized pushover curves and the corresponding plastic mechanisms are presented in figures 3.12 and 3.13. It is clear that the presence of infill walls significantly affects the response of the structure, increasing the maximum base shear force by a factor greater than 4, due to the very strong infill panels (f_{wc}=7.5MPa, t=22cm). It should be noted that infill panels cover all space between the surrounding beams and columns since no openings have been taken into account. As expected, the struts that model the masonry walls are the first elements that fail and there is a significant drop in strength until the base shear is decreased to the value that corresponds to the bare frame. The behavior of the soft story layout (open ground story) frame is very close to the bare one since in both cases the final failure of the building is due to the failure of the first story columns. The Indian index buildings manage to withstand very large displacements due to the fact that the spacing and the diameter of the transverse reinforcement in columns correspond to high ductility (Ø12/75mm). Results from extra analyses where the compressive strength of masonry infill panels was reduced to 1.91MPa are presented in figures 3.14 and 3.15, clearly showing the effect of these elements on the overall response of the structure (maximum V/W is reduced by almost 40%). The failure mechanisms still remain similar.

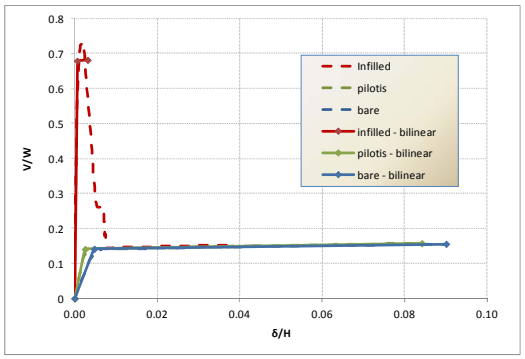

Figure 3. 12 Normalized pushover curves for bare, infilled and soft story layout Indian index frames (f_{wc}=7.5MPa)

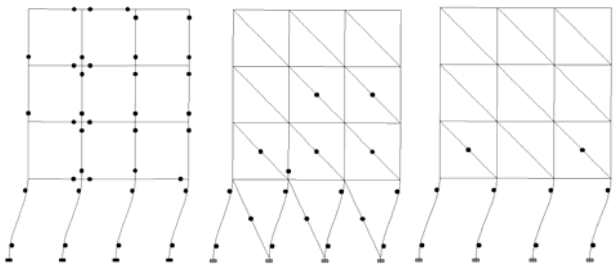

Figure 3. 13 Plastic mechanisms for bare, infilled and soft story layout Indian index frames (f_{wc}=7.5MPa)

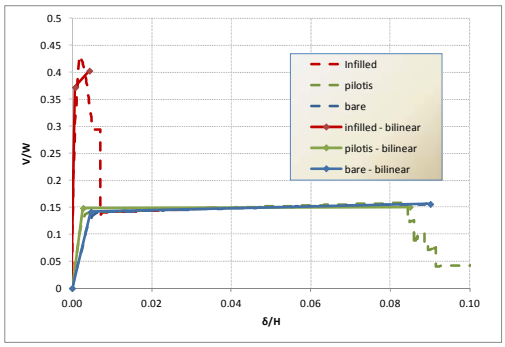

Figure 3. 14 Normalized pushover curves for bare, infilled and soft story layout Indian index frames (f_{wc}=1.91MPa)

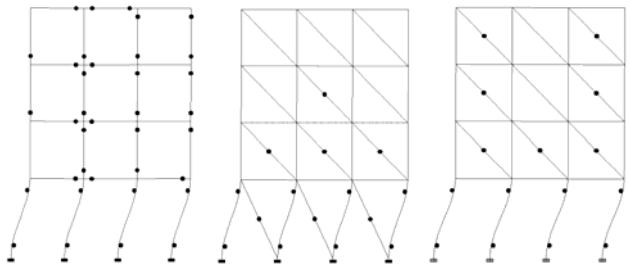

Figure 3. 15 Plastic mechanisms for bare, infilled and soft story layout Indian index frames (f_{wc}=1.91MPa)

Results for building types C4M, C3M (9), C3M-SS (10), with irregularity in plan

Analysis of the 4-story, irregular residential building was carried out using Seismostruct considering separate analysis along x- and y-directions (+y and –y directions were also separately considered due to the asymmetric layout along y-axis, Figure 3.9). Pushover curves are provided both in V/W-δ/H and S_a - S_d terms. Results (displacements) along x direction were plotted not only for the center of mass of the upper story, but also for two external frames: the rear, stiff frame with full-bay infills, and a front facade frame with a more rational opening configuration ("soft" frame). Due to the existing symmetry, results along the y direction were plotted only for the center of mass of the upper story. Capacity curve derivation and bilinear approximations were implemented according to Sections 3.2.3 and 3.2.4.

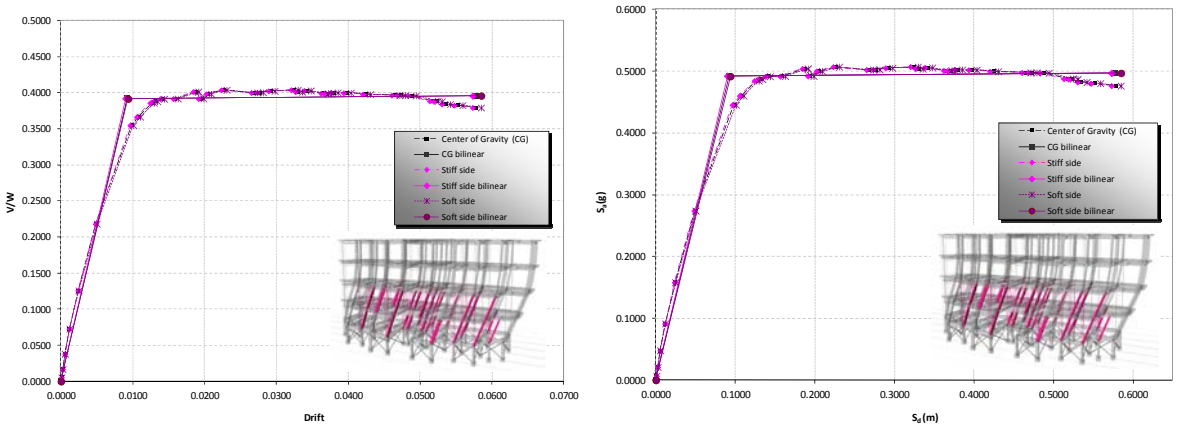

Figure 3.16 Capacity curves for the Indian 4-story residential building, bare frame version, class C4M. Direction of loading is only +x (due to layout symmetry across y axis).

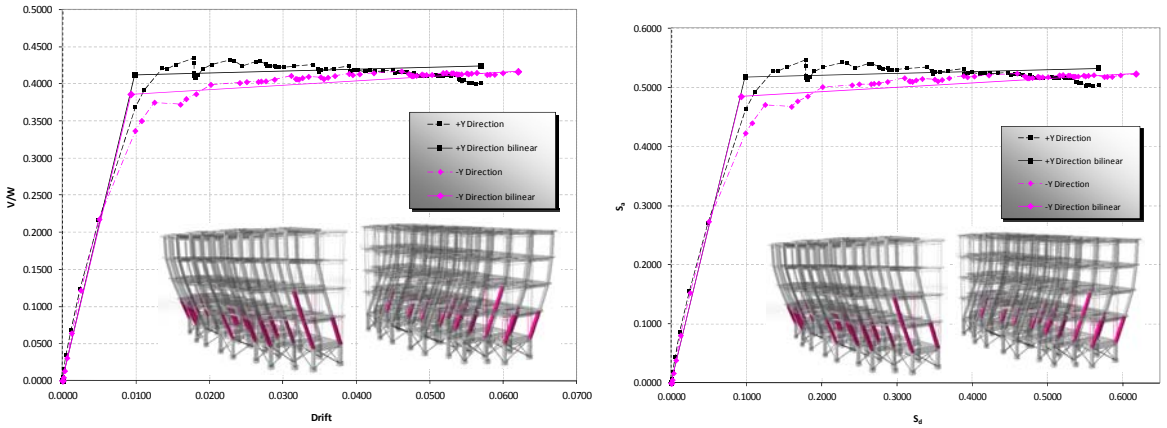

Figure 3.17 Capacity curves for the Indian 4-story residential building, bare frame version, class C4M. Direction of loading is +y and –y.

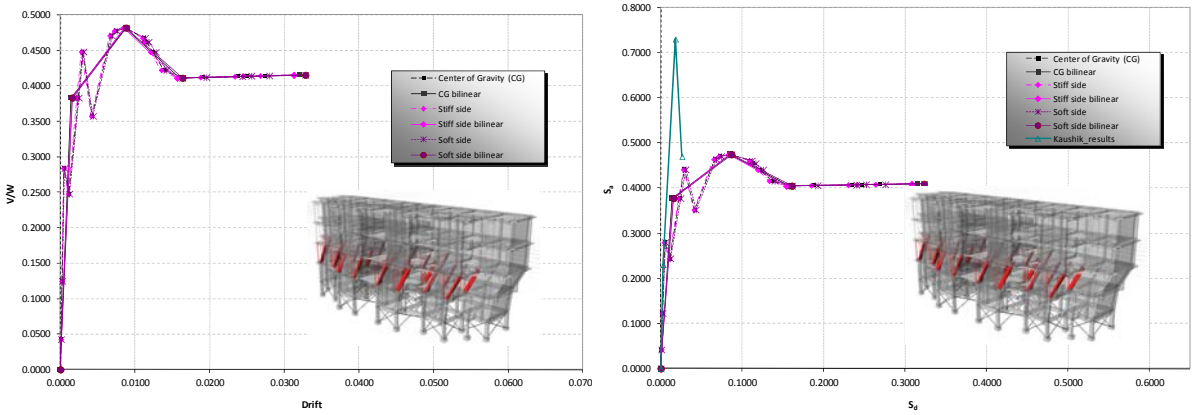

Figure 3. 18 Capacity curves for the Indian 4-story residential building with infills in all stories, class C3M. Direction of loading is only +x (due to layout symmetry across y axis).

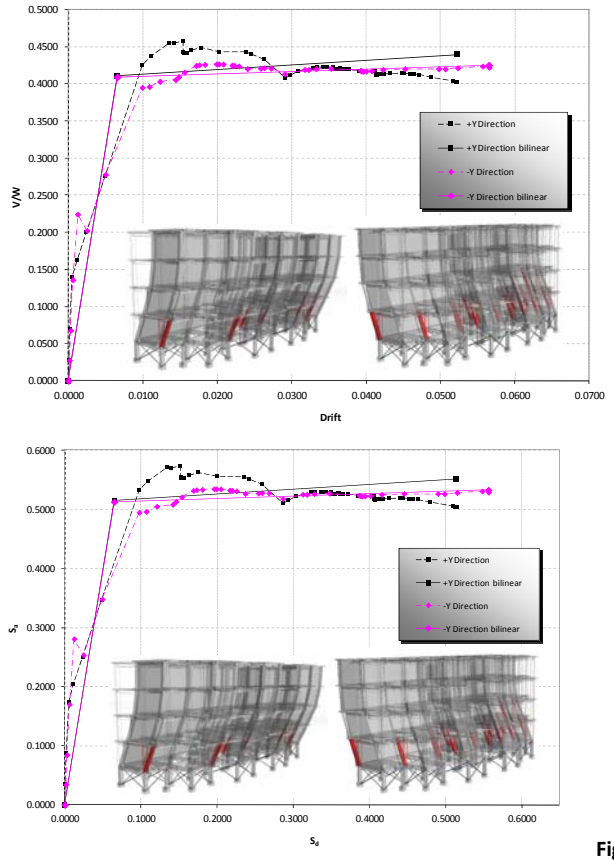

Figure 3.19 Capacity curves for the Indian 4-story residential building with infills in all stories, class C3M. Direction of loading is +y and –y.

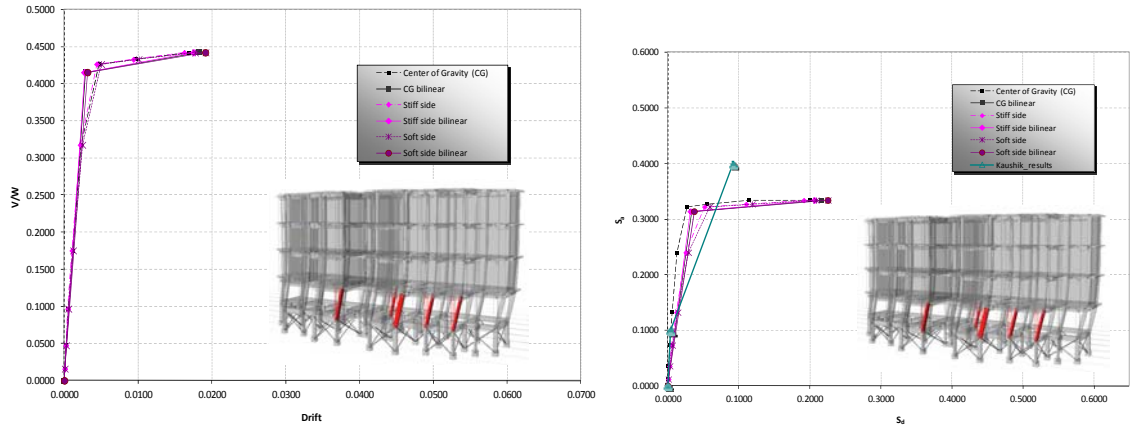

Figure 3. 20 Capacity curves for the Indian 4-story residential building with open first story, class C3M-SS. Direction of loading is only +x (due to layout symmetry across y axis).

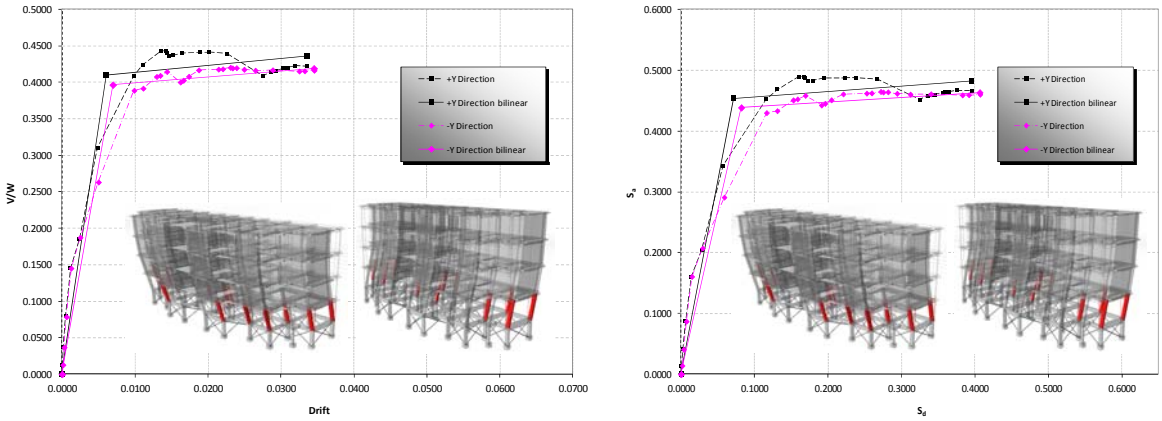

Figure 3. 21 Capacity curves for the Indian 4-story residential building with open first story, class C3M-SS. Direction of loading is +y and –y.

Table 3.2 summarizes the results obtained in terms of spectral displacement and acceleration, effective period, and ductility factor for all Indian buildings analyzed in this study. The values S_{dy} and S_{du} in the Table are those derived from the δ_y and δ_u values in the pushover curves using the well-known SDOF transformation (equation 3.5), i.e. S_{du} corresponds to ≥20% drop in strength in the structure. The high S_{du} values for the frames without infills in the ground story are mainly due to the fact that the spacing and the diameter of the transverse reinforcement in their columns correspond to high ductility requirements.

Table 3.2 Summary of capacity curve parameters for Indian index frames.

PAGER structure .	Building type	Model type	Loading	S_{dy} (cm)	S_{ay} (g)	S_{du} (cm)	S_{au} (g)	T_e (s)	Ductility factor	Failure
C4M (1)	R/C 4-story Frame (Bare)	2D	Pushover 1st mode	5.55	0.15	105.23	0.16	1.23	18.96	Story mechanism
C3M (2)	R/C 4-story Frame Infilled	2D ** f_{wc}=7.5MPa	Pushover 1st mode	0.62	0.78	3.25	0.78	0.18	5.22	Failure of infill walls – story mechanism
		2D ** f_{wc}=1.91MPa		0.84	0.41	4.67	0.45	0.29	5.55	
C3M-SS (3)	R/C 4-story Frame Open First Story	2D f_{wc}=7.5MPa	Pushover 1st mode	3.47	0.14	115.59	0.16	1.00	33.26	Story mechanism
		2D f_{wc}=1.91MPa		3.76	0.15	115.06	0.15	1.01	30.59	
C4M	R/C 4 story Residential Building No Infills	3D	Pushover Dir. X*	9.17	0.49	57.8	0.50	0.864	6.3	Story mechanism
		3D	Pushover Dir. +Y	9.82	0.52	56.8	0.53	0.868	5.78	Story mechanism
		3D	Pushover Dir. -Y	9.26	0.48	61.7	0.52	0.877	6.65	Story mechanism
C3M (9)	R/C 4 story Residential Building with Masonry Infills in all Stories	3D ***	Pushover Dir. X*	8.52	0.41	31.5	0.47	0.850	3.70	Story mechanism
		3D	Pushover Dir. +Y	6.45	0.51	51.4	0.55	0.710	7.97	Story mechanism
		3D	Pushover Dir. -Y	6.46	0.51	55.6	0.53	0.711	8.61	Story mechanism
C3M-SS (10)	R/C 4 Story Residential Building with Open First Story	3D	Pushover Dir. X*	3.40	0.31	21.6	0.33	0.661	6.35	Story mechanism
		3D	Pushover Dir. +Y	7.11	0.45	39.6	0.48	0.794	5.57	Story mechanism
		3D	Pushover	8.19	0.43	40.6	0.46	0.872	4.96	Story

			Dir. -Y							mechanism

** For loading along the x direction, results are provided only for the center of mass of the upper story.*
*** After the drop in strength due to the failure of infill walls the corresponding quantities from the bare frame may be used resulting in a quatrilinear curve (Figure 3.12, 3.14).*
**** A quatrilinear approximation of the pushover curve was calculated for that case (Figure 3.18).*

3.3.2 Input data and results for index frames from Italy provided by ROSE

Basic data for the Italian R/C building typologies are summarized in Table 3.3 and Figure 3.22; details of member detailing can be found in the PAGER report "4 Story RC MRF w/o Infill Panels, "Mediterranean" Design" by H. Crowley, while the methodology used by the ROSE group for analyzing these buildings is presented in Borzi et al. (2008), along with the corresponding results. Pushover analysis has been carried out for 2D frames focusing on the internal frames. The Italian research team has analyzed only bare structures (no infill walls). The AUTh team decided to investigate the effect of the infill walls on the response of the Italian structures, adopting typical values for the compressive strength (f_{wc}=1.2MPa) and the thickness (t=10cm) of masonry infill walls proposed for Italian buildings by Masi (2004). It is noted that these values are closer to the properties of infill that were also adopted within the framework of the WHE PAGER project (f_{wc}=1.5MPa, t=10cm) for the Greek index building but are significantly lower than the values provided for the Indian index building.

The typical frames of the Italian index building have been modeled using the Etabs software (Figure 3.23). The basic approach of the AUTh team focuses on 2D models, therefore it was decided to analyze only the internal frames of the buildings in both directions, with the exception of the non-seismically designed building that is examined only in the x-direction since there are no beams present in the y-direction and diaphragm action is considered to be ensured by the floor slabs alone (Borzi et al, 2008).

Table 3.3 R/C building typologies provided by ROSE School as Italian index buildings

Structure	Detail	Location	Model	Researcher
C4M (RC_PC)	RC frame, No Seismically designed, 4 stories, No Infill walls	Mediterranean	DBELA	ROSE
C4M (RC_5%)	RC frame, Seismically designed (horizontal load:5%), 4 stories, No Infill walls	Mediterranean	DBELA	ROSE
C4M (RC_12.5%)	RC frame, Seismically designed (horizontal load:12.5%), 4 stories, No Infill walls	Mediterranean	DBELA	ROSE

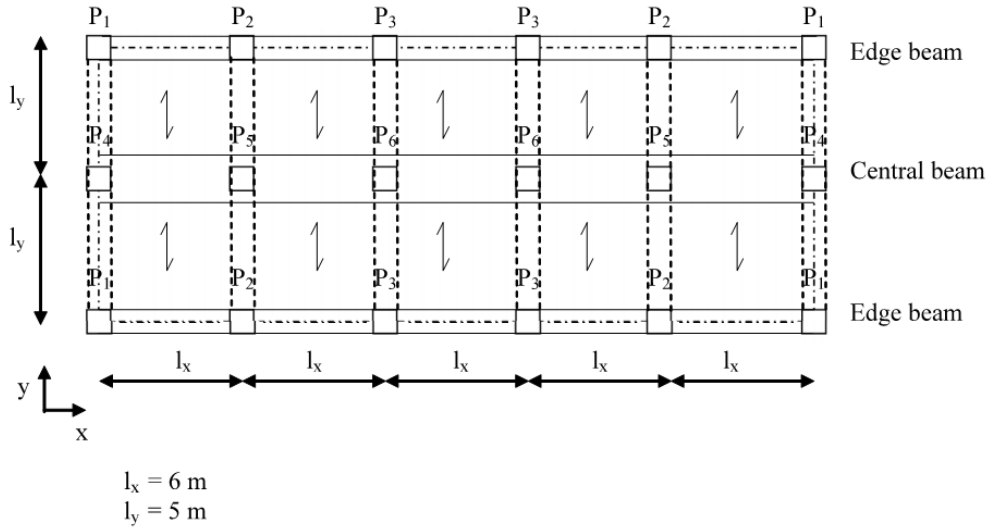

Figure 3. 22 Plan view of Italian index R/C building

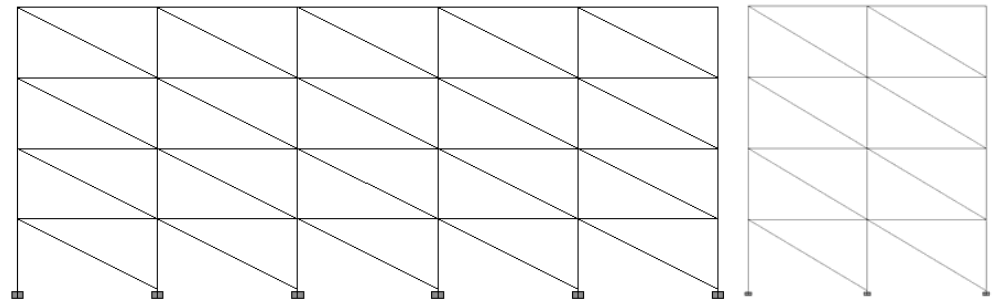

Figure 3. 23 Typical models for Italian regularly infilled index building; x-direction (left), y-direction (right)

Normalized pushover curves and the corresponding plastic mechanisms are presented in figures 3.24 to 3.28. It is notable that for the non-seismically designed building in the x-direction (Figure 3.24), the story mechanism appears at the upper stories, attributed to the decrease in the column dimensions; for example the central column starts with a section of 30x70cm at the base story and is reduced to 30x60cm, 30x40cm and 30x30cm at the 2nd, 3rd and roof story, respectively. As a result the building cannot develop the maximum base shear that corresponds to the capacity of the ground story columns.

For the seismically designed buildings, an increase in strength and, secondarily, in ductility can be noted (Figures 3.25-3.28). It must be emphasized that numerical instabilities of the program occurred in several analyses and very often the results subsequent to 'failure' of the first structural elements were not available. This phenomenon occurred more often when several 'events' (e.g. drop in strength or failure of structural elements) occur during the same step of the analysis. Lowering the step size or the event tolerance may sometimes (but not always) solve the problem. For infilled, regularly or not, buildings after the drop in strength due to the failure of masonry infill walls, the corresponding quantities from the bare frames may be used, resulting in quatrilinear simplified curves.

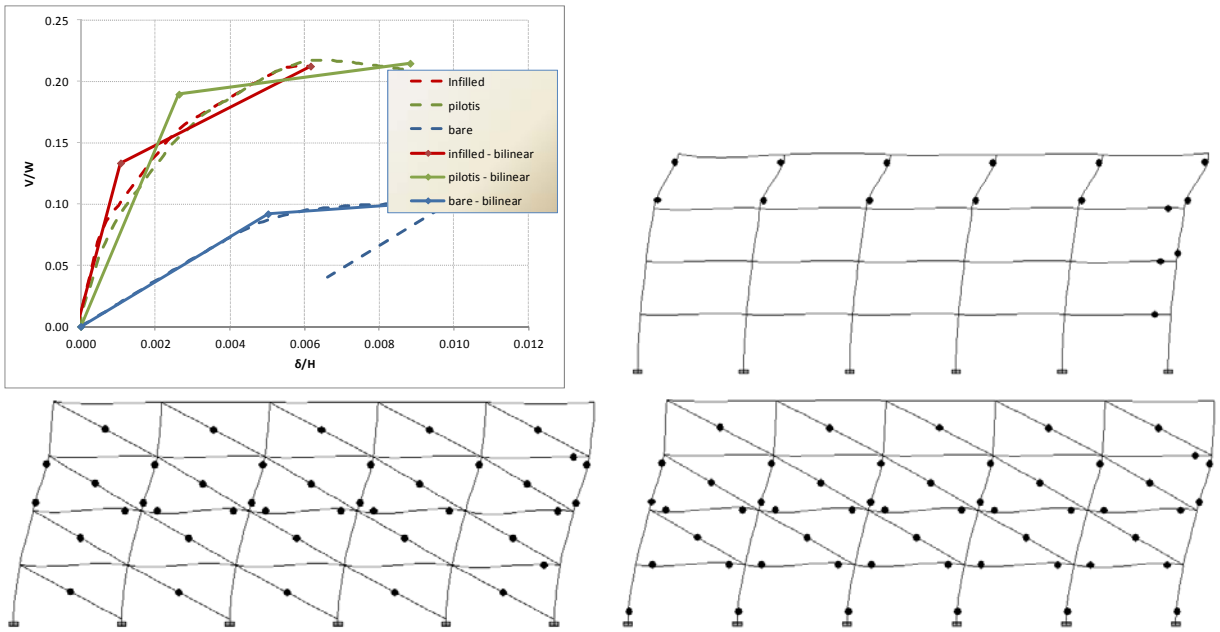

Figure 3.24 Normalized pushover curves and plastic mechanisms for bare C4M (RC_PC), infilled C3M (RC_PC) and soft story layout C3M-SS (RC_PC) Italian index frames (no seismic design, x-direction)

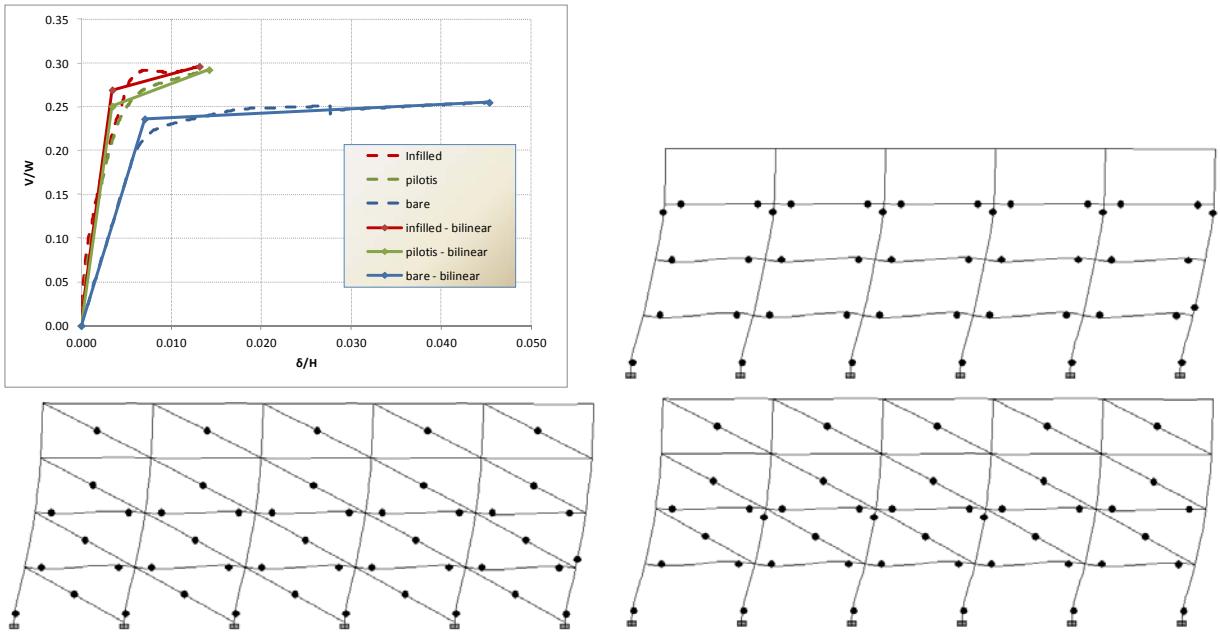

Figure 3.25 Normalized pushover curves and plastic mechanisms for bare C4M (RC_5%), infilled C3M (RC_5%) and soft story layout C3M-SS (RC_5%) Italian index frames (5%, x-direction)

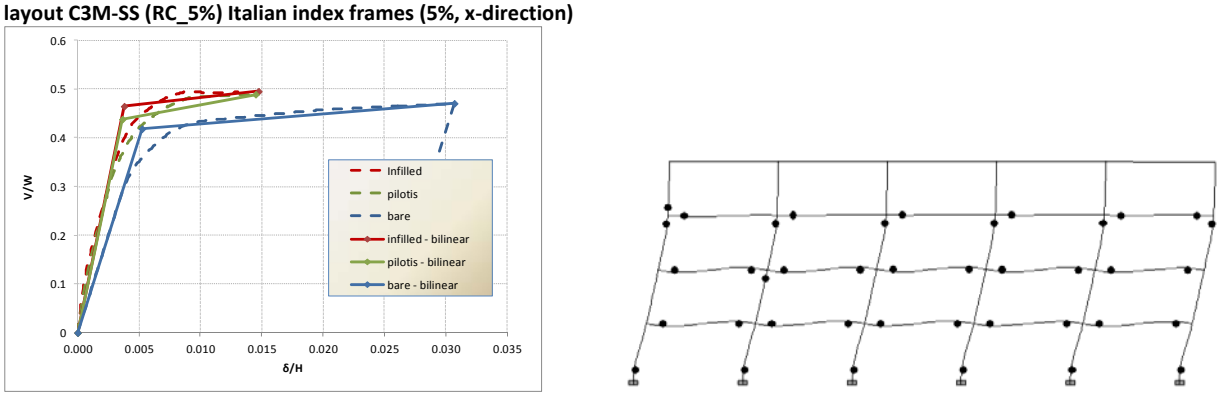

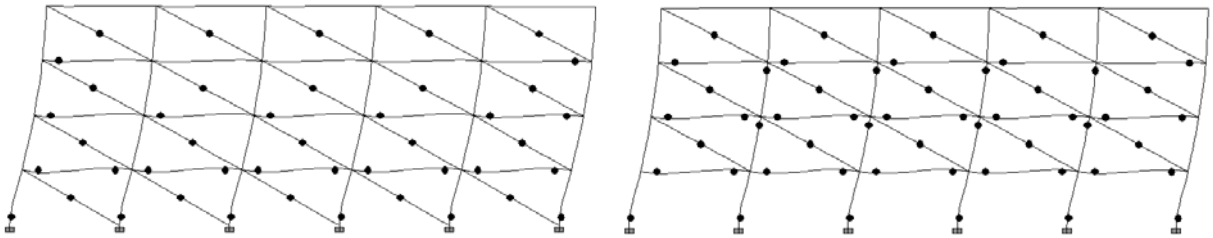

Figure 3.26 Normalized pushover curves and plastic mechanisms for bare C4M (RC_12.5%), infilled C3M (RC_12.5%) and soft story layout C3M-SS (RC_12.5%) Italian index frames (12.5%, x-direction)

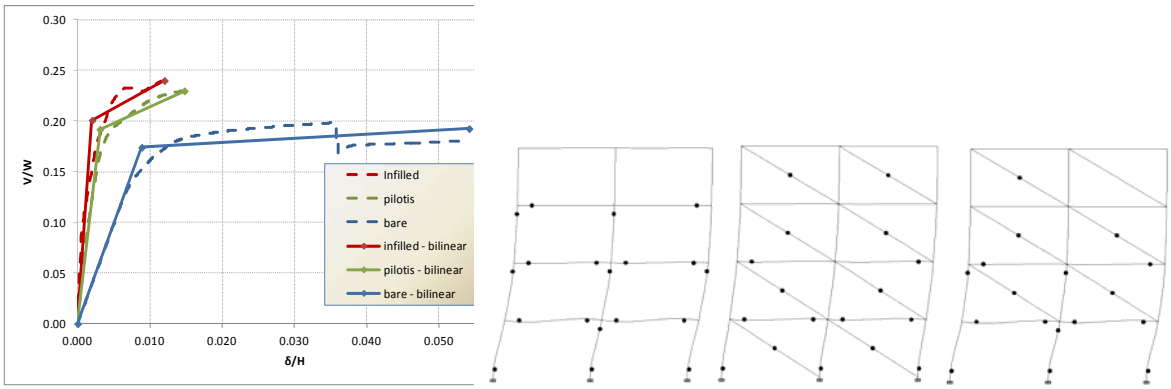

Figure 3.27 Normalized pushover curves and plastic mechanisms for bare C4M (RC_5%), infilled C3M (RC_5%) and soft story layout C3M-SS (RC_5%) Italian index frames (5%, y-direction)

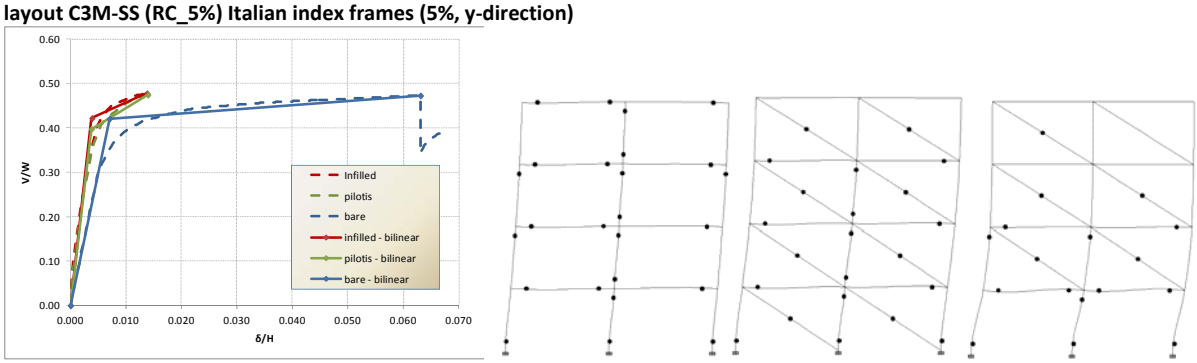

Figure 3.28 Normalized pushover curves and plastic mechanisms for bare C4M (RC_12.5%), infilled C3M (RC_12.5%) and soft story layout C3M-SS (RC_12.5%) Italian index frames (12.5%, y-direction)

Table 3.4 Summary of capacity curve parameters for Italian index frame.

No.	Masonry infills	Model type	Loading - Direction	S_{dy} (cm)	S_{ay} (g)	S_{du} (cm)	S_{au} (g)	T_e (s)	Ductility factor	Failure**
C4M (RC_PC)	Bare	2D	Pushover 1st mode - X	4.58	0.12	8.73	0.14	1.22	1.91	Story mechanism (4th story)
C3M (RC_PC)	Regularly infilled*	2D	Pushover 1st mode - X	1.05	0.15	6.03	0.23	0.54	5.77	Story mechanism (3rd story)
C3M-SS (RC_PC)	Open first story*	2D	Pushover 1st mode - X	2.63	0.20	8.83	0.23	0.72	3.36	Story mechanism (3rd story)
C4M (RC_5%)	Bare	2D	Pushover 1st mode - X	6.70	0.28	43.01	0.31	0.97	6.42	'Story' mechanism – base and top of 3rd floor columns
C3M (RC_5%)	Regularly infilled*	2D	Pushover 1st mode - X	3.31	0.31	12.61	0.34	0.66	3.81	Failure of infill walls at the two lower stories
C3M -SS (RC_5%)	Open first story*	2D	Pushover 1st mode - X	3.48	0.27	14.22	0.31	0.72	4.09	Failure of infill walls at the 2nd story
C4M (RC_12.5%)	Bare	2D	Pushover 1st mode - X	4.95	0.51	28.91	0.58	0.62	5.84	'Story' mechanism – base and top of 3rd floor columns
C3M (RC_12.5%)	Regularly infilled*	2D	Pushover 1st mode - X	3.65	0.53	14.20	0.56	0.53	3.89	Failure of infill walls at the three lower stories
C3M-SS (RC_12.5%)	Open first story*	2D	Pushover 1st mode - X	3.65	0.47	14.51	0.52	0.56	3.97	Failure of infill walls at the 2nd story

C4M (RC_5%)	Bare	2D	Pushover 1st mode - Y	8.45	0.21	51.63	0.23	1.29	6.11	Failure of several base columns
C3M (RC_5%)	Regularly infilled*	2D	Pushover 1st mode - Y	1.91	0.23	11.50	0.27	0.58	6.03	Failure of infill walls at the two lower stories
C3M-SS (RC_5%)	Open first story*	2D	Pushover 1st mode - Y	3.26	0.20	15.67	0.23	0.82	4.81	Failure of infill walls at the 2nd story
C4M (RC_12.5%)	Bare	2D	Pushover 1st mode - Y	6.63	0.51	59.57	0.57	0.72	8.98	Failure of several base columns
C3M (RC_12.5%)	Regularly infilled*	2D	Pushover 1st mode - Y	3.68	0.49	13.15	0.56	0.55	3.57	Failure of infill walls at the two lower stories
C3M-SS (RC_12.5%)	Open first story*	2D	Pushover 1st mode - Y	3.68	0.44	13.64	0.52	0.58	3.70	Failure of infill walls at the 2nd story

** After the drop in strength due to failure of infill walls the corresponding quantities from the bare frames could be used for the regularly or irregularly (open first story) infilled buildings, resulting in quatrilinear curves*

*** 'Failure' sometimes represents the inability of the software to continue the analysis due to convergence problems. The events at the final steps are reported in such cases*

3.4 Comparisons

3.4.1 Comparison for index frames from India

In the following figures, the capacity curves estimated using the AUTh method and 'IITG method' are presented for all Indian frames. The AUTh method usually results in a little lower strength (S_a) than the IITG approach, while the deformation capacity (S_d) is often higher. Bare and soft story layout (open ground story) buildings have similar stiffness, but for infilled buildings the IITG approach results in a more flexible structure. It is interesting that when the lower compressive masonry strength (1.9MPa) has been adopted the AUTh and Kaushik approaches produced results with practically the same stiffness (Figure 3.31); of course, the strength of the AUTh building was now significantly lower.

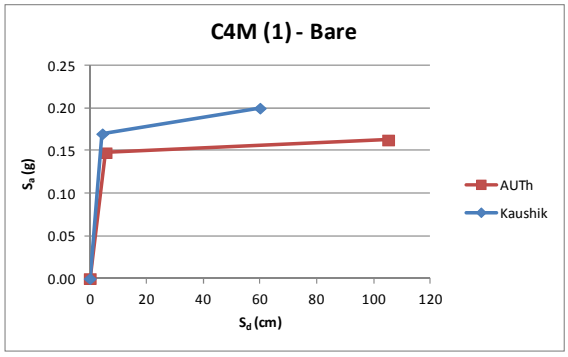

Figure 3.29 Comparisons of IITG and AUTh capacity curves for bare Indian index frames

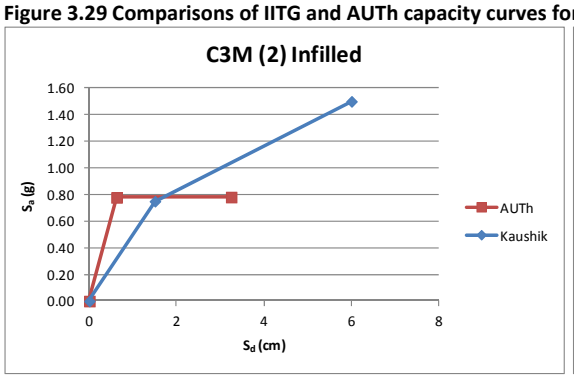

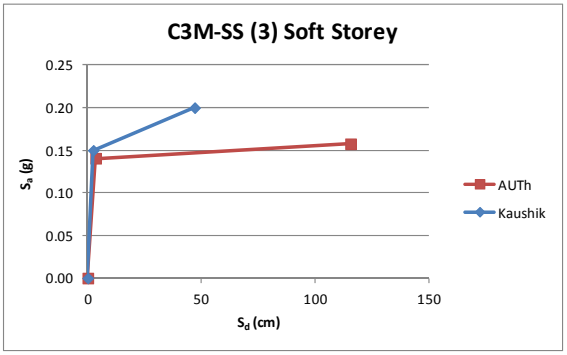

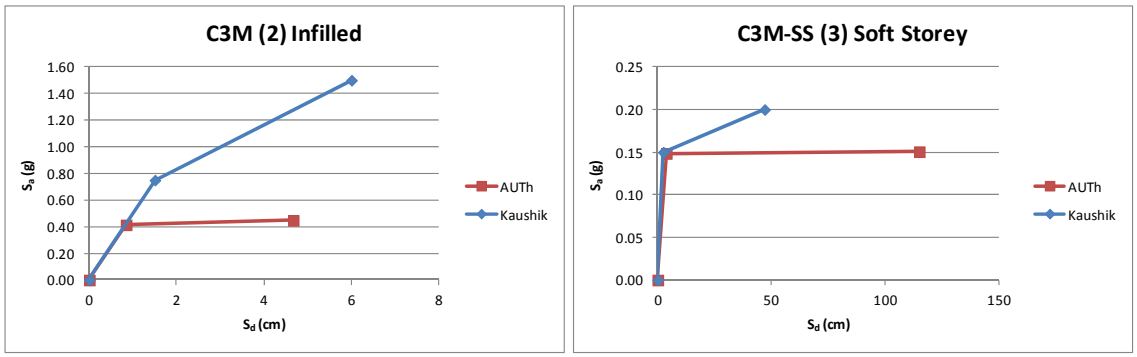

Figure 3.30 Comparisons of Kaushik and AUTh capacity curves for regularly and irregularly infilled Indian index frames (top: f_{wc}=7.50MPa; bottom: f_{wc}=1.91MPa – AUTh, f_{wc}=7.50MPa – Kaushik)

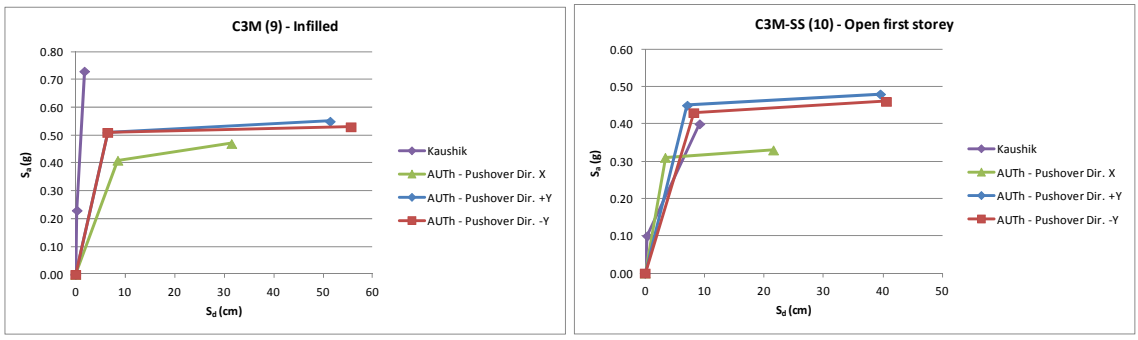

Figure 3.31 Comparisons of Kaushik and AUTh capacity curves for regularly and irregularly infilled Indian index 3D irregular building

With regard to the comparisons shown in Figure 3.31, it has to be emphasized that for the 4-story residential building (where a full 3D model was implemented), rather incomplete results were provided by Kaushik et al (see figs. 3.18 & 3.20). Software or modeling issues were to blame for this paucity of results; recall that this was the main reason for AUTh's software switch from SAP/ETABS to Seismostruct in this demanding 3D analysis. Nevertheless, the difference in the maximum strengths noted in Figure 3.18 (fully infilled frame), may, (to some extent) be attributed to the masonry placement hypothesis (see Figure 3.9) if software limitations are to be mainly attributed to the complexity of interacting masonry and beam-column elements during the post-yield stages.

3.4.2 Comparison for index frames from Italy

In the following figures, the capacity curves estimated using the AUTH and ROSE methods are shown for bare frame buildings. With the exception of the non-seismically designed building where a story mechanism has formed at the upper story, the results of the two teams show that the ROSE approach estimates higher S_a values than the AUTh method. The stiffness of the buildings is generally very close for both approaches and the AUTh team predicts higher available ductilities.

In order to compare different software and analysis options as well, the 5% seismically designed Italian bare frame was also analyzed in Seismostruct, using a 2D finite element model; basic modeling assumptions were the same as in the 3D Indian 4-story residential building (Section 3.3). In figure 3.33 both curves according to AUTh method are provided as well as the one according to ROSE's method. ETABS and Seismostruct models generally predict similar yield base shear and displacement values but they differ in terms of maximum displacement. ROSE 's team's prediction

agrees well with Seismostruct based results only in terms of maximum displacement; yield displacement, as well as maximum strength, are clearly above those predicted by either method used by AUTh.

It is recalled here that the methodology used by ROSE team is very different from that used by the AUTh, i.e. the former is based on a set of empirical equations for the building period and yield displacement, whereas the latter involves detailed finite element modeling of all members, as described in Section 3.2 of this report. In view of the different approaches adopted by the two groups (either approach could be the proper choice depending on the data available for each building and the time available for deriving the capacity curves) the differences found herein are not surprising. The only noticeable difference is in the case of the bare non-seismically designed R/C frame (Figure 3.32) for which the 'generic' empirical equations of the Italian group did not capture the upper story failure mechanism discussed in the previous sections.

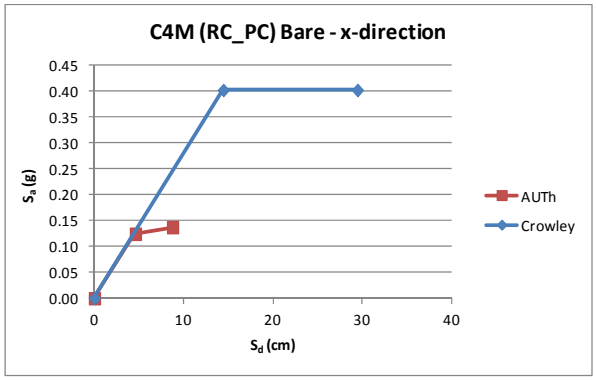

Figure 3.32 Comparisons of ROSE and AUTh capacity curves for bare Italian index frames (non-seismically designed, x-direction)

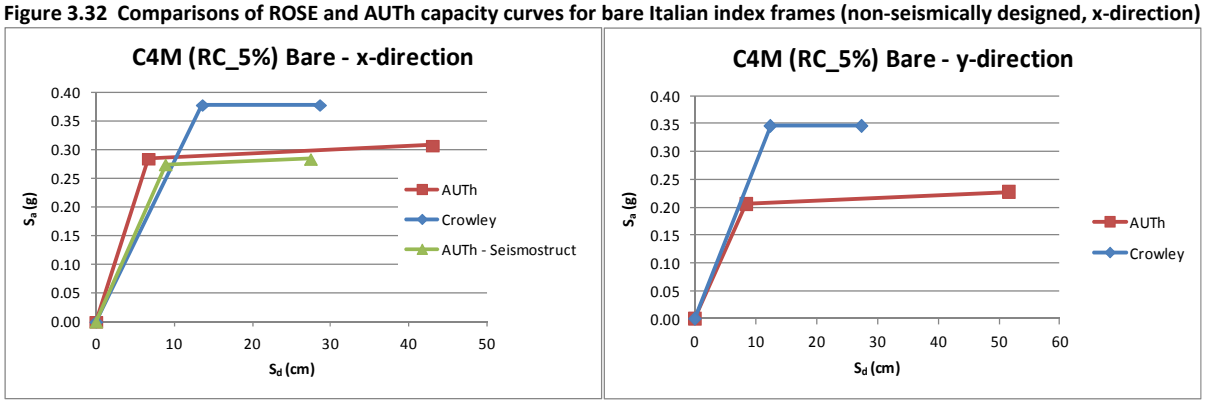

Figure 3.33 Comparisons of ROSE and AUTh capacity curves for bare Italian index frames (5%, x-direction)

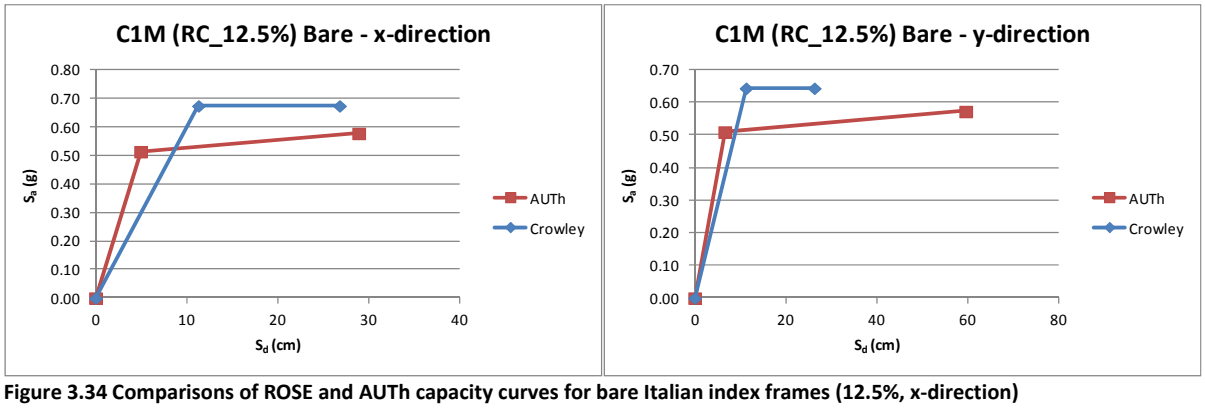

Figure 3.34 Comparisons of ROSE and AUTh capacity curves for bare Italian index frames (12.5%, x-direction)

3.4.3 Further investigation of some key assumptions

In view of the comparisons presented in this section, some additional analyses have been carried out for the Indian 2D frames, considering inferior detailing of structural members, taking into account information provided at a later stage by the Indian participants to PAGER that 135 degree stirrups are generally not provided even in highest seismic zones in India (except for some important structures).

In order to estimate the plastic rotation capacity of concrete members an approach based on the Greek Code for Structural Interventions (EPPO, 2012), which is compatible with EC8-3 but includes more up-to-date information on issues like R/C member ductility, has been adopted. This code prescribes that the ultimate concrete strain for confined elements can be estimated using the expression

$$\varepsilon_{cu}=0.0035+0.1\cdot\alpha\cdot\omega_w \tag{3.6}$$

where the confinement effectiveness coefficient (see Figure 3.35 for notation) is

$$\alpha=\left(1-\frac{s_h}{2\cdot b_c}\right)\left(1-\frac{s_h}{2\cdot h_c}\right)\left(1-\frac{\sum b_i^2}{2\cdot b_c\cdot h_c}\right) \tag{3.7}$$

and ω_w is the mechanical volumetric ratio of transverse reinforcement ($\rho_w\cdot f_{yw}/f_c$)

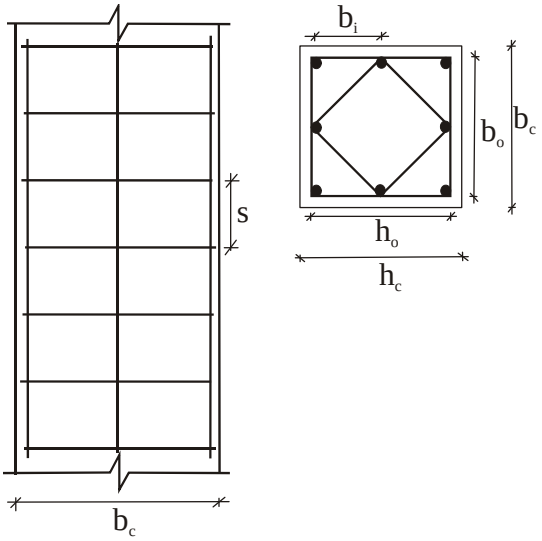

Figure 3.35 Column data for definition of confinement parameters.

The Greek Code for Structural Interventions suggests that for open stirrups confinement must be neglected, assuming $\alpha=0$. In this study, since a deterministic approach is adopted, a less conservative value was assumed for the confinement coefficient, i.e. $\alpha'=0.2\cdot\alpha$.

Using this approach the pushover analyses of the 2D Indian frames have been rerun and the corresponding normalized pushover curves are presented in figures 3.36 to 3.38. It is clear from Figs. 3.37 and 3.38 that the pushover curves estimated by Kaushik et al. do not refer to poor detailing of stirrups and, as shown in Section 3.4.1, they are closer to the curves estimated by the AUTh group assuming proper detailing of transverse reinforcement.

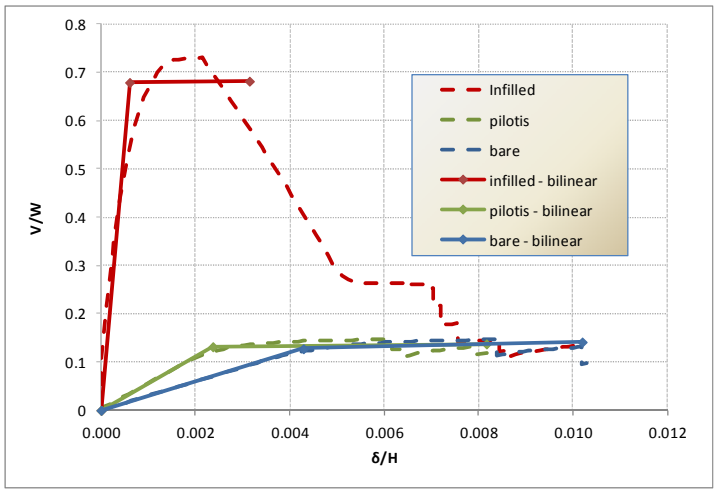

Figure 3.36 Normalized pushover curves for Indian 2D frames assuming open stirrups

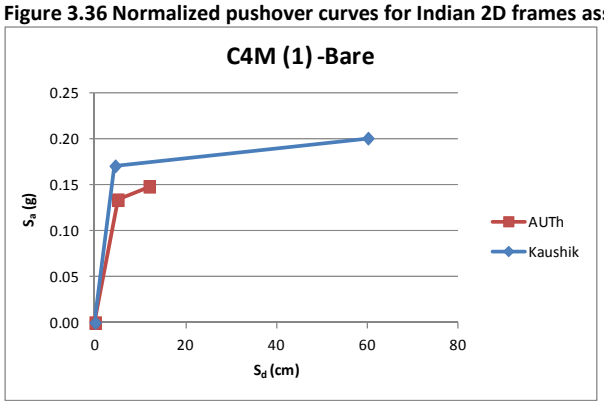

Figure 3.37 Comparisons of Kaushik et al. and AUTh capacity curves for bare Indian index frames assuming open stirrups

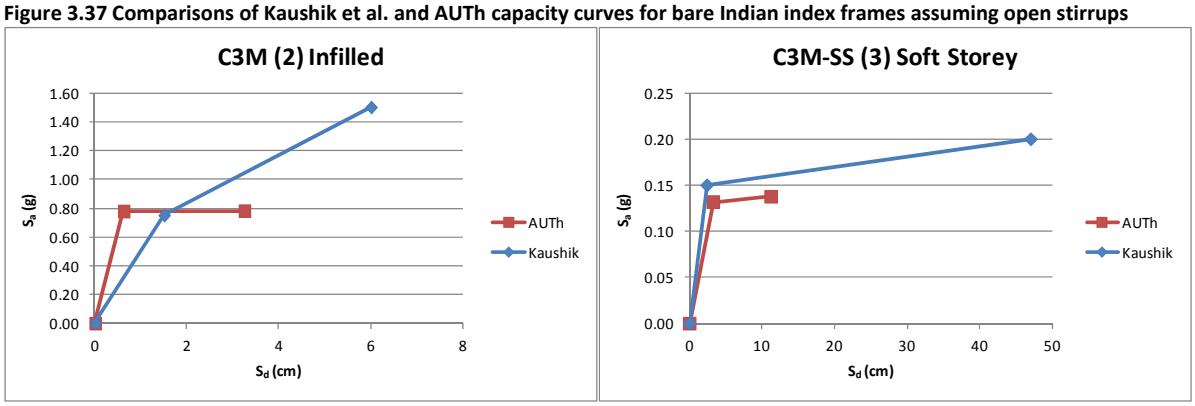

Figure 3.38 Comparisons of Kaushik et al. and AUTh capacity curves for regularly and irregularly infilled Indian index frames (f_{wc}=7.50MPa) assuming open stirrups.

3.5 Derivation of S_d-based fragility curves

3.5.1 Generalities

Fragility curves have been derived for all buildings analyzed by the AUTh team within the PAGER project. The basis for the procedure is the set of the corresponding capacity curves for each building typology, as discussed in the following. The adopted approach is purely analytical, since damage states are expressed in terms of displacements along the capacity curves derived using

nonlinear static (pushover) analysis; hence, it is different from the PGA-based hybrid approach that was developed by the AUTh research group and was used in several vulnerability studies (Kappos et al. 1997, 2006; Kappos & Panagopoulos, 2010).

3.5.2 Methodology

Assuming a lognormal distribution (as commonly done in seismic fragility studies), the conditional probability of being in or exceeding, a particular damage state ds_i, given the spectral displacement (S_d) is defined by the relationship:

$$P[ds \geq ds_i / S_d] = \Phi[\frac{1}{\beta_{ds_i}} \ln(\frac{S_d}{\overline{S}_{d,ds_i}})] \quad (3.6)$$

where:

$\overline{S}_{d,ds_i}$ is the median value of spectral displacement at which the building reaches the threshold of damage state, ds_i.

β_{dsi} is the standard deviation of the natural logarithm of spectral displacement for damage state, ds_i

Φ is the standard normal cumulative distribution function.

3.5.3 Estimation of spectral displacement median values

Each fragility curve is defined by a median value of spectral displacement that corresponds to the threshold of that damage state and by the variability associated with that damage state; these two quantities are derived as described in the following. Defining appropriate values for the damage state thresholds in terms spectral displacement (with the understanding that the actual pushover curve for a building type is reduced to an S_a vs. S_d capacity curve) involves several uncertainties, related i.a. to the qualitative definition of the damage states, the assumptions used for inelastic analysis, and the shape of the derived pushover curve (FEMA-NIBS 2003, Lagomarsino & Giovinazzi 2006, Calvi et al. 2006, Maffei et al. 2008). Tables 3.5 and 3.6 summarize the damage state thresholds in S_d terms, as well as in descriptive terms. The rationale behind using $0.7 \cdot S_{dy}$, rather than S_{dy}, as the threshold of 'slight' damage is that damage states are defined in terms of displacement values along the bilinearized capacity curves and, in general, actual yielding in some members has started well before the conventional yield point (i.e. the breaking point of the bilinear diagram). Also, it should be clarified that for structures wherein S_{du} corresponds to a drop in strength of 20% (in some structures this drop is larger) the definition of the DS5 ('collapse') threshold as S_{du} is generally a conservative assumption, i.e. vertical load carrying capacity of columns could still be maintained at this level of strength degradation, provided the drift is not excessive. Refined analysis of failure due to loss of vertical load capacity was beyond the scope of this study. Further discussion on the definition of damage states can be found in previous works of the team, e.g. Kappos et al. (2006).

It should be noted that additional considerations are necessary for dual systems, as well as masonry infilled R/C frame buildings. For the latter, especially the regularly infilled ones, since failure of infill walls can cause a significant drop in strength in the pushover and therefore the capacity curve of the structure (see figure 3.35 left), it is often noted that S_{du} of infilled structures represents the point where failure of infill walls takes place. This point cannot be considered as the collapse (DS5) of the building, thus it was assumed that this point (S_{du}) of the infilled structure

represents the threshold of DS4, while the threshold of DS5 can be taken as the S_{du} of the corresponding bare building (figure 3.35, left).

Table 3.5 Damage state description for R/C frame buildings

Damage State	Damage state label	Bare Frames Infilled frames with $S_{du,bare}<1.1 \cdot S_{du}$	Infilled frames with $S_{du,bare} \geq 1.1 \cdot S_{du}$
DS1	Slight	$0.7 \cdot S_{dy}$	
DS2	Moderate	$S_{dy} + 0.05 \cdot (S_{du} - S_{dy})$	
DS3	Substantial to heavy	$S_{dy} + (1/3) \cdot (S_{du} - S_{dy})$	$S_{dy} + (1/2) \cdot (S_{du} - S_{dy})$
DS4	Very heavy	$S_{dy} + (2/3) \cdot (S_{du} - S_{dy})$)	S_{du}
DS5	Collapse	S_{du}	$S_{du,bare}$

Nevertheless, this is not always the case for irregularly infilled (soft story layout) R/C frames. Since the collapse mechanism develops at the ground (soft) story, the strength of the building (in terms of base shear) is very close to the one of the corresponding bare frame (figure 3.35, right). Furthermore, the use of modal quantities for the transformation of the pushover curve to capacity curve, or sometimes the termination of the pushover analysis due to convergence reasons, may result in cases that $S_{du,bare}<S_{du,\text{ soft story layout}}$ (figure 3.35, right top). In this case, using the aforementioned approach the median value of DS5 would be lower than the one of DS4 which is obviously inconsistent. To avoid this inconsistency it was decided to make use of the corresponding bare frame only when $S_{du,bare} \geq 1.10 \cdot S_{du,\text{ soft story layout}}$ (figure 3.35, right bottom), otherwise the sole curve to be used in fragility analysis is that of the soft story layout, as it is done in bare frames (figure 3.35, right top).

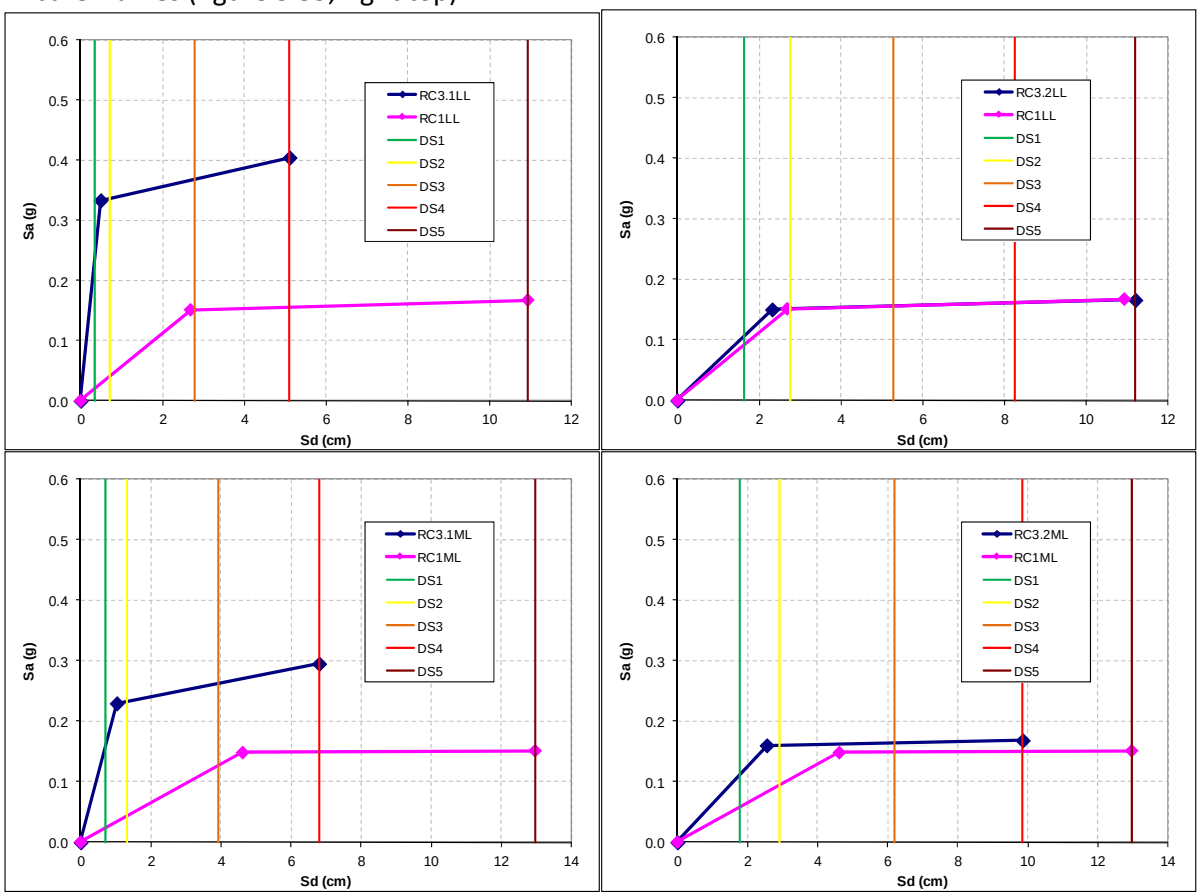

Figure 3.39 Estimation of spectral displacement thresholds for typical R/C frame buildings

For R/C dual systems the presence of infill walls is not as important as for frame systems, since the strength of the shear walls is usually significantly higher than the strength of infill panels, especially for moderate- and high-rise buildings. The end of the bilinear approximation of the pushover curve for infilled dual buildings used for the derivation of the corresponding capacity curve, calculated using the drop in strength criterion, may be reached due to the drop in strength of shear walls (Case A; figure 3.40, left) or due to failure of the infill panels (figure 3.40, right). For the first case (Case A) it is deemed to be very conservative to assume that this drop in strength is the 'complete' damage or 'collapse' level (DS5), taking also into account that the ductility of shear walls (moment – rotation or moment – curvature diagrams) is estimated using rather conservative assumptions. Therefore it was decided to use this point as the threshold for DS4 and (arbitrarily but reasonably) assume that the median value for DS5 is $S_{d,DS5}=1.3\cdot S_{d,DS4}$. It is noted that in this case the end of the capacity curves for both bare and infilled dual systems in terms of S_{du} is very close; therefore the corresponding bare typology is not utilized (figure 3.40, left). In order to automatically determine whether the S_{du} value is reached due to the drop in shear wall strength or due to failure of the infill panels, the expression $S_{du,bare}<1.10\cdot S_{du}$ has been adopted as the limit for the first case.

Table 3.6 Damage state description and spectral displacement thresholds for R/C dual buildings

Damage State	Damage state label	Bare Infilled-Case A	Infilled-Case B
DS1	Slight	$0.7\cdot S_{dy}$	
DS2	Moderate	$S_{dy} + 0.05\cdot(S_{du} - S_{dy})$	
DS3	Substantial to heavy	$S_{dy} + (1/2)\cdot(S_{du} - S_{dy})$	$0.9\cdot S_{du}$
DS4	Very heavy	S_{du}	$S_{du,bare}$
DS5	Collapse	$1.3\cdot S_{du}$	$1.3\cdot S_{du,bare}$

For the second case (i.e. S_{du} reached due to failure of the infill panels; Case B) the threshold of DS3 is estimated as a displacement slightly lower than S_{du}, taken as $S_{d,DS3}=0.9\cdot S_{du}$. For the estimation of the thresholds for DS4 and DS5 the aforementioned approach is also adopted, but in this case the S_{du} values of the corresponding bare typology are used; $S_{d,DS4}=S_{du,bare}$, $S_{d,DS5}=1.3\cdot S_{du,bare}$ (figure 3.40, left). It has to be noted that if quadrilinear capacity curves are available, the entire procedure is simplified; nevertheless, such curves are more cumbersome to use in large-scale vulnerability analyses.
The previously described procedure is presented in the flowchart of figure 3.41.

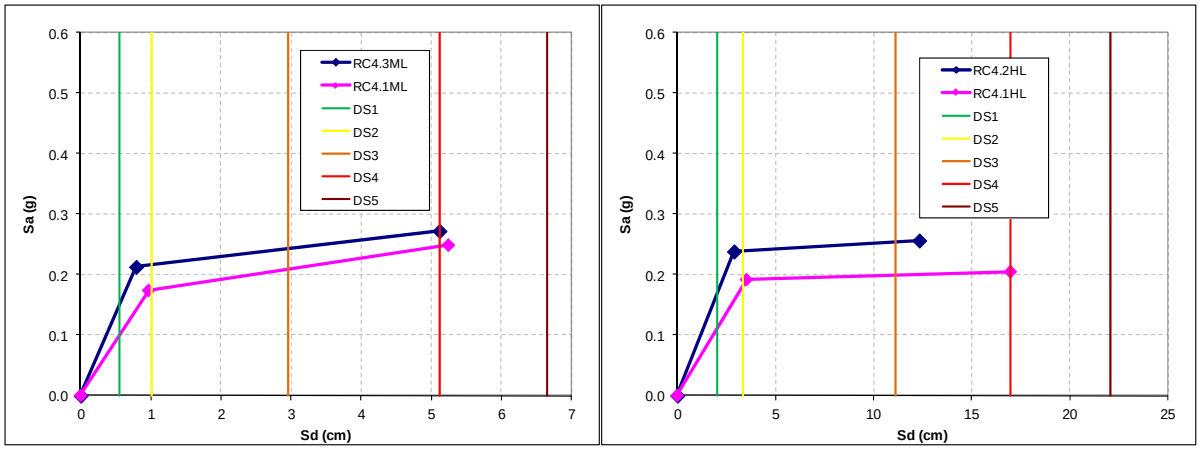

Figure 3.40 Estimation of spectral displacement thresholds for typical R/C dual buildings

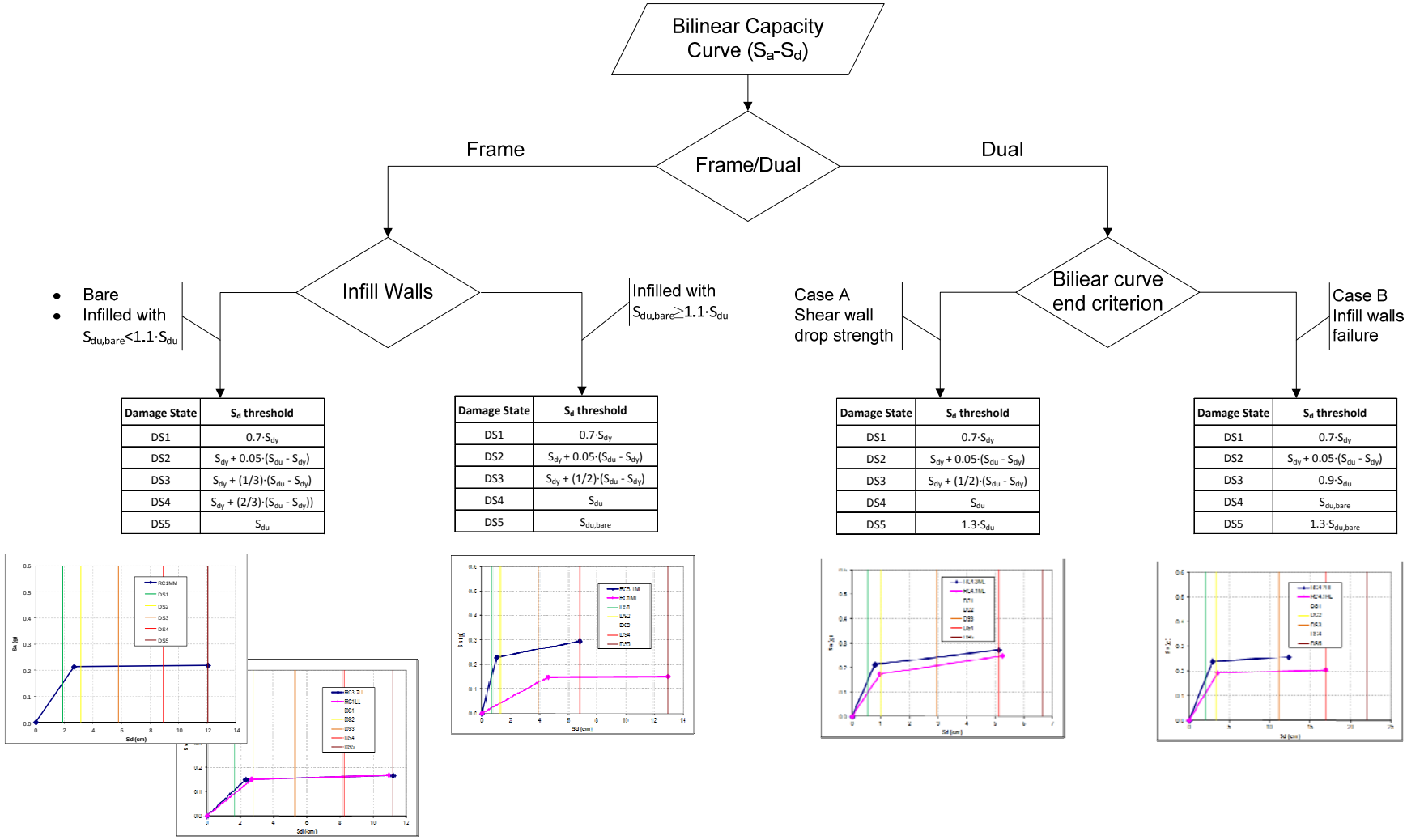

Figure 3.41 Summary of procedure for S_d threshold definition

3.5.4 Estimation of standard deviation

Lognormal standard deviation values (β) describe the total variability associated with each fragility curve. Three primary sources contribute to the total variability for any given damage state (FEMA-NIBS, 2003), namely the variability associated with the discrete threshold of each damage state which is defined using damage indices $\beta_{T,ds}$, the variability associated with the capacity curve of each structural type β_C, and finally the variability in the demand imposed on the structure by the earthquake ground motion β_D. Assuming independence of each source of variability (which is not entirely true), the total variability in the fragility curve can be estimated using the following expression:

$$\beta = \sqrt{\beta_C^2 + \beta_D^2 + \beta_{T,ds}^2} \tag{3.7}$$

In the present study fragility curves were derived from the corresponding capacity curves for a single analysis of each building typology, therefore the variability in fragility curve damage states has not been specifically addressed. Average values adopted from the literature (FEMA-NIBS, 2003) or previous studies of the AUTh group (Kappos & Panagopoulos, 2010) have been used as follows:

- Buildings designed to old codes: β=0.75
- Buildings designed to moderate codes: β=0.70
- Buildings designed to modern codes: β=0.65

It is noted that β-values for all damage states are taken as constant for each building type. This was done on purpose, because if the (generally) different variability associated with each damage state is taken into account, unrealistic fragility curves (for instance, intersecting) result in cases where median values are closely spaced.

3.5.5 Results

Using the aforementioned procedure and the capacity curves derived during the previous phases of the PAGER project for all building typologies, the fragility curves presented in the following sections have been derived.

Table 3.7 Fragility curve parameters for Greek buildings (S_d in cm)

Typology	DS1	DS2	DS3	DS4	DS5	β
C4L (RC1LL)	1.88	3.10	5.43	8.18	10.93	0.75
C3L (RC3.1LL)	0.34	0.72	2.80	5.11	10.93	0.75
C3L-SS (RC3.2LL)	1.62	2.76	5.28	8.24	11.20	0.75
C4M (RC1ML)	3.23	5.04	7.40	10.18	12.96	0.75
C3M (RC3.1ML)	0.72	1.32	3.91	6.80	12.96	0.75
C3M-SS (RC3.2ML)	1.78	2.91	6.20	9.85	12.96	0.75
C4H (RC1HL)	4.80	7.22	9.31	11.77	14.23	0.75
C3H (RC3.1HL)	2.35	3.79	7.68	12.00	14.23	0.75
C3H-SS (RC3.2HL)	2.88	4.46	7.59	11.06	14.23	0.75
C1L (RC1LH)	2.24	4.87	14.29	25.37	36.46	0.65
C1L-I (RC3.1LH)	0.70	1.22	3.20	5.40	36.46	0.65
C1L-SS (RC3.2LH)	1.71	4.21	14.26	26.08	37.91	0.65
C1M (RC1MH)	2.60	5.59	16.24	28.76	41.28	0.65
C1M-I (RC3.1MH)	1.10	1.83	4.13	6.68	41.28	0.65
C1M-SS (RC3.2MH)	1.79	4.03	17.30	32.04	41.28	0.65
C1H (RC1HH)	4.96	8.60	17.14	27.19	37.25	0.65
C1H-I (RC3.1HH)	2.72	4.48	9.86	15.84	37.25	0.65
C1H-SS (RC3.2HH)	3.28	5.66	14.44	24.19	37.25	0.65

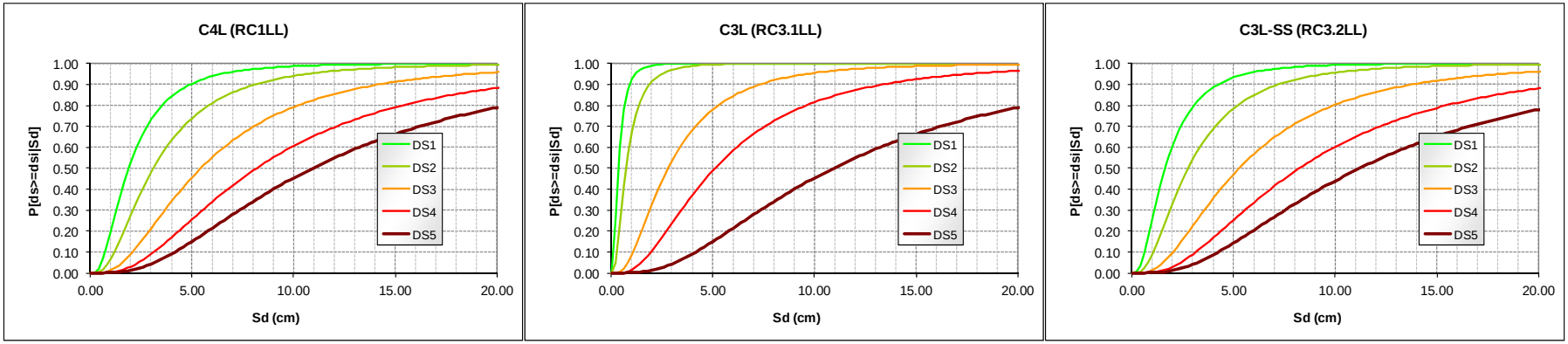

Figure 3.42 Fragility curves for low-rise, low-code R/C frame buildings

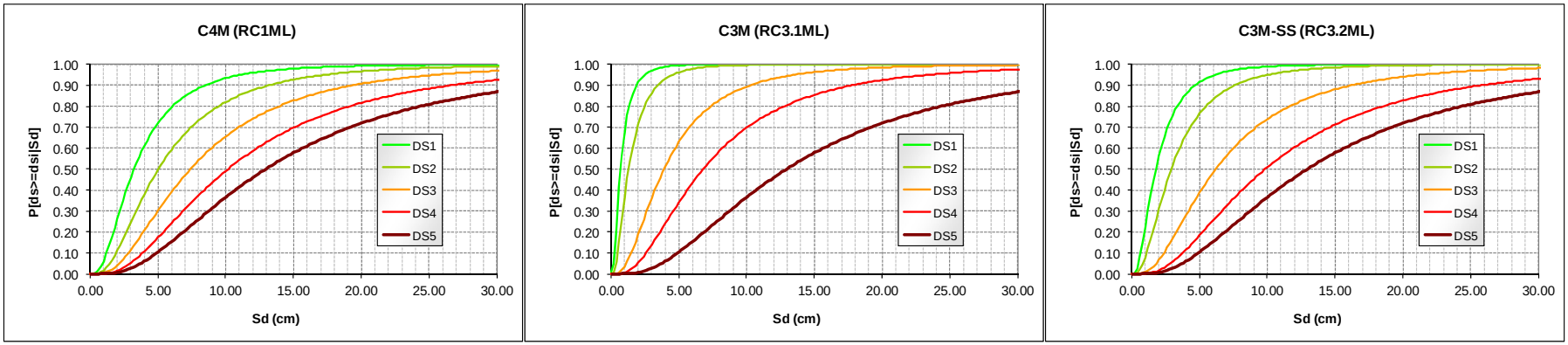

Figure 3.43 Fragility curves for medium-rise, low-code R/C frame buildings

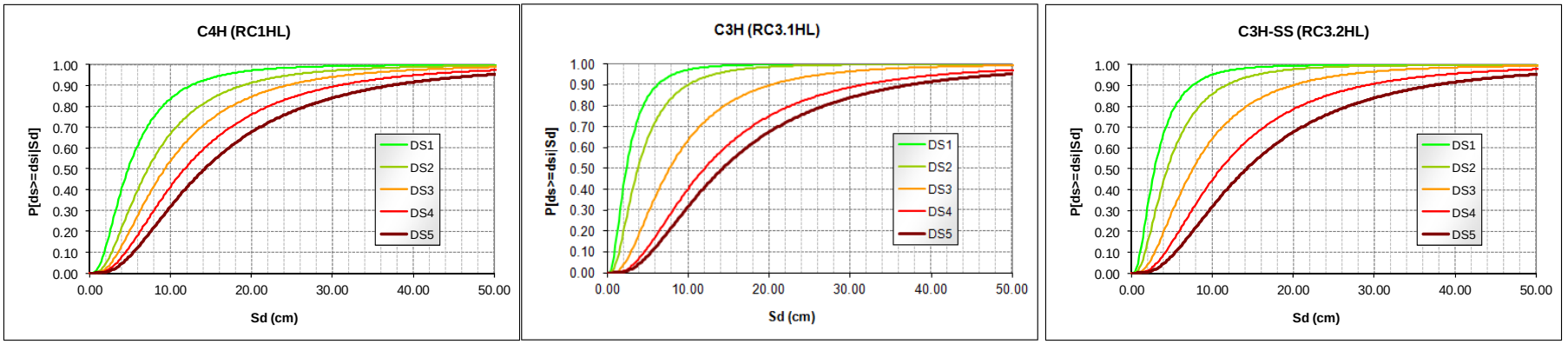

Figure 3.44 Fragility curves for high-rise, low-code R/C frame buildings

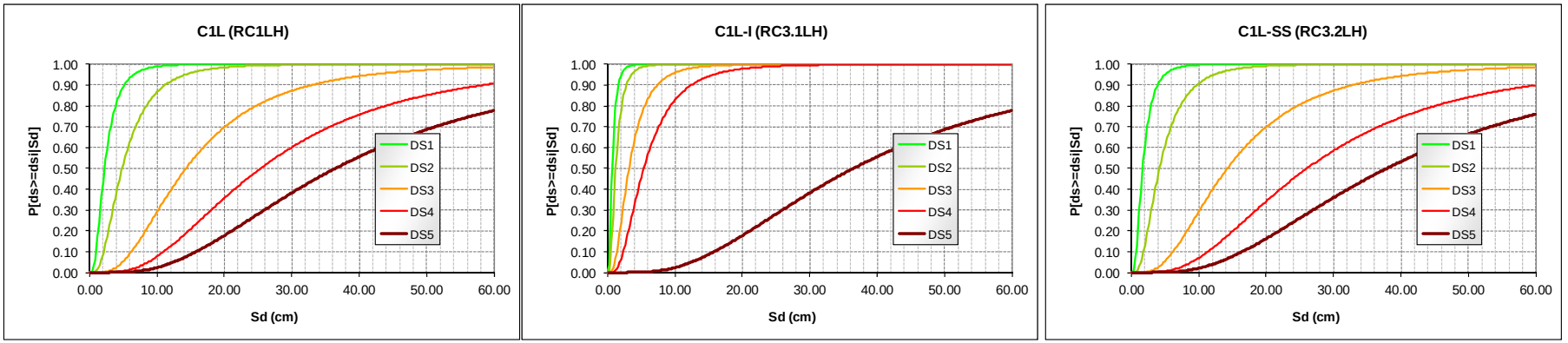

Figure 3.45 Fragility curves for low-rise, high-code R/C frame buildings

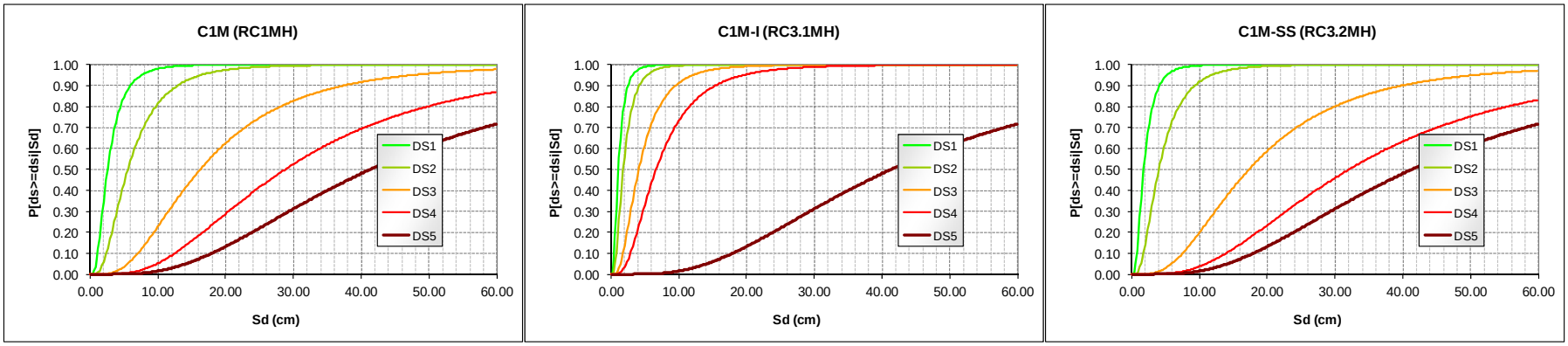

Figure 3.46 Fragility curves for medium-rise, high-code R/C frame buildings

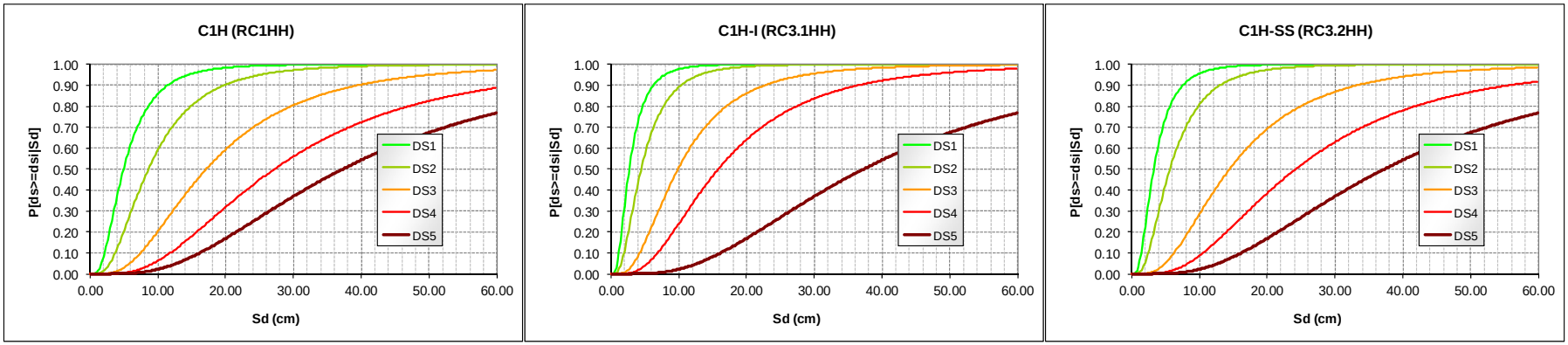

Figure 3.47 Fragility curves for high-rise, high-code R/C frame buildings

Index buildings from India

Using the same procedure, Table 3.8 presents the fragility curve parameters for Indian buildings. For the 2D frame buildings fragility curves adopting f_{wc}=7.5MPa have been used (see Section 3.3.1). For the 3D residential buildings, different sets of fragility curves have been derived based on the corresponding capacity curves according to the direction of the loading; for practical analysis the most critical curve (irrespective of direction) should be adopted for each damage state. In the absence of more specific information, the standard deviation values assumed for 'old' Greek buildings are also used herein.

Table 3.8 Fragility curve parameters for Indian buildings (S_d in cm)

Typology	DS1	DS2	DS3	DS4	DS5	β
C4M (1) - Bare	3.89	10.53	38.78	72.00	105.23	0.75
C3M (2) - Infilled	0.43	0.75	1.93	3.25	105.23	0.75
C3M-SS (3) - Soft Story	2.43	9.08	40.84	78.22	115.59	0.75
C4M bare X	6.42	11.60	25.38	41.59	57.80	0.75
C3M (9) - Infilled X	5.96	9.67	20.01	31.50	57.80	0.75
C3M-SS (10) - Soft Story X	2.38	4.31	12.50	21.60	57.80	0.75
C4M bare +Y	6.87	12.17	25.48	41.14	56.80	0.75
C3M (9) - Infilled +Y	4.51	8.70	28.93	51.40	56.80	0.75
C3M-SS (10) - Soft Story +Y	4.98	8.73	23.35	39.60	56.80	0.75
C4M bare -Y	6.48	11.88	26.74	44.22	61.70	0.75
C3M (9) - Infilled -Y	4.52	8.92	31.03	55.60	61.70	0.75
C3M-SS (10) - Soft Story -Y	5.73	9.81	24.39	40.60	61.70	0.75

It is noted that in the infilled frames substantial loss in strength takes place for small displacement values (e.g. see Figure 3.12), hence the associated damage states (DS1 to DS4) have low thresholds, whereas DS5 starts at a large displacement value, since for this DS the bare frame value ($S_{du,bare}$) is taken as the threshold; as discussed in Section 3.3, these not very convincing values are due to the very high level of confinement assumed by Kaushik et al. for this 'old' building type (very closely spaced stirrups).

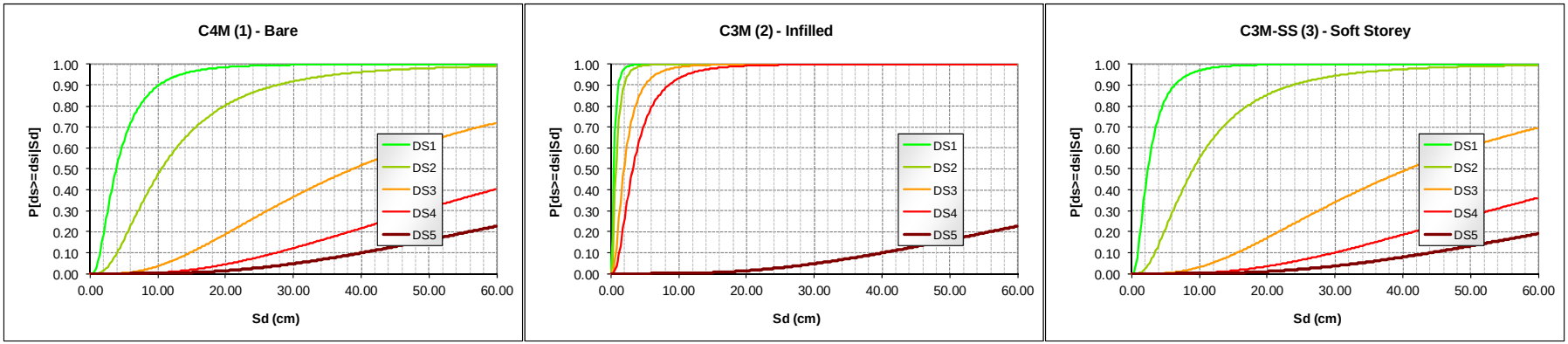

Figure 3.48 Fragility curves for Indian 4-story 2D frames

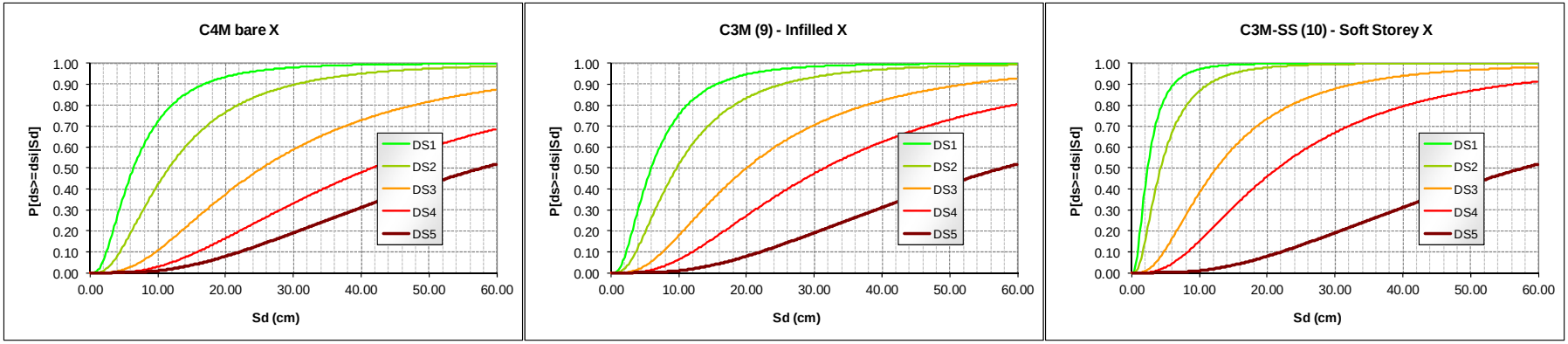

Figure 3.49 Fragility curves for Indian 4-story residential buildings (3D analysis, X direction)

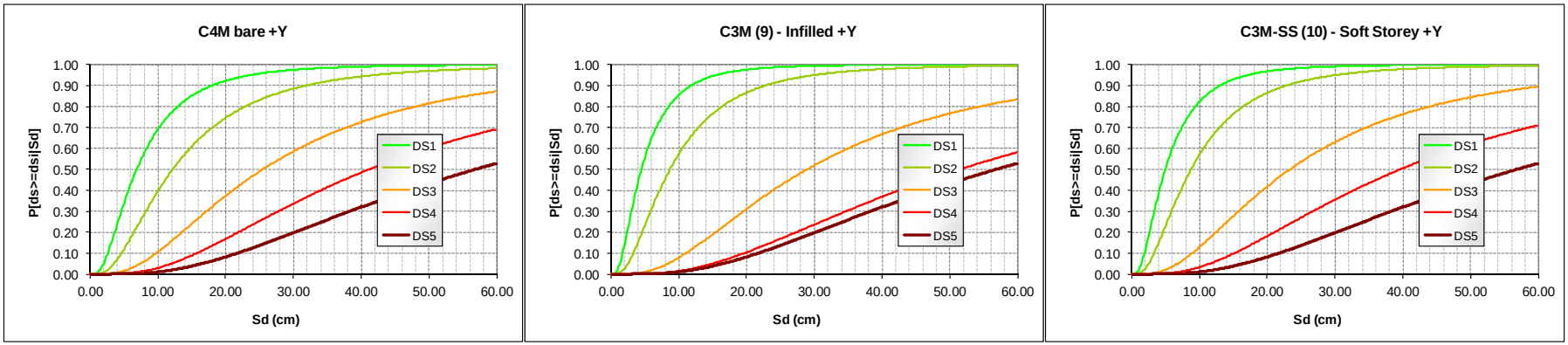

Figure 3.50 Fragility curves for Indian 4-story residential buildings (3D analysis, +Y direction)

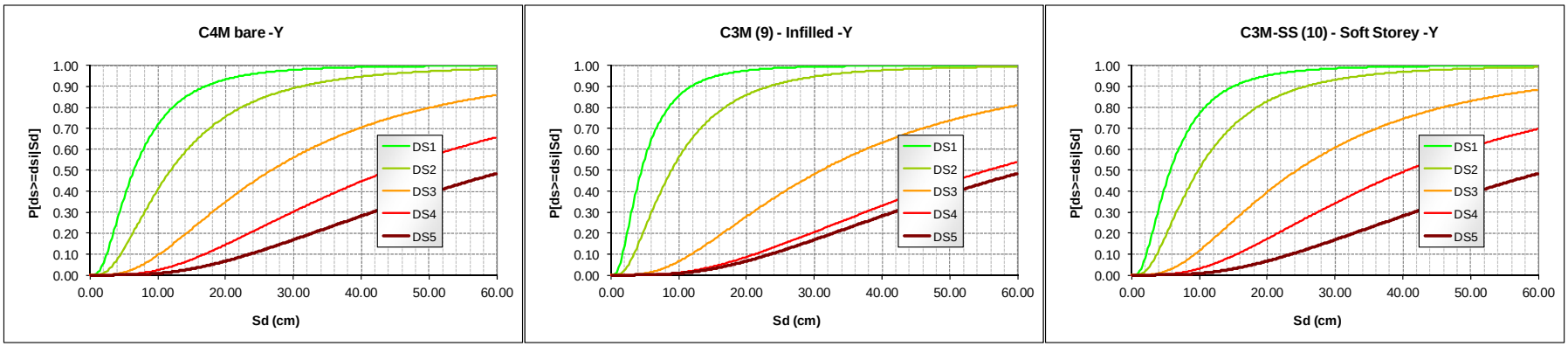

Figure 3.51 Fragility curves for Indian 4-story residential buildings (3D analysis, -Y direction)

Index buildings from Italy

Table 3.9 lists the fragility curve parameters for the Italian buildings (analyzed in Section 3.3.2). As for the Indian buildings, different sets of fragility curves have been derived based on the corresponding capacity curves according to the direction of the loading, although the Italian capacity curves were based on 2D pushover analysis in each direction. In the absence of more specific information, the standard deviation values assumed for the analogous Greek buildings (Low and Moderate Code) are also used herein.

Table 3.9 Fragility curve parameters for Italian buildings (S_d in cm)

Typology	DS1	DS2	DS3	DS4	DS5	β
C4M (RC_PC) X	3.21	4.79	5.96	7.35	8.73	0.75
C3M (RC_PC) X	0.73	1.30	3.54	6.03	8.73	0.75
C3M-SS (RC_PC) X	1.84	2.94	4.70	6.76	8.83	0.75
C4M (RC_5%) X	4.69	8.52	18.80	30.91	43.01	0.70
C3M (RC_5%) X	2.32	3.77	7.96	12.61	43.01	0.70
C3M-SS (RC_5%) X	2.44	4.02	8.85	14.22	43.01	0.70
C4M (RC_12.5%) X	3.46	6.15	12.94	20.92	28.91	0.70
C3M (RC_12.5%) X	2.56	4.18	8.93	14.20	28.91	0.70
C3M-SS (RC_12.5%) X	2.56	4.19	9.08	14.51	28.91	0.70
C4M bare (RC_5%) Y	5.91	10.61	22.84	37.24	51.63	0.70
C3M (RC_5%) Y	1.34	2.39	6.70	11.50	51.63	0.70
C3M-SS (RC_5%) Y	2.28	3.88	9.47	15.67	51.63	0.70
C4M bare (RC_12.5%) Y	4.64	9.28	24.28	41.92	59.57	0.70
C3M (RC_12.5%) Y	2.58	4.15	8.41	13.15	59.57	0.70
C3M-SS (RC_12.5%) Y	2.58	4.18	8.66	13.64	59.57	0.70

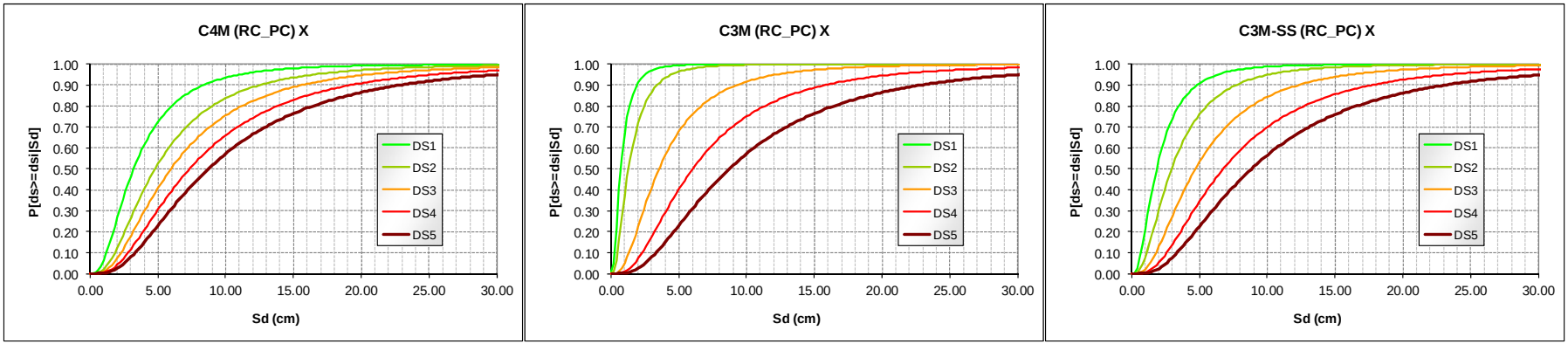

Figure 3.52 Fragility curves for bare, infilled and soft story layout Italian frames (no seismic design, x-direction)

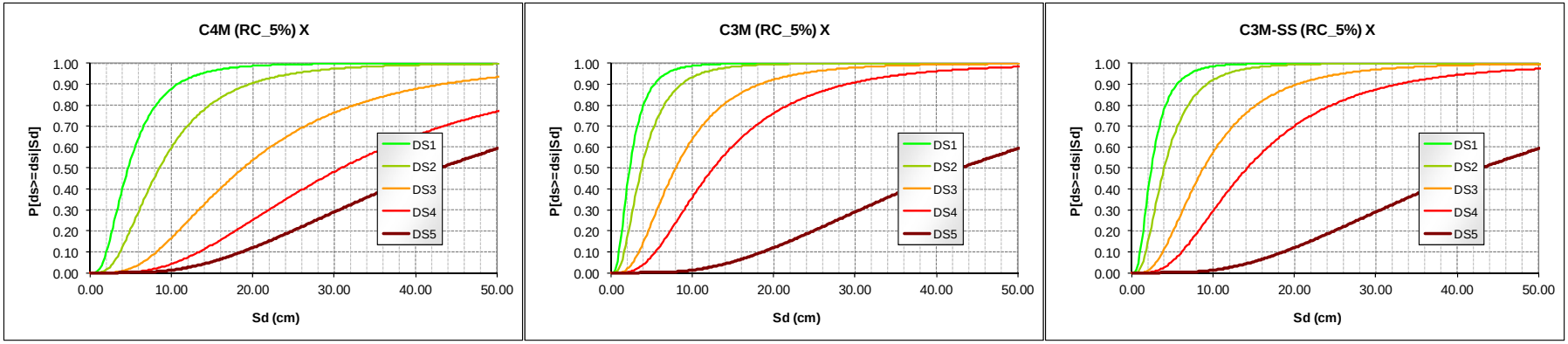

Figure 3.53 Fragility curves for bare, infilled and soft story layout Italian frames (5%, x-direction)

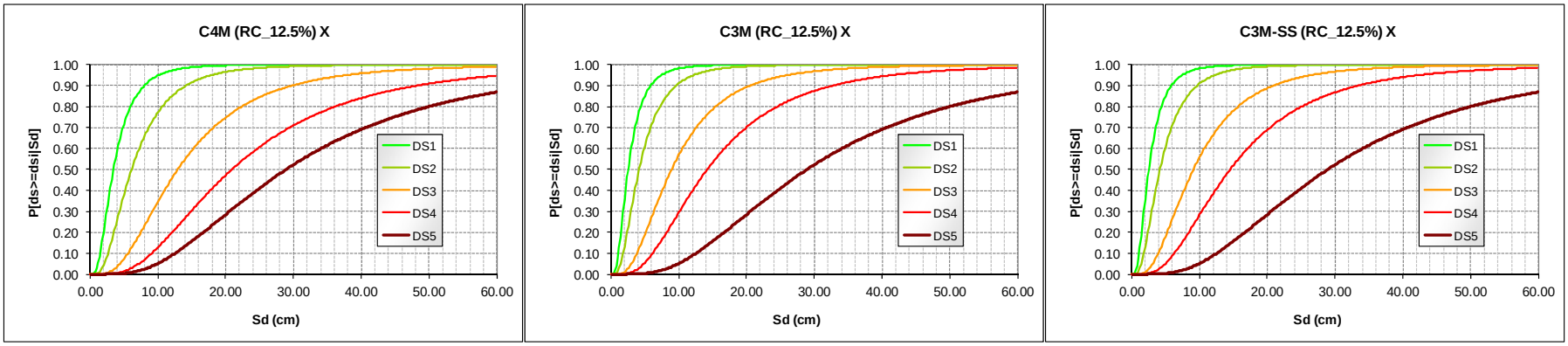

Figure 3.54 Fragility curves for bare, infilled and soft story layout Italian frames (12.5%, x-direction)

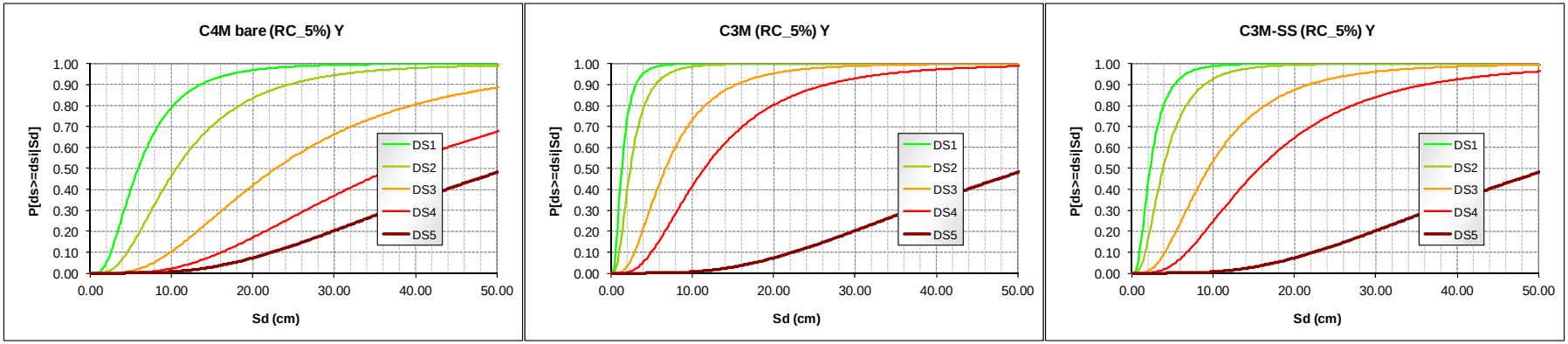

Figure 3.55 Fragility curves for bare, infilled and soft story layout Italian frames (5%, y-direction)

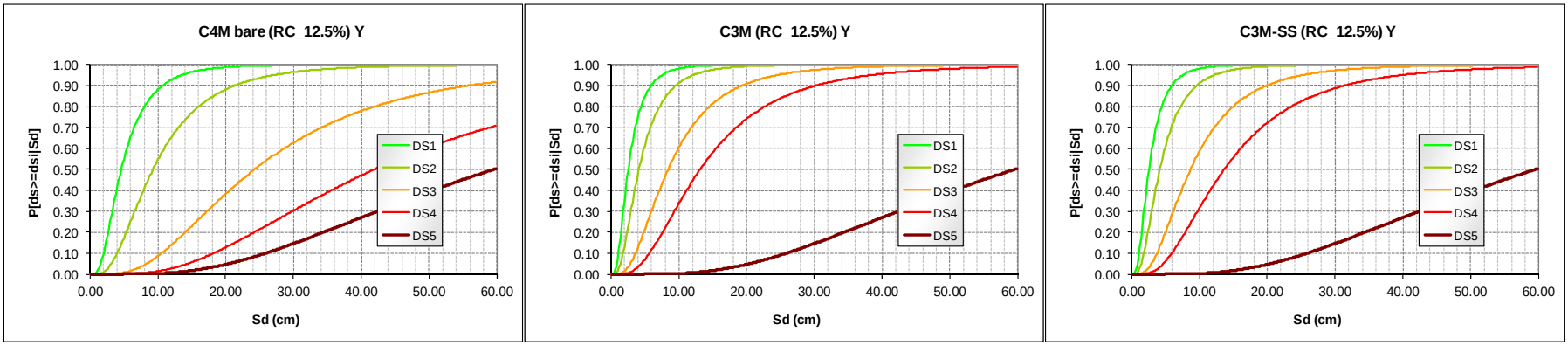

Figure 3.56 Fragility curves for bare, infilled and soft story layout Italian frames (12.5%, y-direction)

4. Application of FaMIVE methodology to masonry typologies from Turkey

Dina D'Ayala[4] & Emre Kishali[5]

4.1 Introduction

For the computation of capacity curves for masonry structures a number of procedures are available in literature. These are based either on the equivalent frame approach or on the mechanism approach. Among the first, in the past decade a relatively significant number of procedures aimed at defining reliable analytical vulnerability function for masonry structures in urban context have been published (Lang and Bachmann (2004), Erberik (2008), Borzi et al. (2008), Erdik et al. (2003)). Although they share similar conceptual hypotheses they differ substantially by modelling complexity, numerical complexity, geographic validity of the model, treatment of uncertainties. Far fewer are the approaches based on mechanical behavior, and among those it is worth mentioning VULNUS (Bernardini et al., 2000) and FaMIVE (D'Ayala & Speranza 2003).

This report presents the comparison in terms of capacity curves of results obtained by applying the procedure FaMIVE and the METU procedure, to data provided by METU and relevant to masonry structures in Turkey (Erberik 2008, Erberik 2010), as indicated in section 1.2. The residential building stock in Turkey is still largely dominated by masonry construction both in rural and urban areas. For the present study METU provided data and description of index buildings for the following PAGER structure typologies: adobe (A1), rubble stone masonry in mud mortar with earth or metal roof (RS2), massive stone masonry in lime mortar with timber floors (MS), unreinforced bricks in mud mortar (UFB1), unreinforced bricks in cement mortar with timber floors (UFB4), unreinforced bricks in cement mortar with reinforced concrete floors (UFB5) and unreinforced concrete blocks in lime/cement mortar (UCB). For each typology typical values of a set of geometric parameters were provided as shown in Table 4.1., together with a set of photos representing typical cases for each class.

The pictorial information allowed deriving further parameters, not included in the numerical dataset but essential to conduct the analysis using FaMIVE, i.enumber and layout of openings, number of stories, and other more specific construction details like the presence of timber bands in rubble construction. The full set of construction typologies sub-classes analyzed is listed in Table 4.2. In the following sections the procedure used by FaMIVE to obtain capacity curves is presented in detail. The rationale used to derive additional input data is discussed and the results are presented in terms of capacity curves, and fragility curves for three limit states are derived for each typology.

[4] Dept. of Architecture and civil Engineering, University of Bath
[5] Faculty of Architecture and Design, University of Kocaeli

Table 4.1 : Parameters by typology as provided by Erberik.

Parameter	Type (A1) - Adobe block, mud mortar, wood roof and floors	Type (RS2) - Rubble stone masonry with mud mortar + earth, or metal roof.	Type (MS) - Massive stone masonry in lime or cement mortar	Type (UFB1) - Unreinforced brick masonry in mud mortar without timber posts	Type (UFB4) - Unreinforced brick masonry in cement mortar with timber floors	Type (UFB5) - Unreinforced brick masonry in cement mortar with rc floors	Type (UCB) - Unreinforced concrete block masonry in lime / cement mortar
Wall dimensions (length/height/thickness)	3.5 / 2.35 / 0.6 m	3.6 / 2.5 / 0.5 m	3.4 / 2.6 / 0.6 m	4.3 / 2.65 / 0.2 m	4.5 / 2.8 / 0.3 m	4.7 / 2.85 / 0.3 m	4.7 / 2.7 / 0.2 m
Wall compression strength	0.4 MPa	1-2 MPa	3-4 MPa	3-4 MPa	6-7 MPa	6-7 MPa	2-3 MPa
Door opening dimensions (width/height)	0.8 / 1.8 m	0.85 / 1.9 m	0.85 / 1.95 m	0.9 / 2.0 m	0.9 / 2.1 m	0.9 / 2.2 m	0.9 / 1.9 m
Window opening dimensions (width/height)	0.9 / 1.05 m	1.0 / 1.2 m	0.9 / 1.0 m	1.3 / 1.1 m	1.3 / 1.3 m	1.4 / 1.4 m	1.25 / 1.25 m
Unit dimensions in mm	120*250*300	Variable	Variable	190*190*135, 190*290*135	190*190*135, 190*290*135	190*190*135, 190*290*135	300*190*190
Type of horizontal structures	Timber	Timber	Timber	Timber	RC	RC	RC
Wall-to-wall connections	Weak	Weak	Weak	Moderate	Good	Good	Moderate
Wall-to-floor connections	Weak	Weak	Weak	Moderate	Moderate	Good	Moderate
Maintenance	Poor	Poor	Poor - Moderate	Poor	Moderate	Moderate	Moderate
Comments	Very common in rural areas	Very common in rural areas	Common both in rural and urban areas	Both in rural and urban regions	Both in rural and urban regions	Very common in urban centers	Cellular hollow units not allowed by the Earthquake Code.

Table 4.2 Set of the building typologies analyzed with FaMIVE method

Structure	Detail	Location	Model	Researcher
A1	Adobe masonry, single story, timber floors, 2 openings on façade	Turkey	FaMIVE	D'Ayala & Kishali
A1	Adobe masonry, single story, timber floors, 3 openings on façade	Turkey	FaMIVE	D'Ayala & Kishali
RS2	Rubble stone masonry, single story, timber floors, 2 openings on façade	Turkey	FaMIVE	D'Ayala & Kishali
RS2	Rubble stone masonry, single story, timber floors, 3 openings on façade	Turkey	FaMIVE	D'Ayala & Kishali
RS2	Rubble stone masonry, two story, timber floors, 2+2 openings on façade	Turkey	FaMIVE	D'Ayala & Kishali
RS2	Rubble stone masonry, two story, timber floors, 2+2 openings on façade with timber bands	Turkey	FaMIVE	D'Ayala & Kishali
RS2	Rubble stone masonry, two story, timber floors, 2+3 openings on façade	Turkey	FaMIVE	D'Ayala & Kishali
RS2	Rubble stone masonry, two story, timber floors, 2+3 openings on façade with timber bands	Turkey	FaMIVE	D'Ayala & Kishali
MS	Massive stone masonry, two story, timber floors, 2+2 opening on façade	Turkey	FaMIVE	D'Ayala & Kishali

UFB1	Unreinforced brick masonry, single story, mud mortar, timber floors, 2 openings on façade	Turkey	FaMIVE	D'Ayala & Kishali
UFB1	Unreinforced brick masonry, single story, mud mortar, timber floors, 3 openings on façade	Turkey	FaMIVE	D'Ayala & Kishali
UFB1	Unreinforced brick masonry, two story, mud mortar, timber floors, 2+3 openings on façade	Turkey	FaMIVE	D'Ayala & Kishali
UFB4	Unreinforced brick masonry, single story, cement mortar, timber floors, 2 openings on façade	Turkey	FaMIVE	D'Ayala & Kishali
UFB4	Unreinforced brick masonry, two story, cement mortar, timber floors, 2+2 openings on façade	Turkey	FaMIVE	D'Ayala & Kishali
UFB4	Unreinforced brick masonry, two story, cement mortar, timber floors, 3+2 openings on façade	Turkey	FaMIVE	D'Ayala & Kishali
UFB5	Unreinforced brick masonry, two story, cement mortar, concrete floors, 2+2 openings on façade	Turkey	FaMIVE	D'Ayala & Kishali
UCB	Unreinforced concrete block masonry, two story, lime/cement mortar, reinforced concrete floors, 2+3 openings	Turkey	FaMIVE	D'Ayala & Kishali
UCB	Unreinforced concrete block masonry, three story, lime/cement mortar, reinforced concrete floors, 3+2+2 openings	Turkey	FaMIVE	D'Ayala & Kishali

4.2 Methodology for the derivation of the capacity curves

The program FaMIVE is based on a limit state determined by the mechanical analysis of the external bearing walls forming a masonry building. The analysis is static equivalent and aims to predict the lateral load collapse multiplier (expressed in g) which will trigger the onset of a specific failure mechanism. The procedure is based on a lower bound approach and the detailed analytical developments for a suite of possible mechanisms are reported in D'Ayala & Speranza (2003) for out of plane mechanisms and in D'Ayala & Casapulla (2006) for in plane failures. The possibility of occurrence of different mechanisms is dependent on the geometric configuration of each analyzed wall or façade of the building and its connections to the other structural elements (vertical and horizontal structures). In order to evaluate the vulnerability of the building, among all possible mechanisms computed for each façade, the procedure chooses the one that shows the worst combination between minimum collapse load factor and maximum extent of façade involved in the collapse according to an algorithm described in D'Ayala & Speranza(2002). On this basis, it is possible to produce a prediction of possible damage modes and levels of vulnerability for individual or groups of buildings, in relation to expected levels of shaking at the site. Application of the procedure to sites in Turkey and Italy are reported in (D'Ayala, 2005) and (D'Ayala and Paganoni, 2011).

Although the collapse load factor might be sufficient to generate fragility curves based on lateral capacity only, in order to obtain performance points, a complete capacity curve for each building or façade analyzed needs to be developed. This allows assessing and predicting levels of damage given a specific demand spectrum, once performance points and damage states are correlated along the capacity curve. To this end the results obtained with the limit analysis and the mechanism approach need to be recast in the framework of the capacity spectrum method by associating an elasto-plastic capacity curve to each mechanism and then further manipulating this to obtain the equivalent SDOF bilinear curve, in the space Sa-Sd.

In the FaMIVE procedure capacity curves are developed by calculating first the effective stiffness for a wall K_{eff}: this is a function of the type of mechanism attained, the geometry of the wall and layout of the opening, the constraints to other walls and floors, and the portion of other walls involved in the mechanism:

$$K_{eff} = k_1 \frac{E_t I_{eff}}{H_{eff}^3} + k_2 \frac{E_t A_{eff}}{H_{eff}} \tag{4.1}$$

where H_{eff} is the height of the portion involved in the mechanism, E_t is the estimated elastic modulus of the masonry as it can be obtained from experimental literature, I_{eff} and A_{eff} are the second moment of area and the cross sectional area, respectively, calculated taking into account extent and position of openings and variation of thickness over height, k_1 and k_2 are constants which assume different values depending on edge constraints and whether shear and/or flexural stiffness are relevant for the specific mechanism.
Next, the effective mass involved in the mechanism is calculated following the same approach:

$$\Omega_{eff} = V_{eff}\delta_m + \Omega_f + \Omega_r \tag{4.2}$$

where V_{eff} is the solid volume of the portion of wall involved in the mechanism, δ_m is the density of the masonry Ω_f, Ω_r are the masses of the horizontal structures involved in the mechanism.
Effective mass and effective stiffness are used to calculate a natural period T_{eff}, which characterise an equivalent single degree of freedom (SDOF) oscillator. The mass is applied at the height of the center of gravity of the collapsing portion with respect to the ground and a constant acceleration distribution over the wall height is assumed. The significant points of the capacity curve can be computed as follows. The elastic limit acceleration A_y is identified as the combination of lateral and gravitational load that will cause a triangular distribution of compression stresses at the base of the overturning portion, just before the onset of partialization. This can be calculated as:

$$A_y = \frac{t_b^2}{6h_0} g \quad \text{with corresponding displacement } \Delta_y = \frac{A_y}{4\pi^2} T_{eff} \tag{4.3}$$

where t_b is the effective thickness of the wall at the base of the overturning portion, h_o is the height of the overturning portion, and T_{eff} the natural period of the equivalent SDOF oscillator. For in-plane mechanisms a similar equation is applied assuming a compressive strut in each pier with t_b and h_o equal to the width of the strut and the interstory height, respectively. The next point on the pushover curve corresponds to the conditions of maximum lateral capacity A_u:

$$A_u = \frac{\lambda_c}{\alpha_1} \tag{4.4}$$

where λ_c is the load collapse multiplier of the collapse mechanism calculated by FaMIVE, and α_1 is the proportion of total mass participating in the mechanism. This is calculated as the ratio of the mass of the façade and sides or internal walls and floor involved in the mechanism, to the total mass of the involved macroelements (walls, floors, and roof). The displacement corresponding to the peak lateral force, Δ_u is

$$3\Delta_y \leq \Delta_u \leq 6\Delta_y \tag{4.5}$$

as suggested by Tomaževič (2007). Given the different types of binders and masonry materials, Equation 4.5 depicts the lower bound chosen for adobe, rubble stone and brickwork in mud mortar, while the upper bound has been used for massive stone, brickwork and concrete blockwork set in cement mortar, to account for the variation in integrity of the masonry under ultimate loads.
Finally the near collapse condition is determined by the displacement Δ_{nc} identified by the condition of loss of vertical equilibrium which, for overturning mechanisms, can be computed as a lateral displacement at the top or for in plane mechanism by the loss of overlap of two units in successive courses:

$$\Delta_{nc} = t_b/3 \text{ or } \Delta_{nc} = l/2 \tag{4.6}$$

where t_b is the thickness at the base of the overturning portion and l is the typical length of units forming the wall.

Figure 4.1 shows a pictorial flow chart of the entire procedure up to the derivation of fragility functions using performance points and the N2 approach (Fajfar 1999) for the derivation of the non-linear spectrum.

In order to compare capacity and demand displacement, in this application the elastic demand spectrum is generated following the Turkish Earthquake Code (TEC 2007). The elastic spectral acceleration coefficient is defined according to the code by assuming the effective ground acceleration local site class Z4 and hence the effective ground acceleration coefficient, $A_0 = 0.3$; the building importance factor is set as I = 1. From this reference elastic design spectrum, the nonlinear response spectra can be produced for different values of ductility, according to the following procedure. For a given value of ductility (μ) the reduction factor can be calculated as follows:

$$R = \begin{cases} c_1(\mu - 1)\dfrac{T}{T_g} + 1 & if \ \dfrac{T}{T_g} \leq 1 \\ c_1(\mu - 1) + 1 & if \ \dfrac{T}{T_g} > 1 \end{cases} \tag{4.7}$$

The reduction factor depends on ductility (μ), period (T), transition period (T_g) and the type of non-linear material constitutive model for the equivalent SDOF. In this case $c_1 = 1$ (D'Ayala, 2005).
The displacement amplification factor (S_{dur}) is taken equal to the formulation of factor C1 in FEMA 356 (FEMA 1999), i.e the modification factor that relates expected maximum inelastic displacements to displacement calculated for linear elastic response:

$$S_{dur} = \begin{cases} \dfrac{\left[1 + (R-1)T_g/T\right]}{R} & if \ T < T_g \\ 1 & if \ T > T_g \end{cases} \tag{4.8}$$

The authors are aware of the proposed changes for C1 in FEMA440 (ATC 2005), however the new formulation is strictly related to soil conditions, and sufficient information for this application is

lacking to determine the most appropriate value of the coefficient as proposed by FEMA440 (ATC 2005).

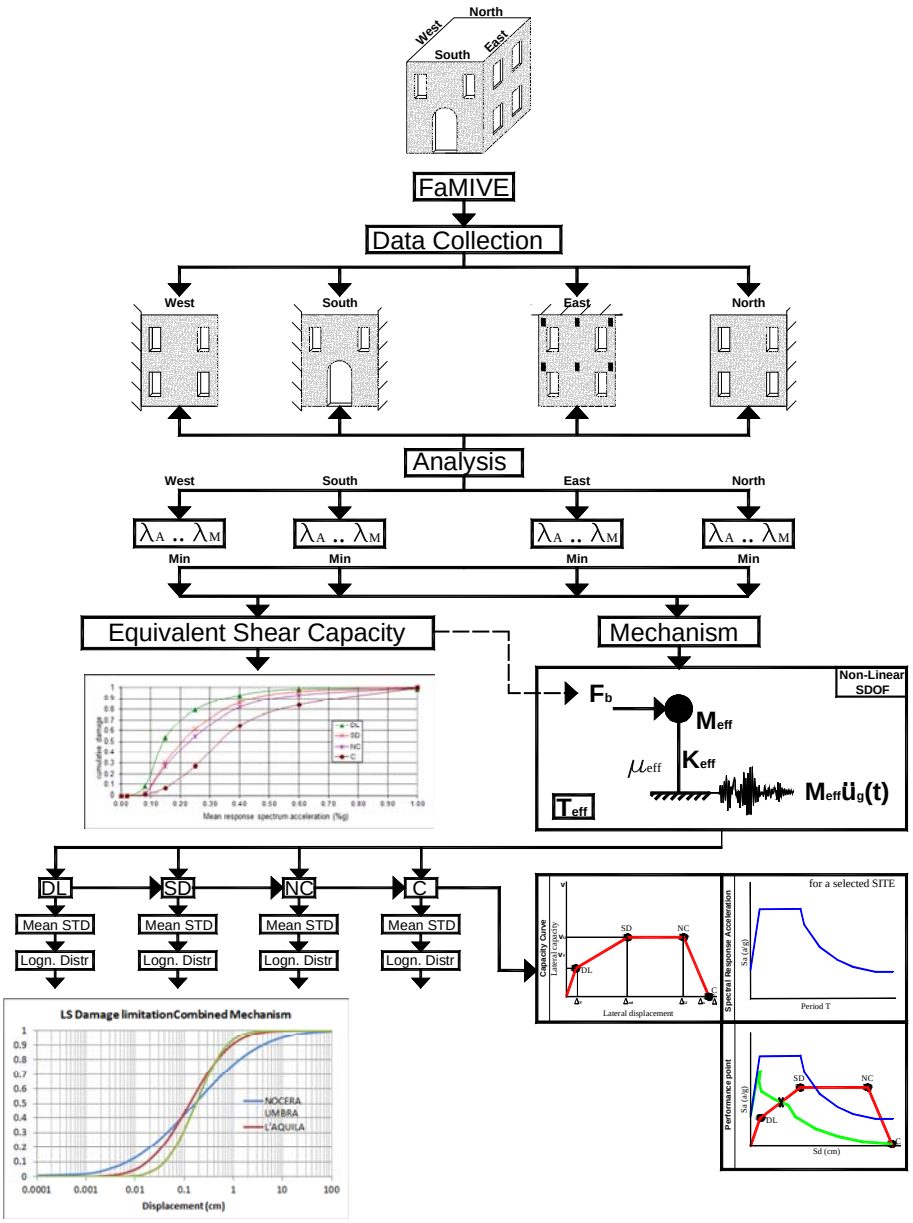

Figure 4.1 Conceptual flowchart of the FaMIVE procedure from data collection to fragility functions.

4.3 Data input and data generation for use in FaMIVE

Seven masonry typologies with different unit type, binders and horizontal structures are studied and the corresponding capacity curves are computed. For each masonry typology METU provided typical or range values for a number of basic parameters as summarised in Table 4.1.
Two issues arise in relation to the application of FaMIVE to this data set. The first issue is that as stated earlier mechanisms and associated collapse load factor are affected by the geometric parameters and their relative variability in a way that is not immediately quantifiable in a single function. So a number of permutations of the parameters need to be generated to define the range

of existence of each mechanism and the associated collapse load multipliers. The second issue is that information is missing for some of the assumptions at the basis of the FaMIVE algorithm.
To tackle the first issue, using a Random Number Generation (RNG) approach, hundreds of random parameters per building typology were sampled, considering a set range of variability. The parameters sampled were the height and width of the wall. The mean values and standard deviation in each RNG set were calculated, and then the minimum and maximum values determined by considering the average value μ provided by the reference data and the standard deviation σ obtained through the RNG.

In order to validate the normal distribution of the ranges so created, these were compared to previous data, collected from 200 houses in the district of Fener–Balat, Istanbul (D'Ayala, 2005) by direct survey. Approximately 182 elevations of this dataset, with 2 stories and 2 openings were considered for the comparison with the generated distributions. The normal distributions of the parameters are calculated according to:

$$f(x, \mu, \sigma) = \frac{1}{\sqrt{2\pi\sigma^2}} e^{-\left[\frac{(x-\mu)^2}{2\sigma^2}\right]} \quad (4.9)$$

The houses in the Fener – Balat district have structural characteristics pertaining to the UFB typologies of the current study with a variety of floor structures. Figure 4.2 shows that both the height of wall and width of wall parameter in Fener - Balat present a greater spread than the range obtained for the sample typologies for the current work, however it overlaps the range of both UFB1 and UFB5 which represent the extremes of brickwork masonry typologies analyzed. It should be noted that the average width of the façade in the Fener –Balat sample is smaller, as it is related to a very densely built urban context, while the distribution obtained on the basis of METU's data relate to both urban and non-urban contexts.

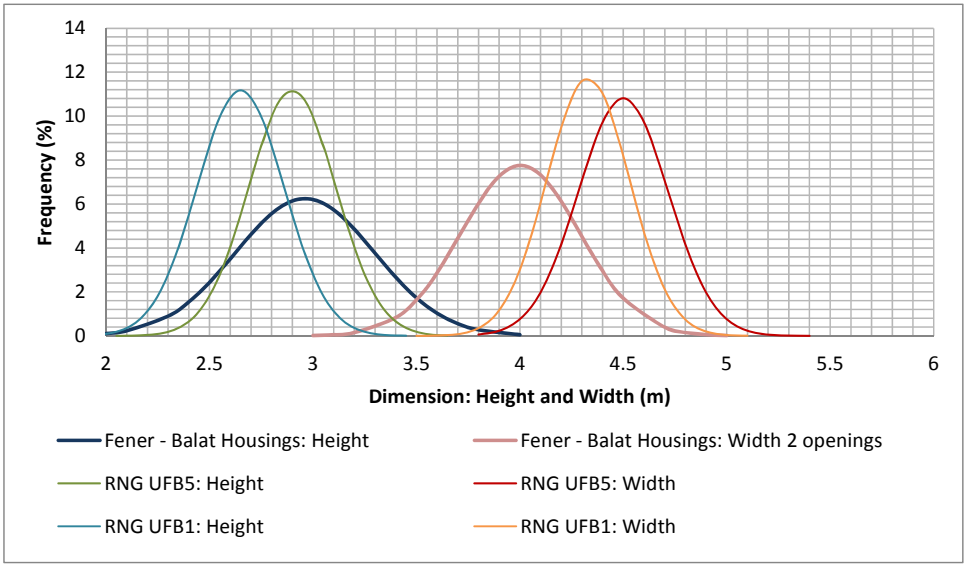

Figure 4.2: Normal distributions of RNG and Fener – Balat samples for height and width of two story façades.

Average, minimum and maximum values calculated by equation (4.9) from RNG were selected to generate the input data for FaMIVE analysis. With these variables of width and height of façade,

nine different combinations are generated for each typology as seen in Tables 4.3 to 4.8. The variability of the thickness of the walls was not accounted for by the RNG analysis, rather, as in FaMIVE the effective structural thickness of the wall is associated to the level of maintenance of the fabric and three different qualitative levels are considered (good, medium, and bad), with corresponding increasing percentage reduction of the geometric value, three different values of effective thickness can be generated. The typical wall thickness indicated by METU's is associated to a good level of maintenance, and this value is reduced by 10% and 25% for medium and bad maintenance level, respectively. Hence by simply varying the geometry of the wall as stated and by varying the thickness, 27 permutations for each typology could be generated. The size of the opening was maintained constant, as it is the size of the units forming the wall, as these are known to be fairly standard within a given typology and regional setting.

The second issue mentioned above relates to the fact that the minimum set of data needed for the application of the FaMIVE procedure is larger than the set provided by METU, as can be seen in Figure 4.3 and these parameters cannot be ignored as they influence both the out-of-plane and in-plane behavior of the façades and whether one would occur in preference over the other. These conditions are discussed in turn.

The relative size of pier to opening has a strong influence on the value of collapse load factor, in particular whether the edge piers are wider or narrower than the opening dimensions (defined as regular or irregular in FaMIVE's form, respectively). However this information is not provided in the original set of data. Hence both cases are considered in the analysis for each permutation. A variable number of opening per story is also considered, ranging from 1 to 3, resulting in different piers geometric ratios and hence in different shear capacity ratio. The distribution of openings also has a consequence on the continuity and width of the piers. As no specific information could be obtained, a regular vertically and horizontally aligned distribution was assumed.

The direction of spanning of the horizontal structure defines whether the analyzed wall is or not load-bearing, but also whether it can be restrained or not in its out-of-plane deflection by the floor or roof structure. This affects values of collapse load factor, the extent of mass involved in collapse, and lateral drift. For each geometric permutation both loadbearing and non-loadbearing conditions are considered.

The edge connection of façades with adjacent structural vertical elements is the parameter indicating presence or absence of box behavior and influencing the formation of different collapse mechanisms and associated values of collapse multipliers. An indication of the quality of the connection is provided by METU, but in the sample both condition of full and no connections are considered. This affects the initial effective stiffness, the effective mass, and the ultimate drift. Finally single, two or three stories high buildings are considered.

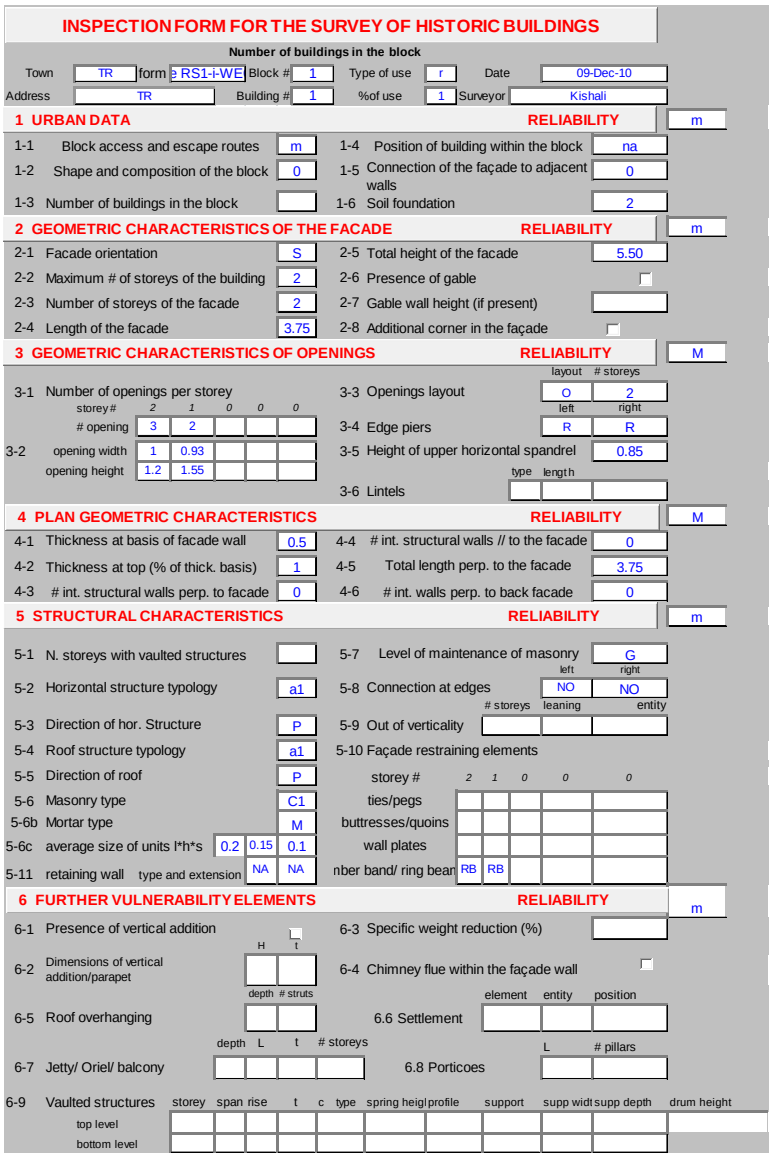

Figure 4.3 Input data screen with typical input requirements for the WHE_PAGER Phase IV FaMIVE application

Considering the various permutations arising from these further assumptions for each of the typologies analyzed about 650 cases are generated leading to a sample of sufficient size to conduct statistical regression analysis and derive fragility curves which can be meaningful. Sketches of each façade typology with the layout of windows are shown in Table 4.9. It should be noted that in general, given the width of façades and openings' dimensions provided by METU the resulting masonry piers are rather slender with relatively deep spandrels, somewhat in contrast with data analysis reported in Erberik (2008). This is reflected in the overall lateral collapse load multipliers and drift capacity.

Table 4.3 Basic data used in FaMIVE to compute capacity curves of adobe masonry structures

Adobe A1	RNG type	Wall dimensions (length/height/thickness)			Door opening (L/H)	Window opening (L/H)	Masonry unit dimension (L*W*H)	Type of horizontal structure
Average value	Type A1-a	3,35	2,2	0,6	0.8/1.8	0.9/1.05	250*300*120	Timber
	Type A1-b	3,35	2,35	0,6	0.8/1.8	0.9/1.05	250*300*120	Timber
	Type A1-c	3,35	2,5	0,6	0.8/1.8	0.9/1.05	250*300*120	Timber
	Type A1-d	3,5	2,2	0,6	0.8/1.8	0.9/1.05	250*300*120	Timber
	Type A1-e	3,5	2,35	0,6	0.8/1.8	0.9/1.05	250*300*120	Timber
	Type A1-f	3,5	2,5	0,6	0.8/1.8	0.9/1.05	250*300*120	Timber
	Type A1-g	3,7	2,2	0,6	0.8/1.8	0.9/1.05	250*300*120	Timber
	Type A1-h	3,7	2,35	0,6	0.8/1.8	0.9/1.05	250*300*120	Timber
	Type A1-i	3,7	2,5	0,6	0.8/1.8	0.9/1.05	250*300*120	Timber

Table 4.4 Basic data used in FaMIVE to compute capacity curves of rubble stone masonry structures

RS2	Typology	Wall dimensions (length/height/thickness)			Door opening (L/H)	Window opening (L/H)	Masonry unit dimension (L*W*H)	Type of horizontal structure
Average value	Type RS2-a	3,25	2,15	0,5	0.85/1.9	1/1.2	200*150*150	Timber
	Type RS2-b	3,25	2,5	0,5	0.85/1.9	1/1.2	200*150*150	Timber
	Type RS2-c	3,25	2,75	0,5	0.85/1.9	1/1.2	200*150*150	Timber
	Type RS2-d	3,5	2,15	0,5	0.85/1.9	1/1.2	200*150*150	Timber
	Type RS2-e	3,5	2,5	0,5	0.85/1.9	1/1.2	200*150*150	Timber
	Type RS2-f	3,5	2,75	0,5	0.85/1.9	1/1.2	200*150*150	Timber
	Type RS2-g	3,75	2,15	0,5	0.85/1.9	1/1.2	200*150*150	Timber
	Type RS2-h	3,75	2,5	0,5	0.85/1.9	1/1.2	200*150*150	Timber
	Type RS2-i	3,75	2,75	0,5	0.85/1.9	1/1.2	200*150*150	Timber

Table 4.5 Basic data used in FaMIVE to compute capacity curves of unreinforced brick masonry (UFB2) structures

UFB1	Typology	Wall dimensions (length/height/thickness)			Door opening (L/H)	Window opening (L/H)	Masonry unit dimension (L*W*H)	Type of horizontal str
Average value	Type UFB1-a	4,1	2,45	0,2	0.9/2.0	1.3/1.1	190*190*135	Timber
	Type UFB1-b	4,1	2,65	0,2	0.9/2.0	1.3/1.1	190*190*135	Timber
	Type UFB1-c	4,1	2,9	0,2	0.9/2.0	1.3/1.1	190*190*135	Timber
	Type UFB1-d	4,3	2,45	0,2	0.9/2.0	1.3/1.1	190*190*135	Timber
	Type UFB1-e	4,3	2,65	0,2	0.9/2.0	1.3/1.1	190*190*135	Timber
	Type UFB1-f	4,3	2,9	0,2	0.9/2.0	1.3/1.1	190*190*135	Timber
	Type UFB1-g	4,55	2,45	0,2	0.9/2.0	1.3/1.1	190*190*135	Timber
	Type UFB1-h	4,55	2,65	0,2	0.9/2.0	1.3/1.1	190*190*135	Timber
	Type UFB1-i	4,55	2,9	0,2	0.9/2.1	1.3/1.2	190*190*135	Timber

Table 4.6 Basic data used in FaMIVE to compute capacity curves of unreinforced brick masonry (UFB3) structures

UFB4	Typology	Wall dimensions (length/height/thickness)			Door opening (L/H)	Window opening (L/H)	Masonry unit dimension (L*W*H)	Type of horizontal str
Average value	Type UFB4-a	4,3	2,6	0,3	0.9/2.1	1.3/1.3	290*190*135	Timber
	Type UFB4-b	4,3	2,8	0,3	0.9/2.1	1.3/1.3	290*190*135	Timber
	Type UFB4-c	4,3	3,05	0,3	0.9/2.1	1.3/1.3	290*190*135	Timber
	Type UFB4-d	4,5	2,6	0,3	0.9/2.1	1.3/1.3	290*190*135	Timber
	Type UFB4-e	4,5	2,8	0,3	0.9/2.1	1.3/1.3	290*190*135	Timber
	Type UFB4-f	4,5	3,05	0,3	0.9/2.1	1.3/1.3	290*190*135	Timber
	Type UFB4-g	4,7	2,6	0,3	0.9/2.1	1.3/1.3	290*190*135	Timber
	Type UFB4-h	4,7	2,8	0,3	0.9/2.1	1.3/1.3	290*190*135	Timber
	Type UFB4-i	4,7	3,05	0,3	0.9/2.1	1.3/1.3	290*190*135	Timber

Table 4.7 Basic data used in FaMIVE to compute capacity curves of unreinforced brick masonry (UFB4) structures

UFB5	Typology	Wall dimensions (length/height/thickness)			Door opening (L/H)	Window opening (L/H)	Masonry unit dimension (L*W*H)	Type of horizontal str
Average value	Type UFB5-a	4,5	2,65	0,3	0.9/2.2	1.4/1.4	290*190*135	RC
	Type UFB5-b	4,5	2,85	0,3	0.9/2.2	1.4/1.4	290*190*135	RC
	Type UFB5-c	4,5	3,1	0,3	0.9/2.2	1.4/1.4	290*190*135	RC
	Type UFB5-d	4,7	2,65	0,3	0.9/2.2	1.4/1.4	290*190*135	RC
	Type UFB5-e	4,7	2,85	0,3	0.9/2.2	1.4/1.4	290*190*135	RC
	Type UFB5-f	4,7	3,1	0,3	0.9/2.2	1.4/1.4	290*190*135	RC
	Type UFB5-g	4,9	2,65	0,3	0.9/2.2	1.4/1.4	290*190*135	RC
	Type UFB5-h	4,9	2,85	0,3	0.9/2.2	1.4/1.4	290*190*135	RC
	Type UFB5-i	4,9	3,1	0,3	0.9/2.2	1.4/1.4	290*190*135	RC

Table 4.8 Basic data used in FaMIVE to compute capacity curves of unreinforced brick masonry (UCB) structures

UCB	Typology	Wall dimensions (length/height/thickness)			Door opening (L/H)	Window opening (L/H)	Masonry unit dimension (L*W*H)	Type of horizontal str
Average value	Type UCB-a	4,5	2,5	0,2	0.9/1.9	1.25/1.25	300*290*190	RC
	Type UCB-b	4,5	2,7	0,2	0.9/1.9	1.25/1.25	300*290*190	RC
	Type UCB-c	4,5	2,95	0,2	0.9/1.9	1.25/1.25	300*290*190	RC
	Type UCB-d	4,7	2,5	0,2	0.9/1.9	1.25/1.25	300*290*190	RC
	Type UCB-e	4,7	2,7	0,2	0.9/1.9	1.25/1.25	300*290*190	RC
	Type UCB-f	4,7	2,95	0,2	0.9/1.9	1.25/1.25	300*290*190	RC
	Type UCB-g	4,95	2,5	0,2	0.9/1.9	1.25/1.25	300*290*190	RC
	Type UCB-h	4,95	2,7	0,2	0.9/1.9	1.25/1.25	300*290*190	RC
	Type UCB-i	4,95	2,95	0,2	0.9/1.9	1.25/1.25	300*290*190	RC

Table 4.9 Sketches of masonry facades for each typology with distribution of openings

Adobe (A1)	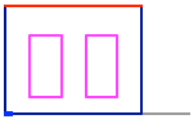	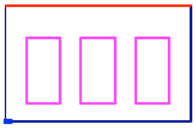		
Rubble (RS2)	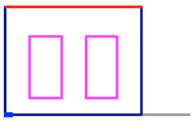	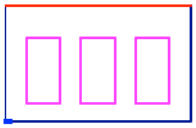	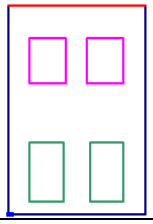	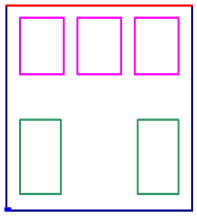
UFB1	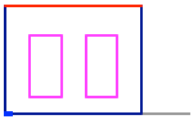	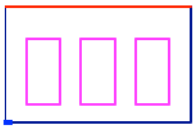	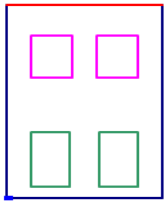	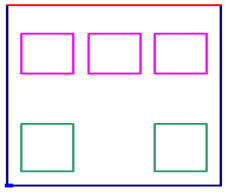
UFB4			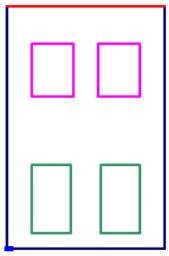	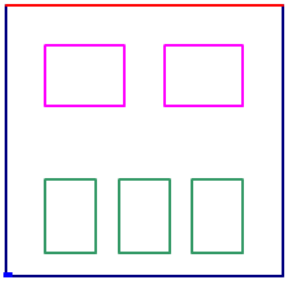
UFB5				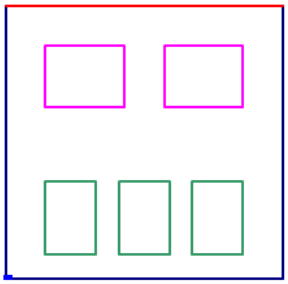
UCB			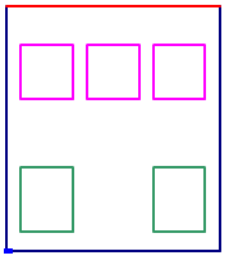	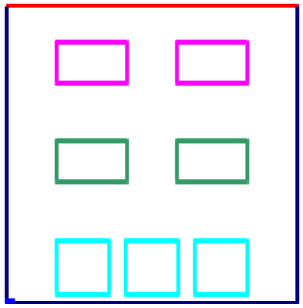

4.4 Results

The analysis shows that the above parameters lead for each typology to results that have substantial variation, not just in terms of collapse load multiplier, but also in terms of critical mechanism and hence in terms of the corresponding capacity curves. For this reason it has been chosen here to provide for each typology, the four capacity curves which yield either maximum or minimum base shear capacity or maximum or minimum ultimate displacement. The results are presented in tabulated format in Table 4.10.

Table 4.10 Capacity curve results for masonry structures.

Structure Group	Layout characteristics	Connections*** and Maintenance**	A_U	D_Y (cm)	D_u(cm)	Choosing criterion	Failure Mechanism
A1	1 story - 2 open. LB	G G	0.28	4.27	12.81	Max Au	E
A1	1 story - 3 open. NLB	B B	0.22	6.29	18.88	Max. Du	A
A1	1 story – 2 open. NLB	B B	0.14	4.36	13.08	Min. Au	D
A1	1 story – 2 open. LB	G G	0.23	0.88	5.26	Min Du	H2
RS2*	1 story – 2 open. LB*	B G	0.29	0.17	1.024	Max Au	A
RS2*	2 stories – 2+2 open. LB*	B B	0.14	8.56	17.11	Max Du	A
RS2*	2 stories – 2+3 open. NLB*	B B	0.17	0.71	4.23	Min Du	A
RS2	2 stories – 2+3 open. LB	G G	0.19	1.63	4.89	Max Au	D
RS2	2 stories – 2+3 open. NLB	B B	0.07	4.81	14.41	Min. Au	D
RS2	1 story – 2 open. LB TB	G G	0.38	1.41	4.23	Max Au	F
RS2*	2 stories-2+3 open NLB TB*	B B	0.17	3.09	9.28	Min. Au	H2
RS2	2 stories-2+3 open NLB TB	B G	0.21	0.60	3.58	Min Du	H2
MS	2story 2+2 open. LB	G G	0.37	1.69	5.08	Max Au	B2
MS	2story 2+2 open. LB	B B	0.12	1.41	3.53	Min. Au	A
MS	2story 2+2 open.N LB	B B	0.13	2.31	5.77	Max Du	D
MS	2story 2+2 open. NLB	G B	0.27	0.58	3.47	Min Du	H2
UFB1	2 stories – 3+2 open. NLB	B-G	0.35	2.57	7.70	Max Au	H2
UFB1	1 story – 2 open NLB	B-M	0.21	3.15	9.46	Max. Du	A
UFB1	2 stories – 3+2 open NLB	B-M	0.13	5.63	11.26	Min. Au	A
UFB1	1 story – 3 open. NLB	B B	0.17	0.70	2.11	Min. Du	A
UFB4	1 story – 2 open. LB	G-G	0.53	0.21	1.27	Max Au	B2
UFB4	2 stories – 2+3 open. LB	B B	0.14	10.90	21.79	Max. Du	D
UFB4	2 stories – 2+2 open. NLB	B M	0.10	4.67	14.01	Min. Au	A
UFB4	2 stories – 2+3 open. LB	B G	0.20	0.16	0.97	Min. Du	A
UFB5	2 stories – 3+2 open. NLB	G G	0.44	2.90	7.25	Max Au	B2
UFB5	2 stories – 3+2 open. LB	B-B	0.39	9.74	19.48	Max. Du	A
UFB5	2 stories – 3+2 open. NLB	B M	0.24	4.33	10.83	Min. Au	A
UFB5	2 stories – 3+2 open. LB	G G	0.37	0.27	1.62	Min. Du	C
UCB	3 stories - NLB	G G	0.32	3.16	7.90	Max Au	B2
UCB	3 stories - LB	B B	0.17	3.95	11.86	Max. Du	D
UCB	3 stories - NLB	B G	0.09	2.84	8.53	Min. Au	D
UCB	2 stories - NLB	B G	0.14	2.01	6.04	Min. Du	D

**Rubble stone masonry with poor unit (200*150*150 mm), in the other case unit dimension is (300*150*150).*
*** Bad maintenance level: B; Medium maintenance level: M; Good maintenance level: G*
****Poor edge connection: B; Good edge connection G.*

Table 4.10 shows the values of lateral capacity in terms of acceleration, yielding displacementand ultimate displacement, alongside the subtype of structure, the layout characteristics providing number of story, number of opening per story and whether affected by floor and roof loads (LB, loadbearing; NLB, non-loadbearing), level of connection, level of maintenance, and the resulting failure mechanism. The suite of possible failure mechanisms considered is shown in Table 4.11.

Some observations are possible: irrespective of the type of masonry in plane failures are rarely critical either in terms of best or worst performance, except when the opening layout makes the piers become rather slender. Best performance is obtained when connections at edges are good and the walls are loadbearing, leading to combined mechanisms, either B2 or C (Table 4.11). However while these deliver good ultimate strength capacity, it is not necessarily accompanied by extended ductile behavior.

Table 4.11: Mechanisms for computation of limit lateral capacity of masonry façades

Combined Mechanisms			
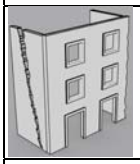 **B1**: façade overturning with one side wall	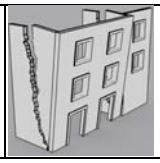 **B2**: façade overturning with two side walls	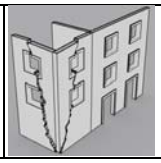 **C**: overturning with diagonal cracks involving corners	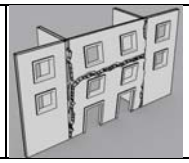 **F**: overturning constrained by ring beams or ties
In plane Mechanisms			
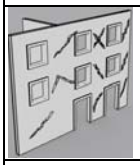 **H1**: diagonal cracks mainly in piers	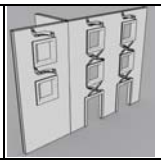 **H2**: diagonal cracks mainly in spandrel	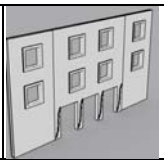 **M1**: soft story due to shear	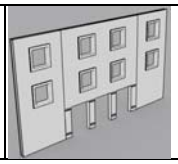 **M2**: soft story due to bending
Out of Plane Mechanism			
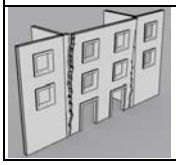 **A**: façade overturning with vertical cracks	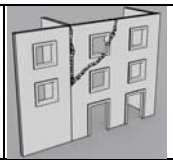 **D**: façade overturning with diagonal crack	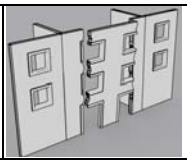 **E**: façade overturning with crack at spandrels	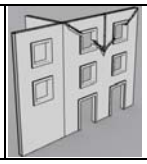 **G:** façade overturning with diagonal cracks

The obtained capacity curves are, where counterparts were available, compared with the curves obtained by METU (personal communication and WHE-PAGER phase III forms, 2011). Curves are represented as bilinear. The collapse point having been omitted in this presentation.

4.5 Comparison between FaMIVE and Erberik curves

To avoid repetition the curves obtained with FaMIVE are presented in this section directly in comparison with the curves produced by METU in Figure 4.4 to 4.9, one for each masonry structure typology. Details of the METU approach are contained in Erberik (2008) and their capacity curves are obtained using the analysis program MAS, which employs a nonlinear model for masonry wall panels assuming that they have resistance in their own plane and have negligible rigidities in the out-of-plane direction. This means that no out-of-plane mechanism is assessed in the analysis and that the walls are assumed to act in parallel. The strength criterion is shear based and energy dissipation is accounted for through a constant value of viscous damping. The only parameter treated as a random variable is the compressive strength, sampled using Latin Hypercube Sampling method (LHSM). Given these assumptions the mean capacity curves obtained by METU and their

lower and upper bounds have a similar shape and ultimate displacement threshold, as these parameters are not related to the random variable, and only one mode of failure is considered. The comparison with the FaMIVE curves shows that when considering different failure mechanisms, brought about not necessarily by material strength, but by variation in geometry and structural connections, the range of both elastic and post elastic behavior is much wider, with substantial differences in initial stiffness, ultimate strength capacity, and elastic and ultimate drift. Hence minimum and maximum performance conditions cannot be obtained from average performance by applying a simple proportional function.

The above variability also proves the necessity of developing a fictitious sample using RNG with sufficient variance of geometric loading and structural parameters, to generate the wide range of possible responses.

As walls' slenderness is one major determinant of both mode of collapse and collapse load multiplier, capacity curves have been presented separately for the same typology and different number of stories. Moreover the effect of traditional strengthening devices, such as timber lacing has also been considered.

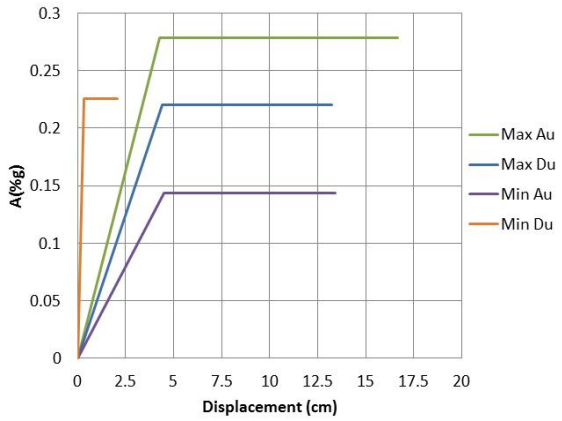

Figure 4.4 Capacity curves for 1 story adobe (A1) Turkey index buildings

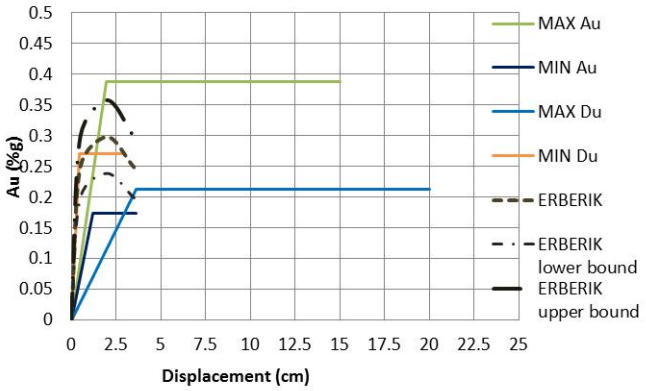

Figure 4.5 Capacity curves for 2 story massive stone (MS) Turkey index buildings

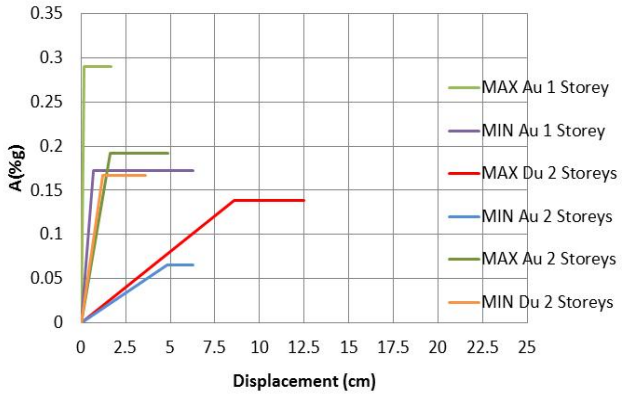

Figure 4.6 Capacity curves for 1 story and 2 story rubble (RS2) Turkey index buildings

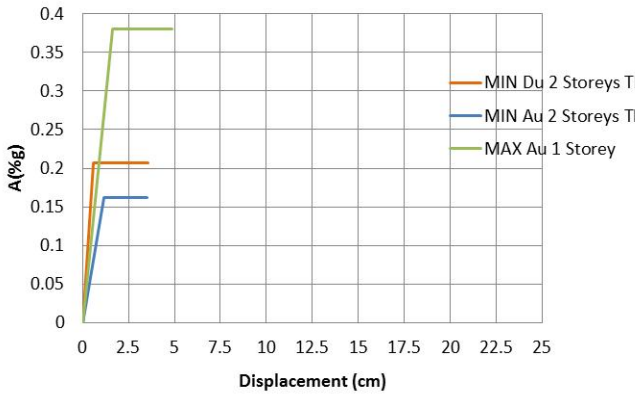

Figure 4.7 Capacity curves for timber laced rubble stone (RS2) Turkey index buildings

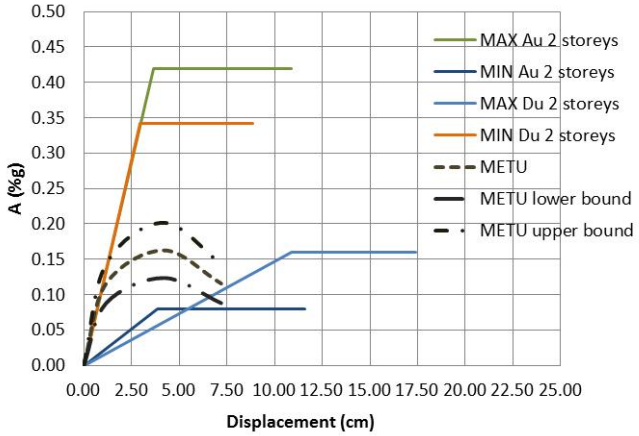

Figure 4.8 Capacity curves for 1 story unreinforced brick masonry in mud mortar (UFB1) Turkey index buildings

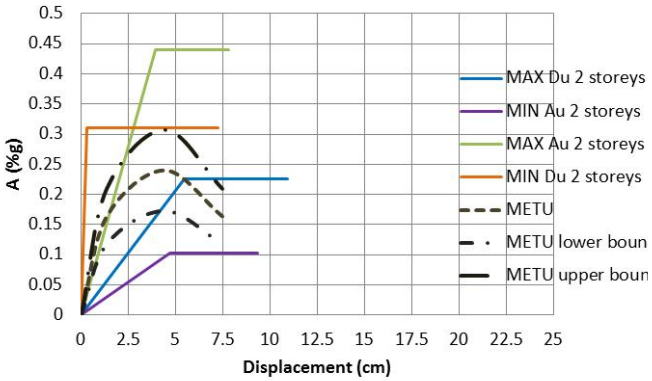

Figure 4.9 Capacity curves for 2 story unreinforced masonry in cement mortar type UFB4 Turkey index buildings

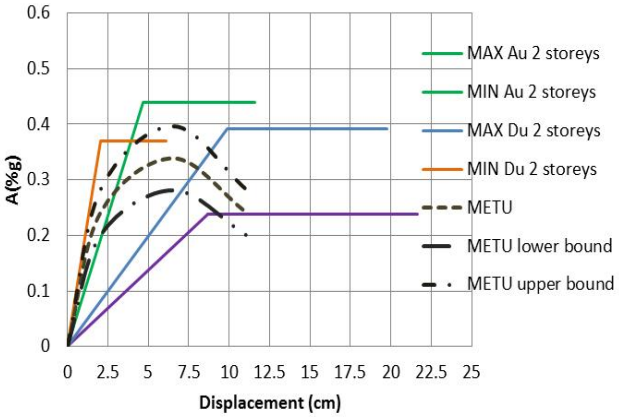

Figure 4.10 Capacity curves for 2 story unreinforced brick masonry in concrete mortar and concrete floors (UFB5) Turkey index buildings

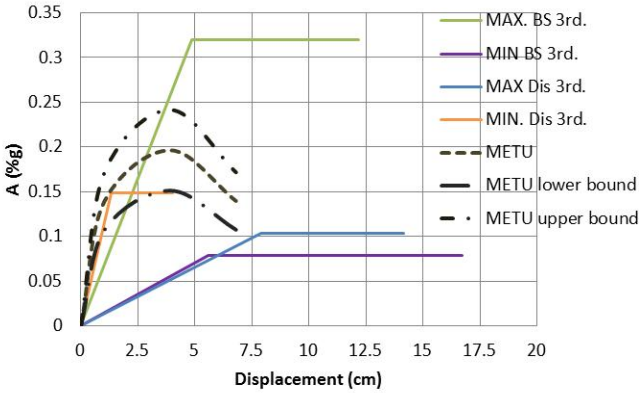

Figure 4.11 Capacity curves for 3 story unreinforced concrete block masonry in cement mortar type UCB Turkey index buildings

4.6 Fragility curves

4.6.1 Generalities

Fragility curves have been computed for each of the typologies analyzed in the previous section. As already mentioned RGN was applied to obtain normal distributions of the geometric input parameters from the typical range of values for each of them, as provided by METU. By considering the realistic variability of constraint conditions that can be found in masonry buildings, further variance has been introduced in the sample resulting in different collapse mechanisms and a large range of capacity curves as the extremes presented in the previous section show clearly. In order to better highlight this, the distribution of ultimate lateral acceleration and yielding limit state displacement are plotted in Figures 4.12 and 4.13. The charts show that while the acceleration has a distribution that can be assimilated to a normal one, the yielding displacement has distributions that are non-symmetric to respect to the median.

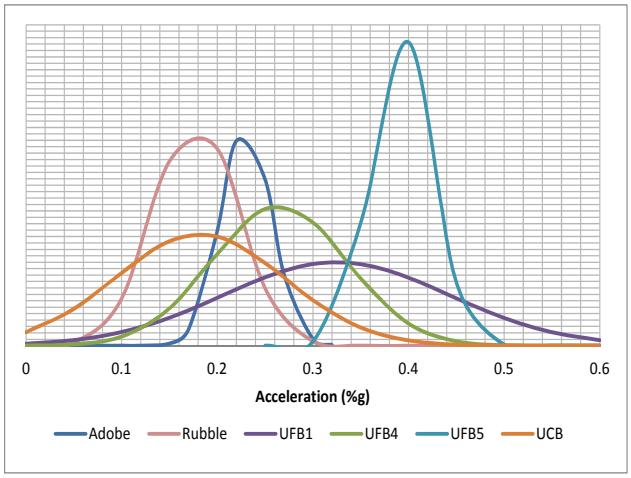

Figure 4.12 Normalised distribution for Au for the different typologies

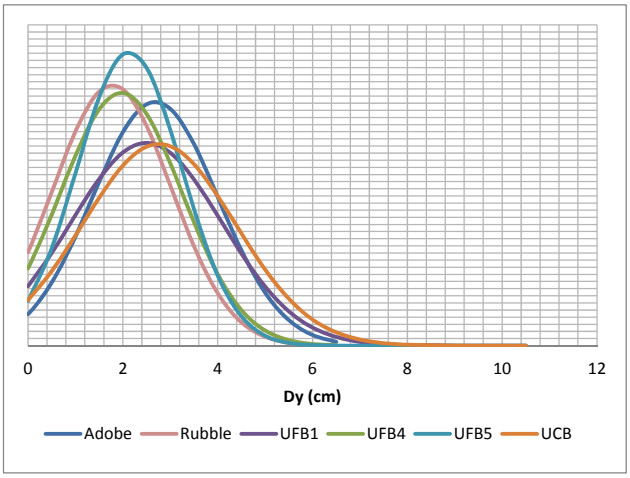

Figure 4.13 Distribution of limit state Dy for the different typologies

Fragility curves for different limit states are obtained by using median and standard deviation values of the limit state displacement and deriving lognormal cumulative distributions. To this end the distribution parameters can be calculated as:

$$\overline{\Delta}_{LS} = e^{\mu} \qquad \text{with} \qquad \mu = \frac{1}{n}\sum(\ln x) \qquad \textbf{(4.10)}$$

and:

$$\beta_{LS} = e^{\mu+\frac{1}{2}\sigma^2}\sqrt{e^{\sigma^2}-1} \qquad \text{with} \quad \sigma = \sqrt{\frac{\sum(\ln x - \ln \bar{x})^2}{n}} \qquad \textbf{(4.11)}$$

where the median and standard deviation of the distribution are obtained for each typology from the capacity curves distributions. Three limit states are considered in agreement with the three representative points defining the push-over curves and capacity curve as introduced in Section 4.2, identifying also three damage states, as shown in Table 4.12.

Table 4.12: Limit states and corresponding damage states and drift ranges

Limit state	Damage state	Drift range (%)
Δy	Slight: cracking limit	0.1-1.2
Δu	Structural damage: maximum capacity	0.6-2
Δnc	Near Collapse: loss of equilibrium	2.0-4.0

It should be noted that the drift ranges are calculated based on all typologies studied above and they are an outcome of the analysis rather than imposed on the basis of code prescriptions or other considerations. Similarly the β_{LS} for each limit state and corresponding fragility curves are quantified only on the basis of the variation for each typology of the capacity curves obtained. The uncertainty associated with the demand has not been included in this study, as it is beyond the scope of the present work. The same approach described in Section 3.5.2 and Equation (3.8) is used to compute the cumulative curves.

4.6.2 Results

Using the procedure described above and the capacity curves derived in the previous section, fragility curves are obtained for each of the masonry typologies, for the three limit states defined in Table 4.12. For each typology separate curves have been derived for different number of stories. This is to highlight the role of slenderness in the fragility of masonry structures: the reduced ductility with increased number of stories can be qualitatively and quantitatively measured by the distance of the median values of the three curves for each typology. In particular it should be noted how close the fragility curve for near collapse, Δ_c, is to the fragility curve for structural damage, Δ_u. It should also be noted that the standard deviation increases with the number of stories, as can be observed by the increasing inclination of the fragility curves for 2 story buildings as compared with the ones for 1 story buildings. Comparing Figures 4.16 and 4.17 it is also apparent the benefit of timber lacing in traditional rubble masonry. Their presence stiffens the structure and shifts the collapse mechanism from simple out-of-plane to in plane and combined mechanisms (see Table 4.11). Although it does not increase the median value for near collapse condition, it does increase the distance between the fragility curves, and provides a wider distribution.

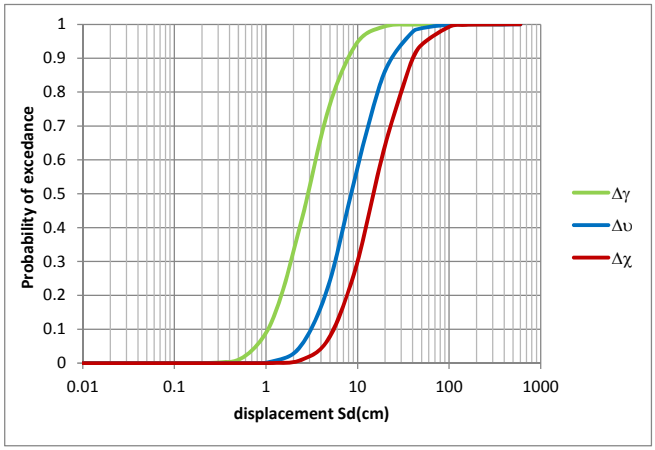

Figure 4.14 Fragility curves: adobe typology 1 story

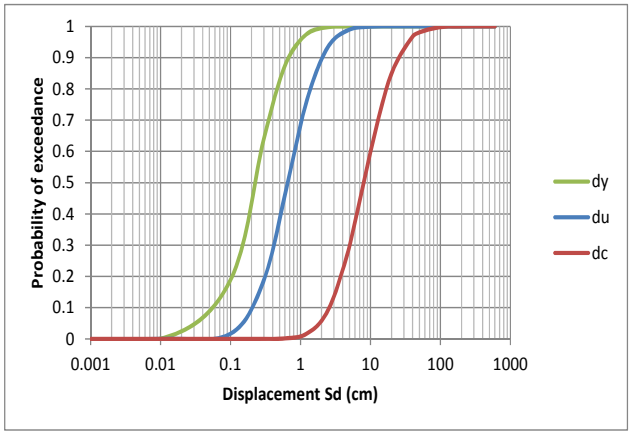

Figure 4.15 Fragility curves: rubble typology 1 story

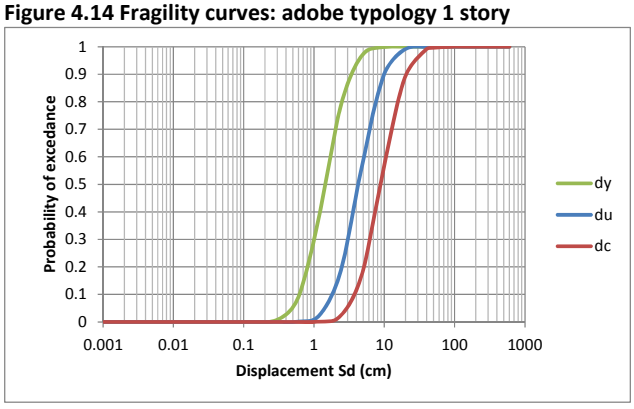

Figure 4.16 Fragility curves: rubble typology 2 story

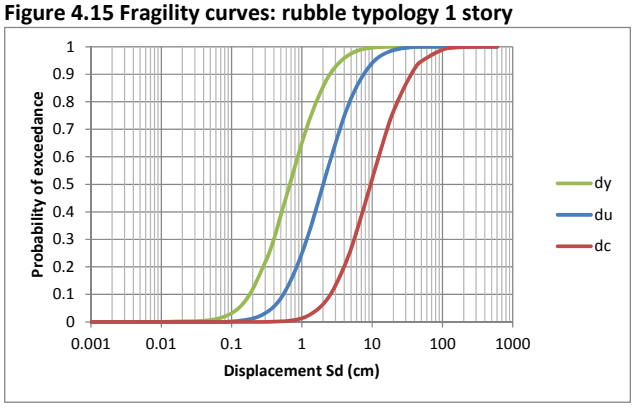

Figure 4.17 Fragility curves: rubble typology 2 stories with timber bands

By comparing UFB1, brickwork set in mud mortar (figure 4.18 and 4.19), with UFB4, brickwork set in cement mortar (figure 4.20 and 4.21), it is possible to quantify the effect of different binders on the fragility curves, noticeable for all 3 limit states and for both number of stories. Similar comparisons

between Figure 4.21 and 4.22 draw out the ffect of floor structures, timber in UFB4 and concrete slabs in UFB5.

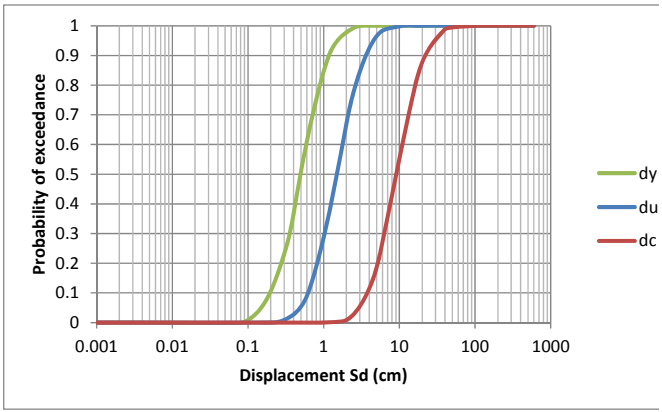

Figure 4.18: Unreinforced brick masonry UFB1 1story

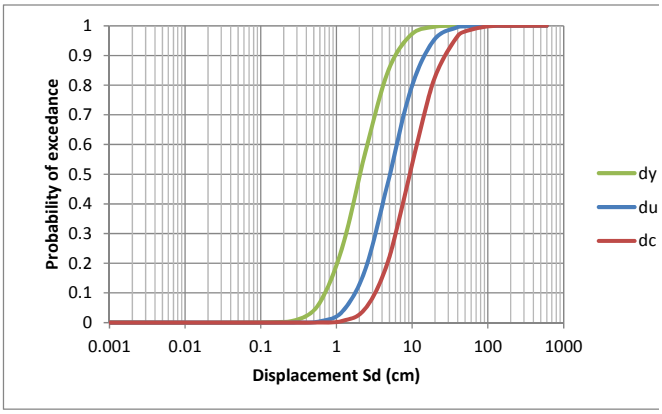

Figure 4.19: Unreinforced brick masonry UFB1 2 story

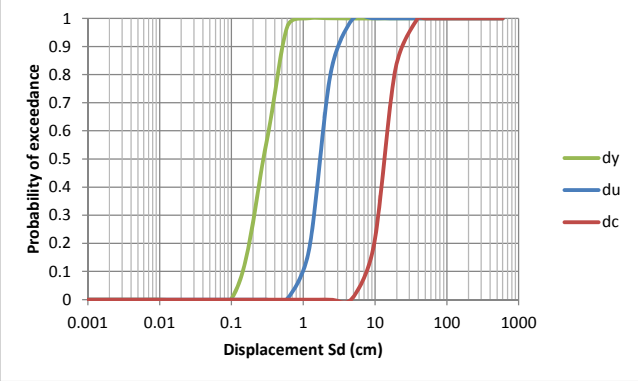

Figure 4.20 Unreinforced brick masonry UFB4 1story

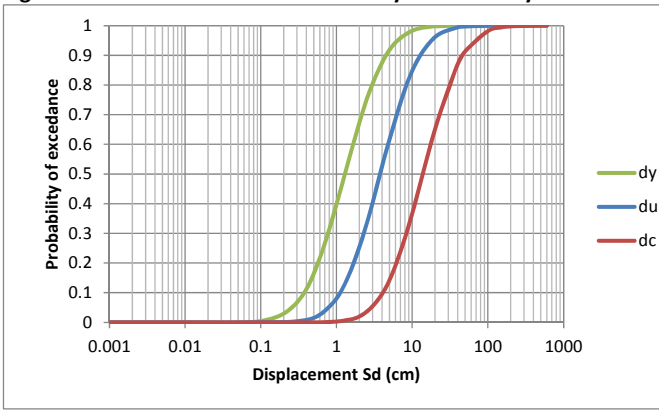

Figure 4.21 Unreinforced brick masonry UFB4 2 story

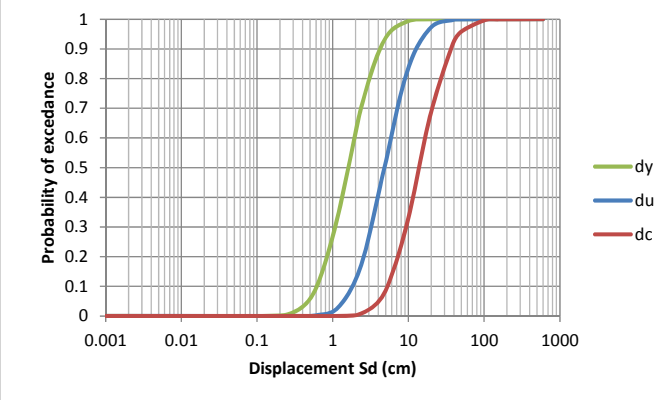

Figure 4.22 Unreinforced brick masonry UFB5 2 story

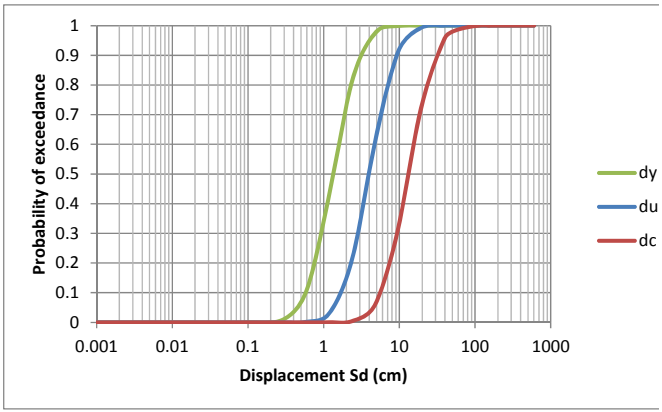

Figure 4.23 Unreinforced Concrete block masonry 2 story

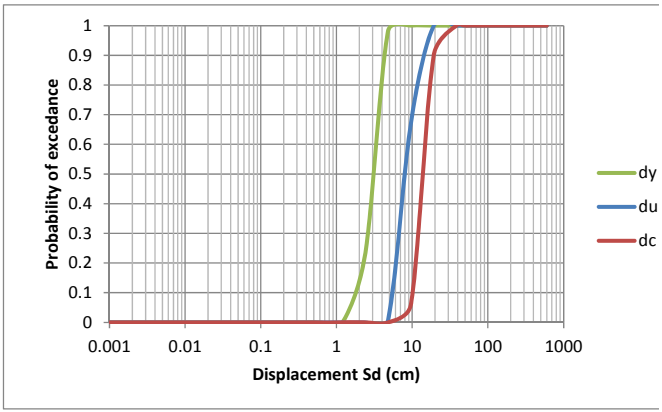

Figure 4.24 Unreinforced Concrete block masonry 3 story

In the fragility curves shown above only the uncertainty associated to the building typology behavior is explicitly accounted for. The uncertainty associated to the model in FaMIVE is taken into account by considering a reliability factor and a range within which the value is likely to fall. The range is greater as the reliability is lower, as this depends on the reliability of the input parameters. As in the present study only average values were provided and their distribution in the samples were randomly generated with limits that have not been confirmed by in situ survey. The reliability is considered low and hence a range of 30% variability from the central value is assumed.
The corresponding fragility curves obtained in this way for UFB4 two stories are shown in Figure 4.25. The standard deviation of the range limit curves and of the central curve remain constant.

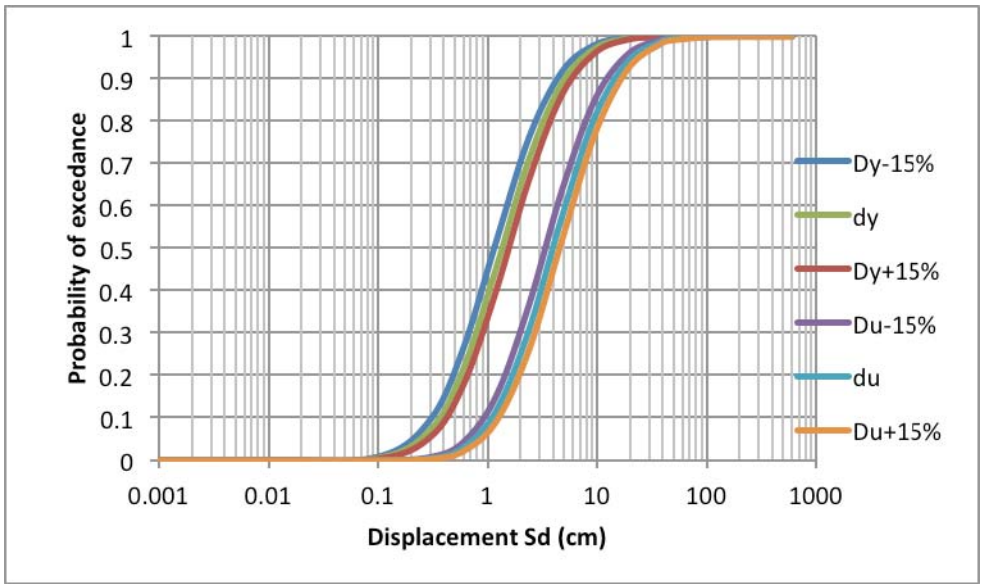

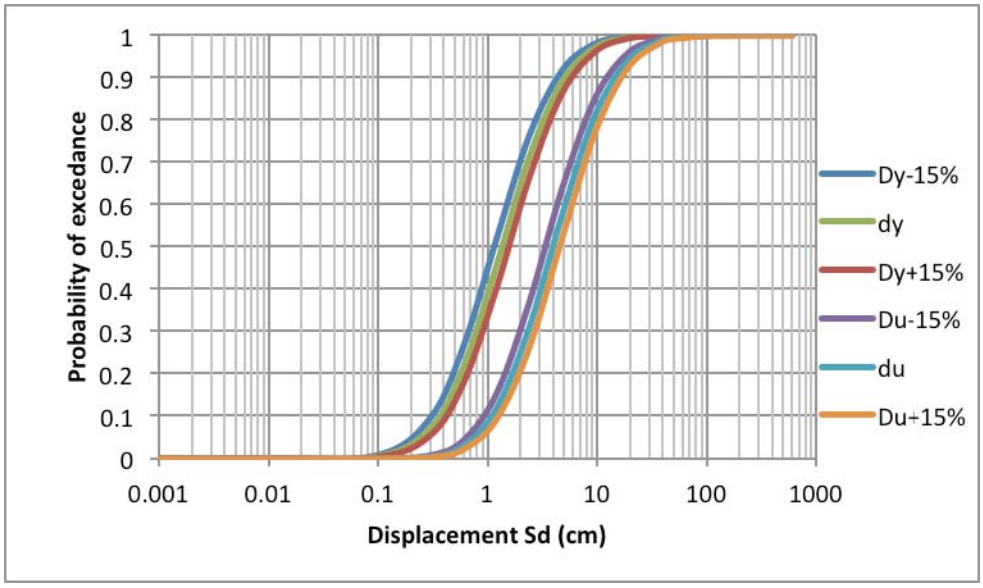

Figure 4.25 Fragility curves for UFB4 2 stories with confidence range .

5. Discussion and conclusions

5.1 Introduction

This chapter compares, summarizes and further discusses the analyses presented in the previous chapters. As indicated in Table 1.2, many of the index buildings chosen in the three approaches belong to the same PAGER typology. This makes it possible to compare results to understand the influence of the analytical approach used on the vulnerability assessment of a given structure as well as the influence of regional differences such as construction practice and code requirements. In the second part of this chapter several critical modeling parameters are reviewed in terms of their effect on the results. For concrete structures these include detailing assumptions, shear failure considerations, and the simulation of the effects of infill on building performance. For masonry structures the effects of window lay-out in determining the size of the piers, of connections of the analyzed façade with its side walls, and of gravitational loads are discussed in terms of their influence on model performance and the level of lateral acceleration capacity. Finally results are compared in terms of capacity curve characteristic points, displacement at collapse, and the value of parameters used to derive the fragility functions. These are also compared with the equivalent parameters used in HAZUS.

5.2 Comparison among results

The most extensive comparison of results for two of the procedures used, DBELA and AUTh Non-linear, was on index frames representative of the building stock of Greece and Italy. The DBELA method seems to consistently overestimate acceleration capacity of the building system when compared with the AUTh method. The overestimate is greater for non-seismically designed structures than either for structures designed according to a code, or for low-rise bare frames. The base shear is obtained from the yield displacement and period; the yield displacement appears to be overestimated for these structures, which thus leads to an overestimation of the shear force. Differences are also noted in terms of ultimate displacement, although these differences are less consistent, as shown in Table 5.1 and 5.2. The DBELA procedure includes empirical relationships for quantities such as the effective period of the structures, the yield displacement, and the failure mechanism as previously highlighted in section 2.2. These quantities may need further calibration, with more numerical models required in particular to constrain the formulae for the period of vibration of bare and infilled frames with differing levels of seismic design, as this assumption affects the estimated base shear (which as mentioned above is often overestimated). The approach used by the AUTh group is, obviously, a more time-consuming one and hopefully leads to more reliable results. However the procedures for the estimation of the plastic hinge properties (see section 3.2.1), the bilinear approximation of moment-curvature (3.2.2) , and the conversion from pushover to capacity curve (3.2.3) also have significant influence on the final value of the representative points of the capacity curves.

5.3 Detailing assumptions for concrete structures

The limit states in DBELA are defined in terms of the displacement of a SDOF equivalent system with a given failure mechanism. The equations to estimate the limit state displacements are a function of the strains attained in the concrete and the steel. If the sections are well-confined, then these limit state strains are assumed to be much higher – the concrete is well-confined and can reach much higher levels of strain before significant levels of damage are observed. Construction deficiencies are not accounted for in the DBELA method. Code requirements in terms of seismic design can be taken into account by modifying the initial period of vibration (as structures designed with a lateral load are stiffer), and modifying the limit state displacement capacities as described above (if the design leads to adequate confinement and thus ductile behavior).

For the Indian buildings, according to the data provided by IITG, 12mm dia. bars at 75mm spacing were used for all columns, and 8mm dia. bars at 100mm spacing for all beams of R/C frames. This resulted, as expected, in high mechanical reinforcement ratios and highly ductile structural members and hence very ductile structures. Note that this ductile behavior has also been reported in the paper by the IITG team (Kaushik et al., 2009). On the other hand, it is notable that for the residential irregular index Indian building analyzed with the 3D model, the transverse reinforcement ratio was substantially lower, 8mm dia. bars at 120mm.

For the Italian buildings, the data on which analysis by the AUTh team was based was "Stirrups Φ12" for some beams but no information concerning their spacing, and no data for the columns. It is noted that such detailed data are not needed in the simplified analysis used by Crowley et al (ROSE). Based on other studies of Italian researchers it was found that, at least for non-seismically designed structures, stirrup bars were often significantly smaller than Φ12, usually 6 or 8mm values that are closer to the Low- (or No-) Code practices in Greece; for example see: Masi, A. (2004); Ricci, et al. (2010).

Hence, in all methods for deriving capacity curves for reinforced concrete frames, results are substantially affected by the assumption made regarding member ductility, which, in turn, is controlled by the assumptions on the confinement of the members.

5.4 Shear failure consideration/omission

Shear failure of R/C members was not explicitly treated in the approximate DBELA approach (though it is recognized that it should be considered for frames without seismic design), whereas it was estimated in terms of ductility-dependent shear strength in the more involved AUTh approach. Consideration of shear proved not to be critical for the structures studied here, since the moment corresponding to the estimated shear capacity level was higher than the flexural capacity of the structural members. Having said this, as noted in §3.2.1 in this report, no reductions were made in shear capacity due to poor detailing of the transverse reinforcement. The differences in the ultimate displacement capacity for the two methods are thus not due to the modeling of shear failure.

5.5 Infill modeling

Masonry infills are known for the high variability associated with their properties (Dymiotis et al. 2001). This was further confirmed in the course of this study, in particular with respect to the strength of the infill walls in the Indian buildings. IITG indicated a masonry strength value of 7.5MPa which is significantly higher than that of masonry commonly used in Greece and, apparently, elsewhere in South Europe. This value resulted in a notable increase in the strength of the infilled frames (compared to the bare ones), as reported in Kaushik et al. (2009). As noted in §3.3.1, extra analyses were run with a lower value of the masonry strength f_{wc} with noticeable effects on the results. In DBELA, the characteristics of the infill panels are not explicitly modelled (i.e. the thickness and strength of the infill panels do not currently influence the formuale used for the period of vibration and displacement capacities), hence this could be a reason for the differences noted between AUTh and ROSE for infilled frames. Additional numerical models with differering infill panel characteristics are needed to calibrate further the equations. However, both AUTh and ROSE assume that once the infill panels fail, the behavior of the structure can be approximated by the behavior of the bare frame, thus leading in most cases to similar estimates of the ultimate base shear capacity.

5.6 Effect of opening layout in masonry structures

One of the parameters that have been analyzed in the present work is the influence and layout of openings on the ultimate capacity of the façade. Especially when masonry buildings are in urban areas, facades tend to have a significant number of relatively large windows or doors. According to the data provided by METU, the opening-to-wall-area ratio ranges from 0.25 to 0.52. The large proportion of openings leads to very slender piers, which tend to fail in-plane in bending for relatively modest collapse load multipliers, after early failure of the spandrel. This might occur even if there are good end connections of the main façade with the side walls, preventing full development of the box behavior.

5.7 Comparison of estimated capacity curves

A comparison of the reference points (S_{dy}, S_{du}, S_{ay}, S_{au}) of the estimated capacity curves for R/C buildings by three different groups (AUTh, ROSE, IITG) is made in table 5.1 while in table 5.2 a similar comparison is made for the masonry structures that were analyzed by UBATH and METU. The differences are quite important in some cases; possible reasons for these discrepancies have been discussed in previous sections of this report (e.g. §3.4), as well as discussed above. As expected, the most dramatic differences occur with regard to the ultimate displacement (S_{du}) which is both difficult to define in a consistent way and to capture properly in an inelastic analysis. Nevertheless, the average difference (between AUTh and ROSE) is lower for S_{du} than S_{dy}. For the unreinforced masonry typologies, differences for stone masonry are quite important, while for brickwork the differences are in the range of 25% for S_{dy} and are smaller for S_{du}.The comparison of results obtained within this study with the corresponding HAZUS-generated capacity curves is summarized in Table 5.3 for typology C4-C1, table 5.4 for typology C3 and table 5.5 for URM.

Table 5.1. Comparison of capacity curves parameters for R/C typologies

BuildingType		AUTh					IITG or ROSE					Difference (%)				
		$S_{dy\,(cm)}$	$S_{du\,(cm)}$	S_{ay}	S_{au}	T*	$S_{dy\,(cm)}$	$S_{du\,(cm)}$	S_{ay}	S_{au}	T	$S_{dy\,(cm)}$	$S_{du\,(cm)}$	S_{ay}	S_{au}	T
Indian 2D f_{wc}=7.50MPa closed stirrups	C4M (1) - Bare	5.6	105.2	0.15	0.16	1.22	4.4	60	0.17	0.2	0.96	26.1	75.4	-11.8	-20.0	27.1
	C3M (2) - Infilled	0.6	3.3	0.78	0.78	0.18	1.5	6	0.75	1.5	0.28	-58.7	-45.8	4.0	-48.0	-36.1
	C3M -SS (3)	3.5	115.6	0.14	0.16	1.00	2.4	47	0.15	0.2	0.8	44.6	145.9	-6.7	-20.0	24.8
Indian 2D f_{wc}=1.91MPa closed stirrups	C4M (1) - Bare	5.5	105.2	0.15	0.16	1.23	4.4	60	0.17	0.2	0.96	26.1	75.4	-13.1	-18.7	28.1
	C3M (2) - Infilled	0.8	4.7	0.41	0.45	0.29	1.5	6	0.75	1.5	0.28	-44.0	-22.2	-44.9	-70.2	2.1
	C3M -SS (3)	3.8	115.1	0.15	0.15	1.01	2.4	47	0.15	0.2	0.8	56.7	144.8	-1.0	-24.7	26.2
Indian 2D f_{wc}=7.50MPa open stirrups	C4M (1) - Bare	5.0	11.9	0.13	0.15	1.23	4.4	60	0.17	0.2	0.96	13.8	-80.2	-21.6	-26.1	28.1
	C3M (2) - Infilled	0.6	3.2	0.78	0.78	0.18	1.5	6	0.75	1.5	0.28	-58.5	-45.9	3.8	-47.9	-35.9
	C3M -SS (3)	3.2	11.2	0.13	0.14	1.00	2.4	47	0.15	0.2	0.8	35.3	-76.2	-12.1	-31.2	24.5
Indian 3D f_{wc}=7.50MPa closed stirrups	C4M bare X	9.2	57.8	0.49	0.50	0.87										
	C3M (9) - Infilled X	8.5	31.5	0.47	0.41	0.85	0.30	1.8	0.23	0.73	0.25	2740	1650	104.3	-43.8	2.416
	C4M (10) - Open Story X	3.4	21.6	0.31	0.33	0.66	0.40	9.2	0.1	0.40	0.45	750.0	134.8	210.0	-17.5	0.476
	C4M bare +Y	9.8	56.8	0.52	0.53	0.87										
	C3M (9) - Infilled +Y	6.5	51.4	0.51	0.55	0.71										
	C3M-SS(10) - Open Story +Y	7.1	39.6	0.45	0.48	0.80										
	C4M bare -Y	9.3	61.7	0.48	0.52	0.88										
	C3M (9) - Infilled -Y	6.5	55.6	0.51	0.53	0.71										
	C3M-SS(10) - Open Story -Y	8.2	40.6	0.43	0.46	0.88										
Italian frames	C4M (RC_PC) X	4.6	8.7	0.12	0.14	1.24	14.4	29.4	0.40	0.40	1.20*	-68.2	-70.3	-70.2	-65.2	3.3
	C3M (RC_PC) X	1.1	6.0	0.15	0.23	0.53										
	C3M-SS (RC_PC) X	2.6	8.8	0.20	0.23	0.73										
	C4M (RC_5%) X	6.7	43.0	0.28	0.31	0.98	13.6	28.6	0.38	0.38	1.20*	-50.7	50.4	-26.1	-18.2	-18.4
	C3M (RC_5%) X	3.3	12.6	0.31	0.34	0.66										
	C3M-SS (RC_5%) X	3.5	14.2	0.27	0.31	0.72										
	C4M (RC_12.5%) X	5.0	28.9	0.51	0.58	0.62	11.8	26.8	0.67	0.67	0.84*	-58.1	7.9	-24.3	-13.9	-25.5
	C3M (RC_12.5%) X	3.7	14.2	0.53	0.56	0.53										
	C3M-SS (RC_12.5%) X	3.7	14.5	0.47	0.52	0.56										
	C4M bare (RC_5%) Y	8.5	51.6	0.21	0.23	1.27	12.4	27.4	0.35	0.35	1.20*	-31.9	88.4	-39.3	-33.6	6.0
	C3M (RC_5%) Y	1.9	11.5	0.23	0.27	0.58										
	C3M-SS (RC_5%) Y	3.3	15.7	0.20	0.23	0.81										
	C4M bare (RC_12.5%) Y	6.6	59.6	0.51	0.57	0.72	11.3	26.3	0.64	0.64	0.84*	-41.3	126.5	-20.8	-11.5	-13.9
	C3M (RC_12.5%) Y	3.7	13.2	0.49	0.56	0.55										
	C3M-SS (RC_12.5%) Y	3.7	13.6	0.44	0.52	0.58										

** Period values for all AUTh analyses were estimated for the corresponding capacity curves using the expression $T=2\pi(S_{dy}/S_{ay})^{0.5}$.The same expression was used for the periods of the Italian buildings derived using the DBELA approach.*

BuildingType		AUTh					ROSE					Difference (%)				
		$S_{dy\ (cm)}$	$S_{du\ (cm)}$	S_{ay}	S_{au}	T	$S_{dy\ (cm)}$	$S_{du\ (cm)}$	S_{ay}	S_{au}	T	$S_{dy\ (cm)}$	$S_{du\ (cm)}$	S_{ay}	S_{au}	T
Greek Frames Low-Base shear	C4L (RC1LL)	2.69	10.93	0.15	0.17	0.84	8.00	14.60	0.57	0.57	0.75	-66.4%	-25.1%	-73.6%	-70.8%	12.8%
	C3L (RC3.1LL)	0.49	5.11	0.33	0.40	0.24	4.20	5.50	0.83	0.48	0.45	-88.4%	-7.1%	-59.8%	-15.4%	-46.2%
	C3L-SS (RC3.2LL)	2.32	11.20	0.15	0.17	0.79										
	C4M (RC1ML)	4.62	12.96	0.15	0.15	1.12	8.60	25.20	0.19	0.19	1.35	-46.3%	-48.6%	-21.5%	-19.9%	-17.3%
	C3M (RC3.1ML)	1.03	6.80	0.23	0.30	0.42	5.30	6.40	0.24	0.17	0.81	-80.6%	6.2%	-28.7%	76.4%	-47.8%
	C3M-SS (RC3.2ML)	2.55	9.85	0.16	0.17	0.80										
	C4H (RC1HL)	6.86	14.23	0.12	0.13	1.54	15.20	47.00	0.08	0.08	2.85	-54.9%	-69.7%	54.0%	70.5%	-45.9%
	C3H (RC3.1HL)	3.36	12.00	0.17	0.21	0.90	7.90	16.80	0.11	0.08	1.71	-57.5%	-28.6%	53.8%	175.6%	-47.4%
	C3H-SS (RC3.2HL)	4.12	11.06	0.14	0.16	1.11										
Greek Frames High-Base shear	C1L (RC1LH)	3.20	36.46	0.61	0.61	0.46	3.90	18.60	0.57	0.57	0.52	-17.9%	96.0%	7.4%	7.4%	-12.5%
	C1L-I (RC3.1LH)	1.00	5.40	0.75	0.87	0.23	3.20	6.20	0.99	0.46	0.36	-68.6%	-13.0%	-24.0%	91.5%	-35.8%
	C1L-SS (RC3.2LH)	2.44	37.91	0.57	0.63	0.41										
	C1M (RC1MH)	3.72	41.28	0.37	0.40	0.64	6.40	32.90	0.29	0.29	0.94	-42.0%	25.5%	28.0%	36.9%	-32.7%
	C1M-I (RC3.1MH)	1.58	6.68	0.44	0.51	0.38	5.00	7.60	0.45	0.20	0.65	-68.5%	-12.1%	-8.7%	157.6%	-41.2%
	C1M-SS (RC3.2MH)	2.56	32.04	0.36	0.39	0.53										
	C1H (RC1HH)	7.09	37.25	0.22	0.23	1.13	11.80	62.20	0.12	0.12	2.00	-39.9%	-40.1%	86.8%	96.3%	-43.3%
	C1H-I (RC3.1HH)	3.88	15.84	0.26	0.31	0.77	9.20	10.80	0.20	0.08	1.37	-57.8%	46.7%	33.8%	299.6%	-43.8%
	C1H-SS (RC3.2HH)	4.69	24.19	0.24	0.25	0.89										

Table 5.2. Comparison of capacity curves parameters for masonry typologies

BuildingType	UBATH					METU					Difference (%)				
	$S_{dy\ (cm)}$	$S_{du\ (cm)}$	S_{ay}	S_{au}	T_{eff}	$S_{dy\ (cm)}$	$S_{du\ (cm)}$	S_{ay}	S_{au}	T_{eff}	$S_{dy\ (cm)}$	$S_{du\ (cm)}$	S_{ay}	S_{au}	T_{eff}
Adobe A1	2.85	8.56	0.064	0.23	0.79										
Rubble RS2 1story	0.26	0.79	0.06	0.22	0.22										
Rubble RS2 2 story	1.43	4.28	0.03	0.145	0.84										
Rubble RS2 2 story timber lacing	0.90	2.79	0.03	0.27	0.43										
Massive stone MS	4.60	8.7	0.04	0.34	0.79	0.5	2.0	.249	.298		89.1	77.0	-83.9	12.3	
Unreinforced brick UFB1 1 story	0.63	1.90	0.06	0.35	0.28										
Unreinforced brick UFB1 2 story	2.50	6.14	0.04	0.30	0.99	1.2	4.2	.116	.163		52	31.5	-65.5	45.6	
Unreinforced brick UFB4 1 story	0.31	1.86	0.062	0.309	0.21										
Unreinforced brick UFB4 2 story	1.85	5.28	0.03	0.25	0.75	1.4	4.4	.164	.240		24.3	16.6	-81.7	4	
Unreinforced brick UFB5 2 story	2.00	6.41	0.035	0.32	0.56	2.1	6.5	.242	.339		-4.7	-1.38	-85.5	-5.6	
Unreinforced concrete block UCB 2 story	1.31	3.93	0.032	0.16	0.60	1	3.9	.14	.196		23.6	0.76	-77.1	-18.3	
Unreinforced concrete block UCB 3 story	2.87	8.61	0.024	0.19	0.99										

Table 5.3. Comparison of capacity curves parameters for R/C bare frame typologies with Hazus capacity curves

Source	Type	Description	Dy (cm)	Du, (cm)	Ay, (g)	Au, (g)	T (sec)
HAZUS	C1Mh	RC moment frame midrise high code (USA)	2.921	46.8376	0.208	0.624	0.75
HAZUS	C1MM	RC moment frame midrise mid code (USA)	1.4732	17.5514	0.104	0.312	0.75
INDIA	C4M (1) - Bare	AUTh open stirrups	5	11.9	0.13	0.15	1.23
INDIA	C4M (1) - Bare	AUTh closed stirrups	5.6	105.2	0.15	0.16	1.22
INDIA		IITG	4.4	60	0.17	0.2	0.96
INDIA	C4M bare X	AUTh	9.2	57.8	0.49	0.5	0.87
INDIA	C4M bare -Y	AUTh	9.3	61.7	0.48	0.52	0.88
ITALY	C4M (RC_PC) X	AUTh	4.6	8.7	0.12	0.14	1.24
ITALY		ROSE	14.4	29.4	0.4	0.4	1.20*
HAZUS	C1Mp	RC moment frame midrise pre-code (USA)	0.7366	8.7884	0.052	0.156	0.76
ITALY	C4M (RC_5%) X	AUTh	6.7	43	0.28	0.31	0.98
ITALY		ROSE	13.6	28.6	0.38	0.38	1.20*
ITALY	C4M bare (RC_5%) Y	AUTh	8.5	51.6	0.21	0.23	1.27
ITALY		ROSE	12.4	27.4	0.35	0.35	1.20*
HAZUS	C1MM	RC moment frame midrise mid code (USA)	1.4732	17.5514	0.104	0.312	0.75
ITALY	C4M (RC_12.5%) X	AUTh	5	28.9	0.51	0.58	0.62
ITALY		ROSE	11.8	26.8	0.67	0.67	0.84*
ITALY	C4M bare (RC_12.5%) Y	AUTh	6.6	59.6	0.51	0.57	0.72
ITALY		ROSE	11.3	26.3	0.64	0.64	0.84*
HAZUS	C1Mh	RC moment frame midrise high code (USA)	2.921	46.8376	0.208	0.624	0.75

Table 5.4. Comparison of capacity curves parameters for R/C infilled frame typologies with Hazus capacity curves

Source	Type	Description	Dy (cm)	Du, cm	Ay, g	Au, g	T (sec)
INDIA	C3M (2) - Infilled	AUTh (high strength)	0.6	3.3	0.78	0.78	0.18
INDIA		IITG	1.5	6	0.75	1.5	0.28
INDIA	C3M (2) - Infilled	AUTh (low strength)	0.8	4.7	0.41	0.45	0.29
INDIA	C3M (2) - Infilled	AUTh (high strength) open stirrup	0.6	3.2	0.78	0.78	0.18
INDIA		IITG	1.5	6	0.75	1.5	0.28
INDIA	C3M (9) - Infilled X	AUTh	8.5	31.5	0.47	0.41	0.85
INDIA		IITG	0.3	1.8	0.23	0.73	0.25
INDIA	C3M (9) - Infilled -Y	AUTh	6.5	55.6	0.51	0.53	0.71
HAZUS	C3ML	RC frame masonry infill midrise low code (USA)	0.6604	4.953	0.083	0.188	1.45
ITALY	C3M (RC_PC) X	AUTh	1.1	6	0.15	0.23	0.53
HAZUS	C3Mp	RC frame masonry infill midrise pre-code (USA)	0.6604	4.953	0.083	0.188	0.57
ITALY	C3M (RC_5%) X	AUTh	3.3	12.6	0.31	0.34	0.66
ITALY	C3M (RC_5%) Y	AUTh	1.9	11.5	0.23	0.27	0.58
HAZUS	C3ML	RC frame masonry infill midrise low code (USA)	0.6604	4.953	0.083	0.188	1.45
ITALY	C3M (RC_12.5%) X	AUTh	3.7	14.2	0.53	0.56	0.53
ITALY	C3M (RC_12.5%) Y	AUTh	3.7	13.2	0.49	0.56	0.55

Table 5.5. Comparison of capacity curves parameters forURM typologies with Hazus capacity curves

Source	Type	Description	Dy (cm)	Du (cm)	Ay (g)	Au (g)	T (sec)
TURKEY	Adobe A1	UBATH	2.85	8.56	0.064	0.23	0.79
TURKEY	Rubble RS2 1story	UBATH	0.26	0.79	0.06	0.22	0.22
HAZUS	URMLp	Unreinforced masonry, lowrise, pre-code (USA)	0.6096	6.096	0.2	0.4	0.35
TURKEY	Rubble RS2 2 story	UBATH	1.43	4.28	0.03	0.145	0.84
TURKEY	Rubble RS2 2 story timber lacing	UBATH	0.9	2.79	0.03	0.27	0.43
TURKEY	Massive stone MS	UBATH	4.6	8.7	0.04	0.34	0.79
TURKEY		METU	0.5	2	0.249	0.298	
HAZUS	URMML	Unreinforced masonry, midrise, low-code (USA)	0.6858	4.5974	0.111	0.222	0.5
TURKEY	Unreinforced brick UFB1 1 story	UBATH	0.63	1.9	0.06	0.35	0.28
HAZUS	URMLp	Unreinforced masonry, lowrise, pre-code (USA)	0.6096	6.096	0.2	0.4	0.35
TURKEY	Unreinforced brick UFB1 2 story	UBATH	2.5	6.14	0.04	0.3	0.99
TURKEY		METU	1.2	4.2	0.116	0.163	
HAZUS	URMML	Unreinforced masonry, midrise, low-code (USA)	0.6858	4.5974	0.111	0.222	0.5
TURKEY	Unreinforced brick UFB4 1 story	UBATH	0.31	1.86	0.062	0.309	0.21
HAZUS	URMLp	Unreinforced masonry, lowrise, pre-code (USA)	0.6096	6.096	0.2	0.4	0.35
TURKEY	Unreinforced brick UFB4 2 story	UBATH	1.85	5.28	0.03	0.25	0.75
TURKEY		METU	1.4	4.4	0.164	0.24	
TURKEY	Unreinforced brick UFB5 2 story	UBATH	2	6.41	0.035	0.32	0.56
TURKEY		METU	2.1	6.5	0.242	0.339	
TURKEY	Unreinforced concrete block UCB 2 story	UBATH	1.31	3.93	0.032	0.16	0.6
TURKEY		METU	1	3.9	0.14	0.196	
TURKEY	Unreinforced concrete block UCB 3 story	UBATH	2.87	8.61	0.024	0.19	0.99
HAZUS	URMML	Unreinforced masonry, midrise, low-code (USA)	0.6858	4.5974	0.111	0.222	0.5
Mexico	UFB	Unreinforced brick masonry	0.2032	0.381	0.15	0.15	0.23
INDIA	UFB4	Unreinforced brick masonry lintel bands RC slab (N India)	0.6096	1.2954	0.9	1.2	0.16

6. References

Abo El Ezz, A. (2008). Deformation and strength based assessment of seismic failure mechanisms for existing RC frame buildings, *MSc dissertation*, European School for Advanced Studies in Reduction of Seismic Risk (ROSE School), University of Pavia, Italy.

(ATC) Applied Technology Council (1996). ATC-40: Seismic evaluation and retrofit of concrete buildings, Rep. SSC 96-01, CSSC-ATC, Redwood City, California, USA.

(ATC) Applied Technology Council (2005). Improvement of Nonlinear Static Seismic Analysis Procedures, FEMA-440. Redwood City, California, USA.

Bal I., Crowley H., Pinho R., Gulten Gulay F. (2007). Structural characteristics of Turkish RC building stock in northern Marmara Region for loss assessment applications. Research Report No ROSE 2007/03.

Bal I. (2008). Displacement-Based Earthquake Loss Assessment: Method Development and Application to Turkish Building Stock. *PhD Thesis*, European School for Advanced Studies in Reduction of Seismic Risk (ROSE School), University of Pavia, Italy.

Bernardini A., Gori R, Modena C. (1990). An application of coupled analytical models and experiential knowledge for seismic vulnerability analyses of masonry buildings. In A. Koridze (ed) Engineering Aspects of Earthquake Phenomena, Vol. 3: 161-180. Oxon: Omega Scientific, 1990.

Borzi B., Crowley H., Pinho R. (2008). Simplified pushover-based earthquake loss assessment (SP-BELA) method for masonry buildings. *International Journal of Architectural Heritage; Conservation, Analysis, and Restoration*; Vol. 2 n.4, October-November pp.353-376.

Borzi, B., Pinho, R., & Crowley, H. (2008). Simplified pushover-based vulnerability analysis for large-scale assessment of RC buildings. *Engineering Structures*, 30(3), 804-820.

Calvi, G. M., Pinho, R., Magenes, G., Bommer, J. J., Restrepo-Vélez, L. F., & Crowley, H. (2006). Development Of Seismic Vulnerability Assessment Methodologies Over The Past 30 Years. *ISET Journal of Earthquake Technology*, 43(3), 75-104.

Computers and Structures Inc. (2010). ETABS Nonlinear Version 9.7.2

Crisafulli, F. J., Carr, A. J., and Park, R. (2000). Analytical modeling of infilled frame structures—A general review. *New Zealand Nat. Soc. Earthquake Eng. Bull*, 33(1), 30–47.

Crowley, H., Pinho, R. and Bommer, J.J. (2004). A probabilistic Displacement-based Vulnerability Assessment Procedure for Earthquake Loss Estimation. *Bulletin of Earthquake Engineering,* Vol. 2, 173-219.

Crowley, H., Borzi, B., Pinho, R., Colombi, M., Onida, M. (2008). Comparison of two mechanics-based methods for simplified structural analysis in vulnerability assessment. *Advances in Civil Engineering*, Vol. 2008, Article ID 438379, 19 pp.

D'Ayala, D. and Speranza, E. (2002). An integrated procedure for the assessment of the seismic vulnerability of historic buildings, Proc. 12th European Conference on Earthquake Engineering: Paper No. 561, London, United Kingdom.

D'Ayala, D. (2003). EU-Fatih Municipality Programme: Rehabilitation of Fener and Balat Districts: Seismic vulnerability and strengthening of historic building*, in Fener and Balat Districts*, Istanbul, Turkey.

D'Ayala, D. and Speranza, E. (2003). Definition of Collapse Mechanisms and Seismic Vulnerability of Historic Masonry Buildings. *Earthquake Spectra,* Volume 19, pp. 479--509.

D'Ayala, D. (2005). Force and Displacement Based Vulnerability Assessment for Traditional Buildings. *Bulletin Of Earthquake Engineering,* Volume 3, 235-265.

D'Ayala, D. F. (2009). Seismic Vulnerability and Conservation Strategies for Lalitpur Minor Heritage. *In:* M. Hardy, C. Cancino and G. Ostergren ed. *Proceedings of the Getty Seismic Adobe Project 2006 Colloquiu*. Los Angeles: The Getty Conservation Institute, pp. 120 – 134.

D'Ayala , D. F., Jaiswal, K.S., Wald, D.J., Porter, K. and Greene, M. (2010). Collaborative effort to estimate collapse fragility for buildings worldwide: The WHE-PAGER project. Proc. of the 9th US and 10th Canadian Conference on Earthquake Engineering: Reaching Beyond Borders, July 25-29, 2010, Toronto, Canada.

D'Ayala , D. F. and Paganoni, S. (2011). Assessment and analysis of damage in L'Aquila historic city centre after 6th April 2009. Bulletin of Earthquake Engineering, 9 (1), pp. 81-104.

Dymiotis, C., Kappos A.J., and Chryssanthopoulos, M.C. (2001). Seismic reliability of masonry infilled r/c frames. Journal of Structural Engineering, ASCE, 127 (3), 296-305.

(EPPO) Earthquake Planning and Protection Organization (2012). Code for Structural Interventions (KANEPE). Athens, Greece.

Erberik M.A. (2008). Generation of fragility curves for Turkish masonry buildings considering in-plane failure modes. *Earthquake Eng. and Str. Dyn*. 37, 387-405.

Erberik M.A. (2010). Seismic Risk Assessment of Masonry Buildings in Istanbul for Effective Risk Mitigation. *Earthquake Spectra* 26, pp. 967-982.

Erdik, M., N.Aydinoglu, Y.Fahjan, K.Sesetyan, M.Demircioglu, B.Siyahi, E.Durukal, C.Ozbey, Y.Biro, H.Akman and O.Yuzugullu (2003). Earthquake Risk Assessment for Istanbul Metropolitan Area. *Earthquake Engineering and Engineering Vibration*, V.2- N-1, pp.1-25

Federal Emergency Management Agency (2000). Prestandard and Commentary for the Seismic Rehabilitation of Buildings, FEMA-356, Washington, D.C.

Glaister and Pinho R. (2003). Development of a Simplified Deformation-Based Method for Seismic Vulnerability Assessment. *Journal of Earthquake Engineering,* Vol. 7, pag 107-140.

Jaiswal, K. S., and Wald, D. J. (2010a). An Empirical Model for Global Earthquake Fatality Estimation. *Earthquake Spectra*, 26, No. 4, 1017-1037.

Jaiswal, K. S., and Wald, D. J. (2010b). Development of a semi-empirical loss model within the USGS Prompt Assessment of Global Earthquakes for Response (PAGER) System. Proc. of the 9th US and 10th Canadian Conference on Earthquake Engineering: Reaching Beyond Borders, July 25-29, 2010, Toronto, Canada.

Kappos, A. J. (1991). Analytical Prediction of the Collapse Earthquake for R/C Buildings: Suggested Methodology. *Earthquake Engineering & Structural Dynamics*, 20(2), 167-176.

Kappos, A.J. (1993). RCCOLA-90: A microcomputer program for the analysis of the inelastic response of reinforced concrete sections. *Rep. of the Lab. of Concrete Structures*, Dept. of Civil Engng. Aristotle Univ. of Thessaloniki,.

Kappos, A. J., Stylianidis, K. C., and Michailidis, C. N. (1998) Analytical models for brick masonry infilled R/C frames under lateral loading. *Journal of Earthquake Engineering*, 2(1), 59-87.

Kappos, A. J., and Panagiotopoulos, C. G. (2003). Inelastic static analysis of infilled R/C buildings. Proceedings of the 2003 International Conference on Computational & Experimental Engineering & Sciences. Corfu, Greece.

Kappos, A.J. and Panagopoulos, G. (2010). Fragility curves for R/C buildings in Greece. *Structure & Infrastructure Engineering*, 6(1), 39 – 53.

Kappos, A.J., Panagopoulos, G., Panagiotopoulos, Ch. and Penelis, Gr. (2006) A hybrid method for the vulnerability assessment of R/C and URM buildings*. Bull. of Earthquake Engineering* 4 (4): 391-413.

Kaushik, H. B., Rai, D. C., and Jain, S. K. (2009). Effectiveness of Some Strengthening Options for Masonry-Infilled RC Frames with Open First Story. *Journal of Structural Engineering*, 135(8), 925-937

Kaushik, H.B., and Manchanda, S.V. (2010). Influence of ductile detailing on behaviour of masonry infilled RC frames, Proceedings of the 14th European Conference on Earthquake Engineering, 30 August-03 September 2010, Ohrid, FYROM, Paper No. 1575

Lagomarsino, S., and Giovinazzi, S. (2006). Macroseismic and mechanical models for the vulnerability and damage assessment of current buildings. Bulletin of Earthquake Engineering, 4(4), 415-443

Lang, K. and Bachmann, H. (2004). On the seismic vulnerability of existing buildings: a case study of the city of Basel. *Earthquake Spectra* 20(1), 43–66.

Maffei, J., Telleen, K., and Nakayama, Y. (2008). Probability-Based Seismic Assessment of Buildings Considering Post-Earthquake Safety. *Earthquake Spectra*, 24(3), 667-699.

Mahin, S. A., Bertero, Vitelmo, V. (1977). RCCOLA: A computer program for reinforced concrete column analysis: User's manual and documentation. Dept. of Civil Engineering, University of California, Berkeley, USA.

Mander, J. B., Priestley, M. J. N., and Park, R. (1988). Theoretical Stress-Strain Model for Confined Concrete. *Journal of Structural Engineering*, 114(8), 1804–26.

Masi, A. (2004). Seismic Vulnerability Assessment of Gravity Load Designed R/C Frames. *Bulletin of Earthquake Engineering*, 1(3), 371-395

(NIBS-FEMA) National Institute of Building Sciences-Federal Emergency Management Agency (2008). Multi-hazard Loss Estimation Methodology - Earthquake Model: HAZUS®MH Technical Manual, Washington DC.

Park, R. and Sampson R.A. (1972). Ductility of reinforced concrete column sections in seismic design, *Journal of the ACI*, 69 (9), 543-551.

Paulay, T. and Priestley, M.J.N. (1992). Seismic design of reinforced concrete and masonry buildings. Wiley, New York

Penelis, G.G. and Kappos, A.J. (1997). *Earthquake-resistant Concrete Structures*. E & FN SPON (Chapman & Hall), London.

Penelis, G.G., Kappos, A.J., and Stylianidis, K.C. (2003). Assessment of the seismic vulnerability of unreinforced masonry buildings", *STREMAH 2003, 8th International Conference on Structural Studies, Repairs and Maintenance of Heritage Architecture* (Chalkidiki, Greece 2003), WIT Press, 575-584.

Porter, K. A. (2009). Cracking an open safe: HAZUS vulnerability functions in terms of structure—independent spectral acceleration. *Earthq. Spectra*, 25(2), 361-378.

Ricci, P., De Luca, F., & Verderame, G. M. (2011). 6th April 2009 L'Aquila earthquake, Italy: reinforced concrete building performance. *Bulletin of Earthquake Engineering*, **9**(2):285–305

Shah, S.K.A. (2009). Review of stiffness-based index for infilled RC frame. *MSc dissertation*, European School for Advanced Studies in Reduction of Seismic Risk (ROSE School), University of Pavia, Italy.

Tomazevic, M. **(**2007). Damage as a Measure for Earthquake-Resistant Design of Masonry Structures: Slovenian Experience. *Can. J. Civ. Eng.* 34: 1403-1412, 2007

(TEC) Turkish Earthquake Code (2007). *Specifications for the Buildings to be constructed in Disaster Areas*. Ministry of Public Works and Settlement, Ankara, Turkey.